Analysis of Hydrologic and Geochemical Time Series Data at James Cave, Virginia: Implications for Epikarst Influence on Recharge

Sarah Denise Eagle

Thesis submitted to the faculty of the Virginia Polytechnic Institute and State University
in partial fulfillment of the requirements for the degree of

Master of Science
In
Geosciences

Madeline E. Schreiber
J. Donald Rimstidt
William D. Orndorff

April 22, 2013
Blacksburg, VA

Keywords: karst, epikarst, time series, groundwater, recharge

Analysis of Hydrologic and Geochemical Time Series Data at James Cave, Virginia: Implications for Epikarst Influence on Recharge

Sarah Denise Eagle

ABSTRACT

Karst aquifers are productive groundwater systems around the world, supplying approximately 25% of the world's drinking water. However, they are highly vulnerable to contamination due to rapid groundwater transit in the transmission zone (KWI 2006). The epikarst, also known as the subcutaneous zone, is an interface between the soil overburden and the transmission zone. The epikarst is considered a critical zone as it can control hydrologic and geochemical characteristics of recharge to the underlying karst aquifer. The overall goal of this thesis is to utilize time series hydrologic and geochemical data collected at James Cave, Virginia, to examine the influence of epikarst on the quantity, quality, and rates of recharge to aquifers in Appalachian karst.

Results of this study indicate a strong seasonality of both the hydrology and geochemistry of recharge. The conceptual model of the epikarst developed in this study identifies three hydrologic seasons: recharge, recession, and baseflow. Seasonality of recharge geochemistry coincides with these three hydrologic seasons. These results have implications for management of karst aquifers. First, recharge to Appalachian karst aquifers is seasonal, reaching a maximum during the winter-early spring; the onset of recharge depends on antecedent climatic conditions. Second, water that infiltrates into the epikarst will have seasonally variable residence times due to changes in hydrologic storage; these variations in attenuation affect geochemical reactions in the epikarst, which can influence recharge quality. Overall, these results point to the complex influence of epikarst on karst recharge, which necessitates collection of long-term and high resolution datasets.

ACKNOWLEDGEMENTS

I would like to acknowledge the Virginia Water Resources Research Center, the National Institutes for Water Resources, the Cave Conservancy of the Virginias and the Virginia Tech Geosciences Department for providing funding for research. Additionally, I would like to thank the Geological Society of America for research and travel funding as well as the Virginia Water Resources Research Center for awarding me the William R. Walker fellowship award; this award greatly increased my professional productivity while a graduate student at Virginia Tech.

Second, I would like to thank the numerous people who have assisted this project in field, laboratory, and technical capacities. My committee has provided me with unparalleled intellectual feedback. I would like to thank my advisor Madeline Schreiber for being certainly the most approachable, encouraging graduate advisor. There was never an issue too small, personal or professional, for her to take the time to discuss with me. I would like to thank my committee member Don Rimstidt for his unyielding enthusiasm for my project, his numerous hours of geochemical discussion with me, and his academic pragmatism. I would like to thank my committee member Wil Orndorff for all his previous and current work on this project, for stimulating intellectual discussion about James Cave, and helping me rediscover the intrigue and appeal of caving. I would also like to thank each of my officemates by name: Denise Levitan, Yinka Oyewumi, Luke Joyce, and Zack Munger for their patience with my unending lines of question, for being a partner in commiseration, and for also indulging me in discussion when my productivity had ceased. I thank Hector Lamadrid for making coffee—so much coffee, without which, this thesis would've certainly turned out very differently. I would also like to thank those other contributors that have been helpful to the overall James Cave project and to my general graduate experience, these people include: the Ferrell family for land access, Benjamin Schwartz for obtaining the initial funding and research goals, Tom Malabad for the cave survey, Heather Scott for extended field sampling, Athena Tilley for sample analysis, Anna Hardy for laboratory assistance, Jim Langridge for amazing tech support, Connie Lowe for managing the papers and bureaucracy of graduate school, and many others whose names have been lost through time.

Finally, I would like to thank my long term professional mentors: Gary Dwyer, Peter Haff, and Heather Stapleton all of Duke University—they were instrumental in my development into the scientist I am today. I would like to thank all my dear friends, and especially Nick Downs and Melissa Crowe for their friendship through this time; with their sarcasm and delightful stubbornness reminding me that school is not everything in life. I would like to thank my immediate family and in-laws—but especially my mother and my sister Kathleen for attempting to understand my circumstance in life, but always being my advocate. Lastly, I would like to thank most of all, my husband Ben Shelton—my partner in all obstacles and triumphs and the person there for and with me at the end and beginning of each day. My most sincere gratitude goes out to each of the people and organizations above.

TABLE OF CONTENTS

LIST OF FIGURES

LIST OF TABLES

CHAPTER 1

Background and Methods of the James Cave Monitoring Site in Pulaski County, Virginia

1.1 INTRODUCTION

Karst aquifers are very productive groundwater systems around the world but are also highly vulnerable to contamination due to the presence of large solution conduits and therefore rapid groundwater transit. Globally, approximately 25% of the world's population obtains drinking water from or live atop karst aquifers and in the United States 40% of drinking water is from karst aquifers (KWI 2006). As such, it is imperative to examine how water infiltrates and how contaminants are potentially transported from the surface to the underlying aquifer.

The epikarst, also known as the subcutaneous zone, is the recharge controlling portion of a karst aquifer. It is a region of highly weathered rock in the vadose zone of a karst aquifer and is an interface between the transmission zone, where conduits are frequent, and the soil overburden. In the epikarst, hydraulic conductivity and degree of weathering and therefore transmissivity decrease with depth creating the potential for transient storage of infiltrating water in a local vadose zone (Williams 2008). Due to variations in the porosity, permeability, and connectivity of conduits, the epikarst is highly heterogeneous. This thesis presents results of research on the epikarst overlying James Cave in Pulaski County, Virginia. The overall research goal is to examine the influence of epikarst on the quantity, quality, and rates of recharge to the underlying karst aquifer.

1.2 CONCEPTUAL BACKGROUND

1.2.1 Karst and Epikarst Formation

Following deposition, lithification, and any structural events of calcareous or evaporite sediments, dissolution commences, leading to common features, such as sinkholes, caves, conduits, which are characteristic of karst terrains. The dissolution of evaporites can occur with exposure to any undersaturated solution. The leading chemical mechanism contributing to the dissolution of calcareous rocks is the equilibrium between water and gaseous carbon dioxide, with the product releasing a hydrogen ion and therefore making the solution acidic:

$$CO_2(gas) + H_2O \rightarrow H_2CO_3^{\ 0} \quad (2.1)$$

$$H_2CO_3^{\ 0} \rightarrow HCO_3^{\ -} + H^+ \quad (2.2)$$

Acidification of water due to carbon dioxide increases the dissolution of carbonates. The general example of calcite dissociation and dissolution in the presence of carbon dioxide is given below:

$$CaCO_3(calcite) + CO_2(gas) + H_2O(aq) \rightarrow Ca^{2+} + 2HCO_3^{\ -} \quad (2.3)$$

Other carbonates such as dolomite ($CaMg(CO_3)_2$) and aragonite ($CaCO_3$) follow the same sequence as above, though they have different kinetics and equilibrium constants.

The inherent solubility of these rocks in a variety of solutions is what allows for the formation of karst terrain. Karst terrain is characterized by dissolution features, including enlarged fissures, conduits, caves, and sinkholes. These features develop as a confluence of both physical and chemical factors. Physical factors which contribute to the development of karst include the release of stress, uplift, or other tectonic strain. As a result the media often exhibits triple porosity, as the rock may retain its initial physical properties, this portion is known as the matrix, while in direct proximity to the matrix are fractures, large caves, sinkholes and conduits.

Due to the epikarst's proximity to the surface and proximity to the main source of CO_2 (i.e. atmosphere, soil zone microbial activity), it is subject to an influx of undersaturated (i.e., aggressive) water and a result, the epikarst matrix exhibits high permeability and porosity (Williams 2008). Due to microbial respiration, the soil zone further enriches epikarst water with CO_2. These chemical effects can be magnified by physical factors in the epikarst, such as fractures from tectonic activities or high primary porosity due to the lack of burial.

1.2.2 Epikarst Hydrologic and Geochemical Function

The epikarst is an important control on recharge in a karst system as it is the interface between the transmission zone, where conduits are frequent, and the soil overburden (Williams 2008). In the epikarst, hydraulic conductivity and the degree of weathering decrease with depth, creating the potential for recharge storage as a transient perched aquifer (Williams 2008). Figure 1.1 is a schematic which shows major physical components of the epikarst hydrologic system including the epikarst zone of storage. Previous research has shown that the epikarst can transmit

surges of recharge to the karst aquifer due to accumulated pressure head in the zone of storage which has been described as a “piston effect” (Williams 2008). However, conduits connected to the surface via sinking streams or sinkholes may bypass the epikarst, allowing recharge to move directly to the aquifer without attenuation.

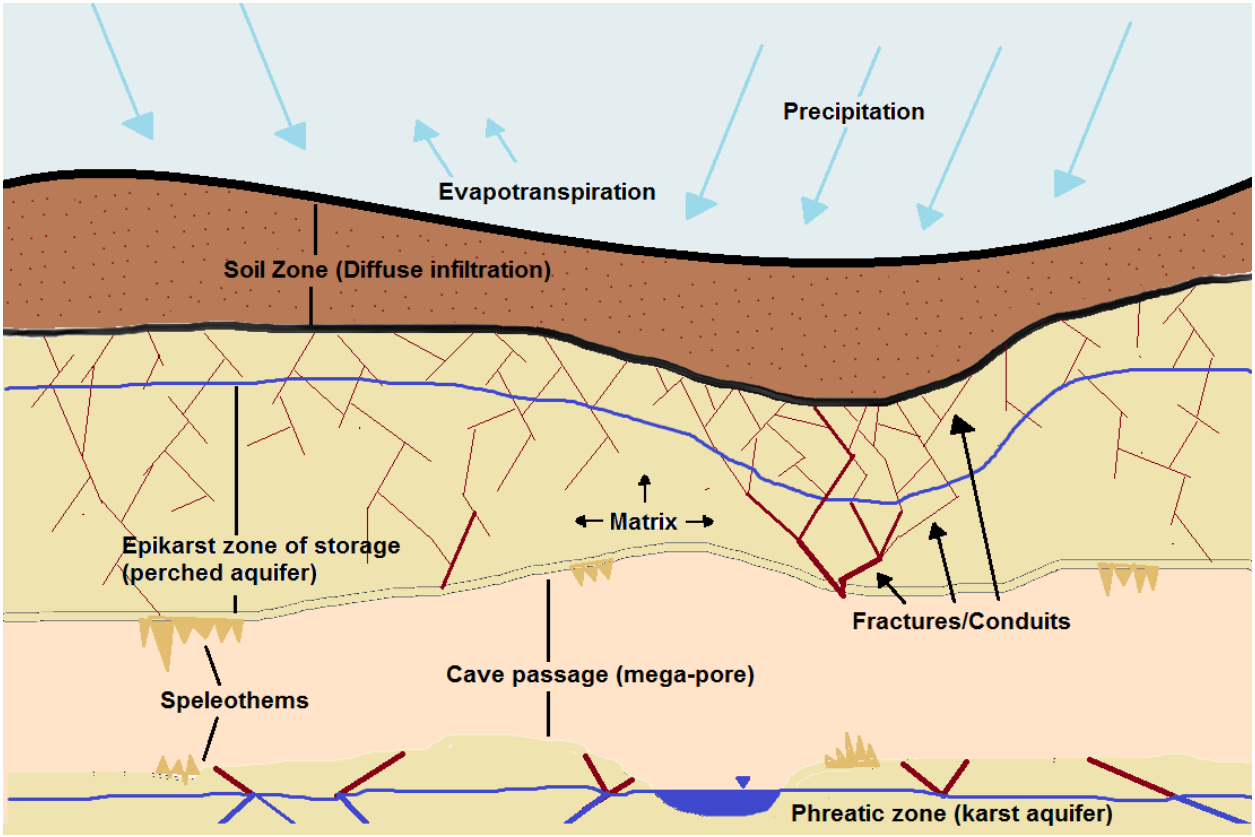

Figure 1.1. Schematic diagram of the epikarst.

The flow mechanisms discussed above have implications for the hydrographs of epikarst discharge. Baseflow through the epikarst has been defined as slowly transported recharge water with long residence time; this is often referred to as diffuse flow. In contrast, quick flow is most often attributed to storm surges and flow through isolated conduits. However, the concepts of baseflow and quick flow in the epikarst hydrologic regime are both subject to the pressure impact of the piston effect—meaning that high head above and within the epikarst can force flow through the epikarst in media associated with both base (matrix) flow and quick (conduit) flow (Bailly-Comte, Martin et al. 2010).

The geochemical function of the epikarst is linked to the hydrologic function as it is influenced by residence time of water as well as interaction of water with soil and rock. As

shown in figure 1.2, the geochemical influence along the flow path may be conceptualized as the mixing of two source waters (precipitation and soil water) and then interaction of the mixture with the carbonate rock. The model proposed in figure 1.2 does not include kinetics; however, a water undersaturated or far from equilibrium can have the same geochemistry of a saturated, equilibrated water mixed with a dilute water.

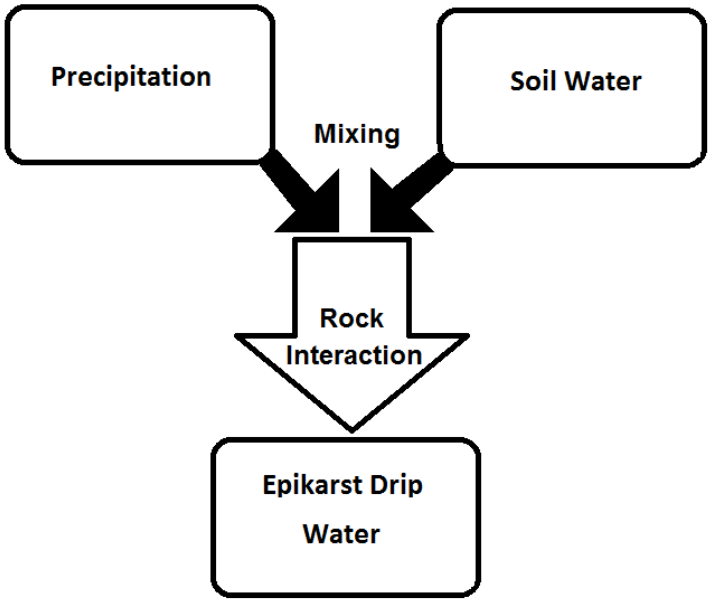

Figure 1.2. Geochemical conceptual model of the epikarst. Precipitation describes dilute water with low concentration of all elements. Soil water is water enriched in elements associated with anthropogenic sources and soil minerals (Na, K, Mg, Cl, SO_4, NO_3). Epikarst drip water is water enriched in products of carbonate mineral dissolution (Mg, Ca, Sr) and comparatively dilute in soil water components (Na, K, Cl, SO_4, NO_3).

1.2.3 Karst and Epikarst Classification

The majority of karst terrains may be classified in one of three categories which describe the geologic history, the current state of the unit with respect to the rock cycle, and the hydrologic characteristics of the carbonate unit: telogenetic, mesogenetic, or eogenetic (Choquette and Pray 1970). Eogenetic carbonate units are diagenetically immature and have not been deeply buried. Therefore, they exhibit higher primary porosity and typically have significant diffuse flow. Mesogenetic describes a state of deep burial and would translate to lower primary porosity but being so deeply buried would likely cause reduced ability for karst to form. In contrast, telogenetic carbonate units are those that have been previously buried to some

extent, thereby reducing primary porosity but due to offloading of overburden and reduction of stress, significant fractures may develop. Flow in telogenetic karst is dominated by secondary porosity, including conduits or fractures (Choquette and Pray 1970).

Classification of epikarst depends on three characteristics: karst classification (as described above), time duration since exposure, and thickness of overburden. Due to the higher primary porosity and relatively efficient diffuse flow, epikarst on eogenetic karst exhibits different hydrologic characteristics than classic telogenetic epikarst, particularly with regard to transient storage (Mylroie, Jenson et al. 2003). Telogenetic karst is typically older and has experienced more of the events discussed above which forms the epikarst. As such the classification for telogenetic epikarst ranges from newly emerged to long since exposed with varying degrees of soil cover. Klimchouk developed a classification scheme where age since exposure positively correlates to the hydraulic conductivity of the epikarst and as soil cover increases, the distribution of fissures and conduits is more even (Klimchouk 2003).

1.3 FIELD SITE BACKGROUND

1.3.1 Location and Land Use

The field site for this project is at James Cave in Pulaski County, Virginia. Figure 1.3, below shows the location of Pulaski County in southwestern Virginia.

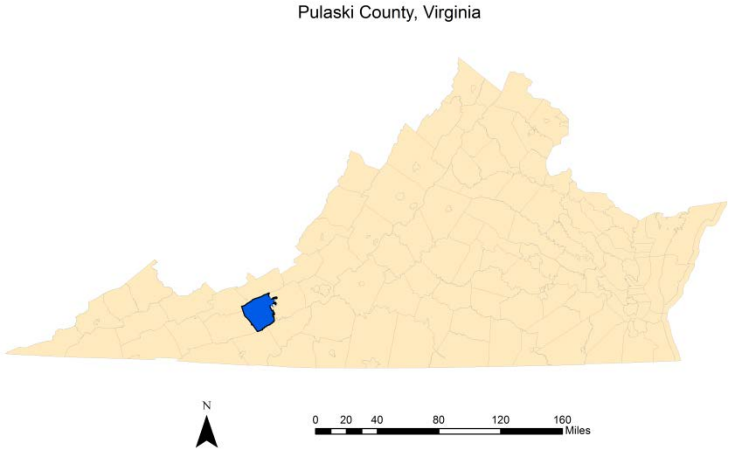

Figure 1.3. Pulaski County, Virginia. Data from Bureau of the Census and NRCS (2002).

The majority of the county is forest of mixed variety and pasture or hay fields (MRLC 2006). The karst areas in the region, not only this county, are also dominated by agricultural land—making this field site important and relevant not just locally, but also regionally. Figure 1.4 shows the distribution of land cover in the county and the specific location of the field site within an area of pasture. The grey areas indicate developed regions, from east to west: outskirts of the independent city of Radford and the towns of Dublin and Pulaski.

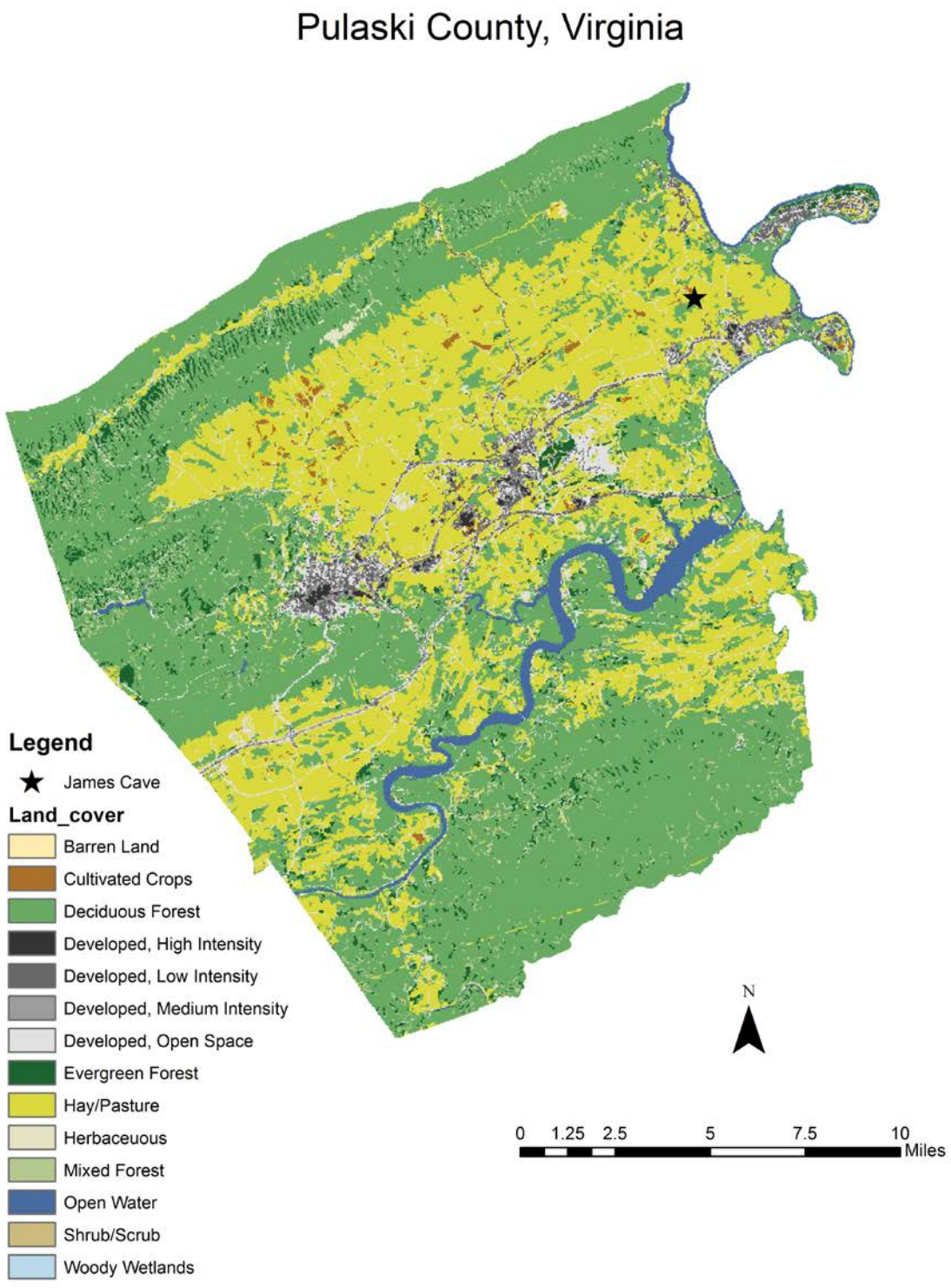

Figure 1.4. Land cover in Pulaski County, Virginia. Data from MRLC (2006). The entrance of James Cave is indicated by a black star in the northeast region of the county, east of the large bend in the New River as shown by the northeast county boundary.

Figure 1.5 shows the topography of the vicinity around James Cave and the cave survey of the section of study and instrumented sites.

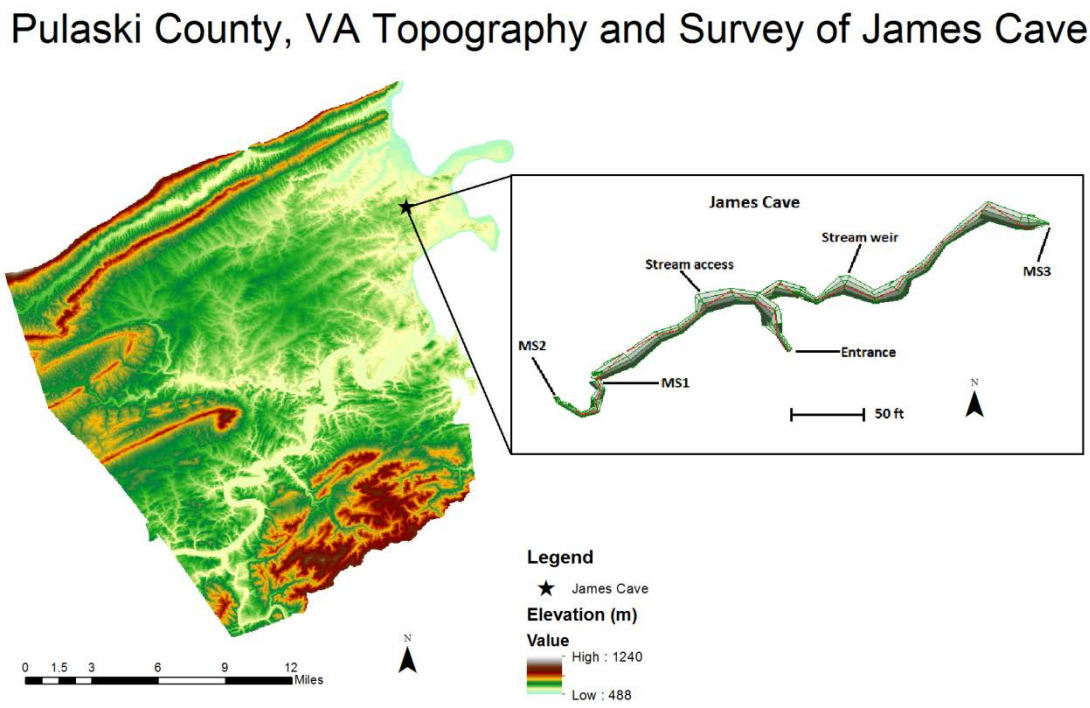

Figure 1.5. Pulaski County, VA Topography and Survey of James Cave with monitoring stations. Topographic data from USGS-EROS (2012), Cave survey data collected by Tom Malabad.

Figure 1.6 shows the full cave survey of James Cave. There are two known entrances to the cave, both of which are located within sinkholes. The depth of the cave below the surface is highly variable and includes several divergent passages. The elevation of the cave ranges from the zero datum at the entrance, to nearly 27 meters below the entrance elevation at the north-eastern extent of the cave. The known full length of James Cave, as indicated in the full survey, is 2.2 kilometers. Also worth noting is the existence of a cave stream which flows eastward.

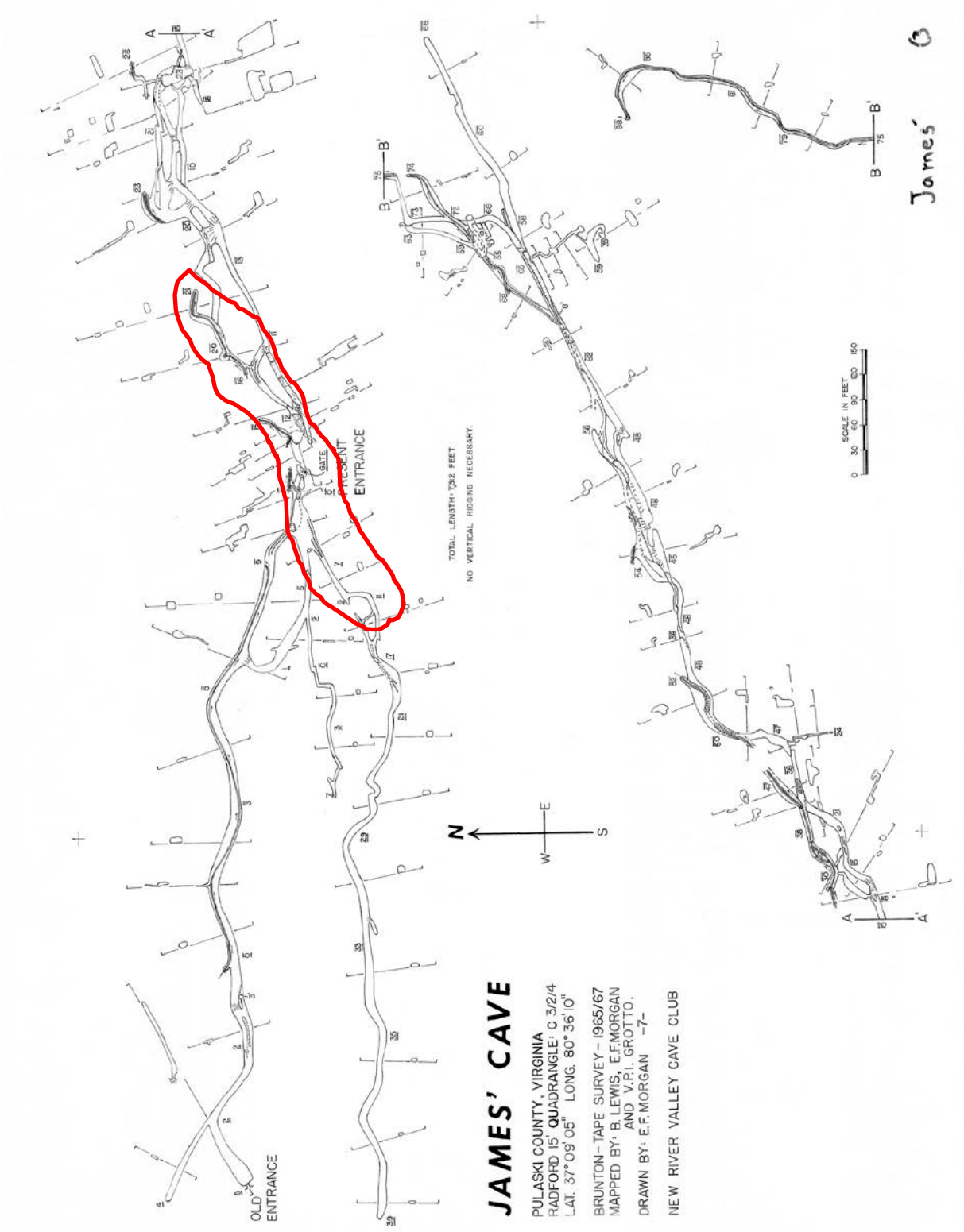

Figure 1.6. Full survey of James Cave. Courtesy of B. Lewis, E.F. Morgan, and the New River Valley Cave Club. The section of study is outlined in red.

1.3.2 Geology and Soils

Pulaski County is located within the Valley and Ridge physiographic province. The Pulaski Fault system dominates the structural geology in this region. As described by Bartholomew (1987) the Pulaski Fault system is a series Alleghanian thrust faults responsible for more than 100 km of westward displacement of the Pulaski thrust sheet over units as young as Mississippian age. James Cave formed within limestone and dolomite units exposed due to this thrust system in the Cambro-Ordovician Conococheague formation. The proximity of secondary faults and current groundwater flow paths likely played a role in the development of this cave. Figure 1.7 depicts the geology of Pulaski County along with the James Cave section of study. Figure 1.8 depicts the more local geology surrounding the site of study, including alluvial deposits.

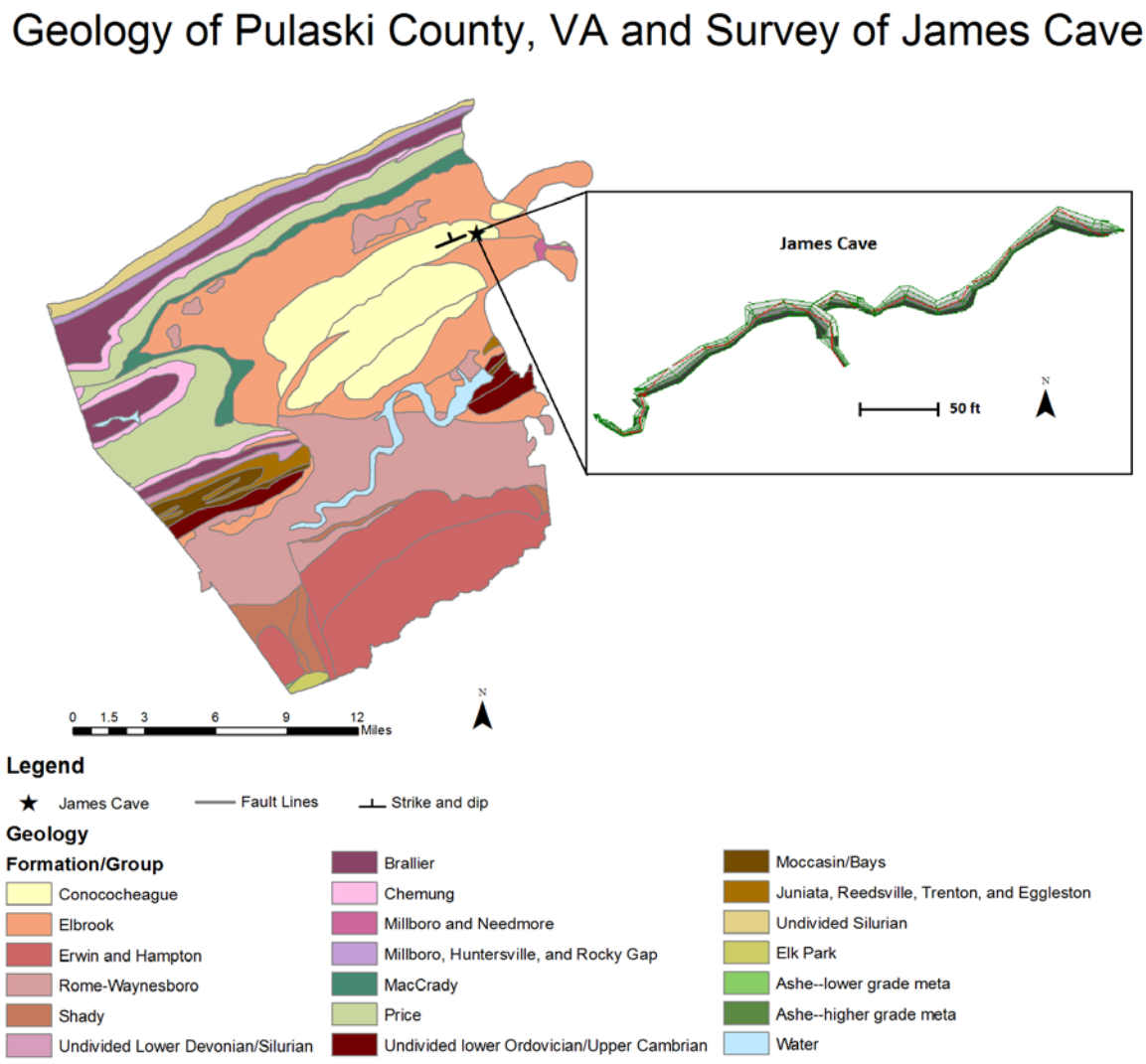

Figure 1.7. Geology of Pulaski County, VA and survey of James Cave. Geologic data from USGS-Mineral Resources Program (2005). Cave survey (inset) conducted by Tom Malabad.

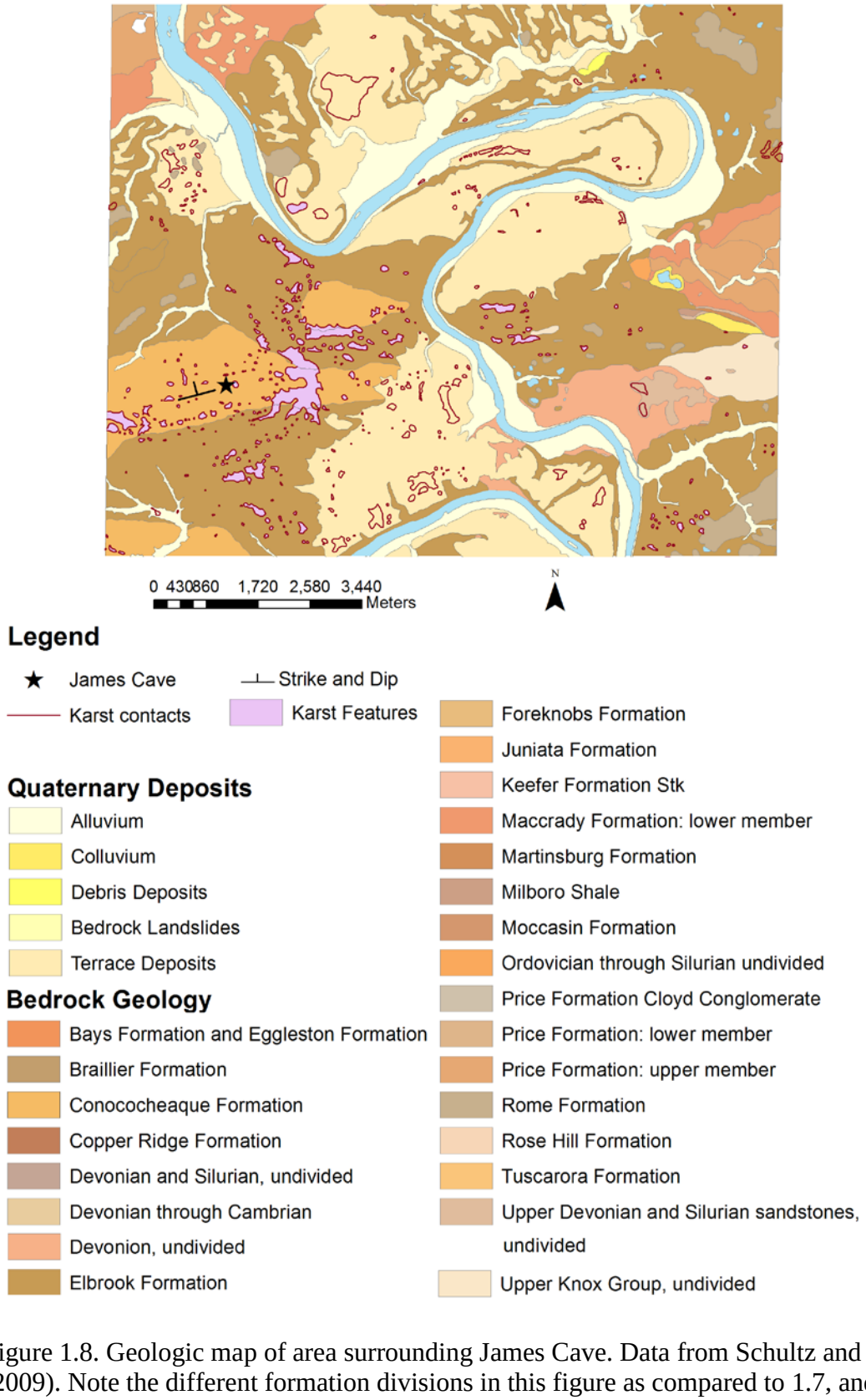

Figure 1.8. Geologic map of area surrounding James Cave. Data from Schultz and Bartholomew (2009). Note the different formation divisions in this figure as compared to 1.7, and the corresponding differences in formation color symbology.

James Cave is located within the Conococheague formation, and is underlain and surrounded by the Elbrook formation due to a synclinal feature. The Conococheague formation has been described in this area as a fine-grained bluish-gray limestone (Hergenroder 1957). The Conococheague also contains thin laminations of argillaceous material, varying amounts of dolomite with the limestone, as well as shale and calcareous sandstone interbeds (Hergenroder 1957). The Elbrook is described as a thin-bedded to shaly dolomite that also contains dolomitic to pure calcareous limestone as well as some shale interbeds (Hergenroder 1957).

The soil units of Pulaski County are shown in figure 1.9. Soils in the vicinity of James Cave, the Wurno-Newbern-Faywood silt loams and the Lowell silt, are described as silt loams with slopes between 7-15%. Additionally, there is carbonate regolith at depth.

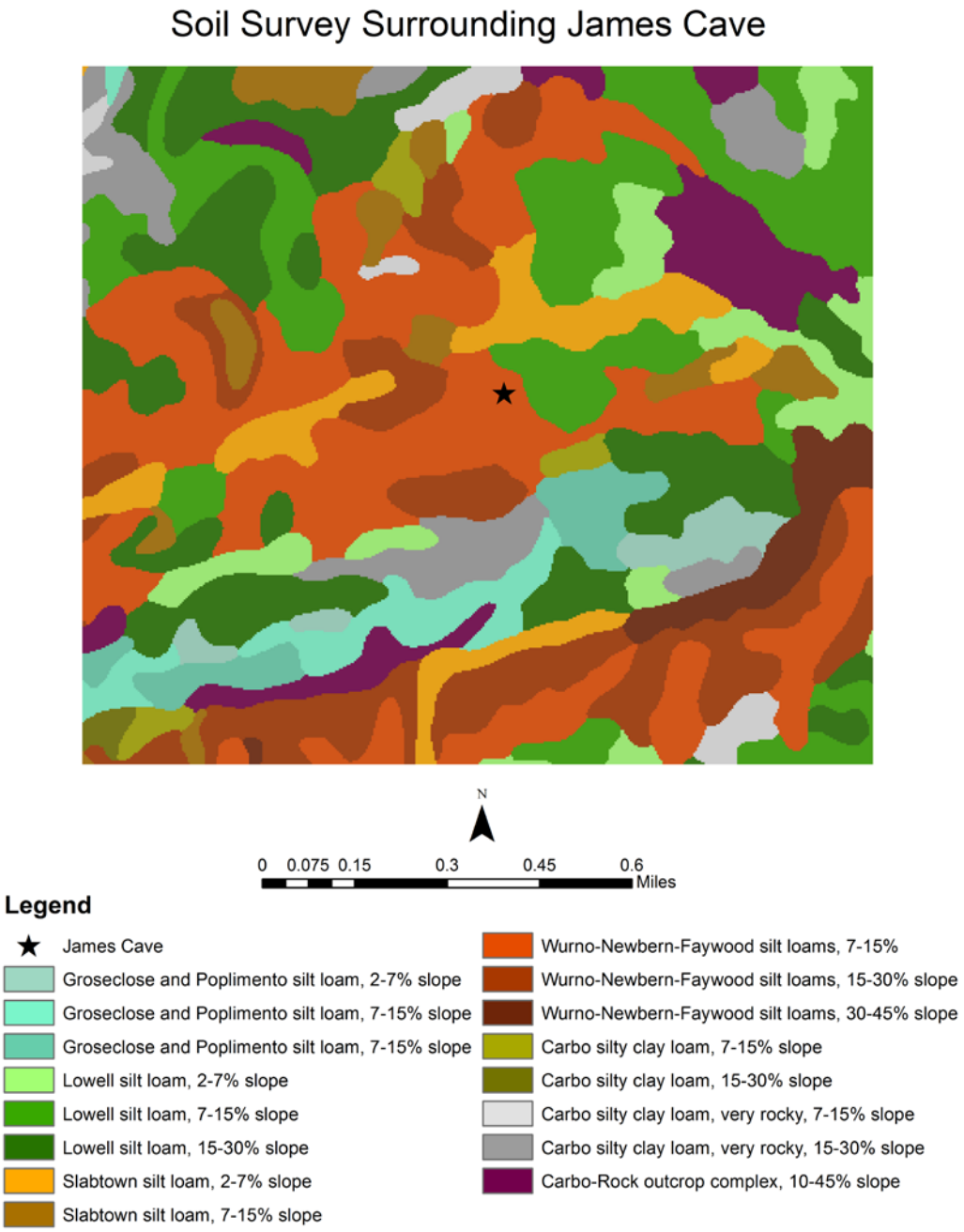

Figure 1.9. Soils in area above and surrounding James Cave. Data from USDA-NRCS (2010).

A general description of the dominant soils overlying James Cave are included in table 1.1.

Table 1.1. General characteristics of soil units near James Cave. Data from USDA-NRCS 2010.

Soil Unit	**Sand (%)**	**Silt (%)**	**Clay (%)**	**pH**	**Cation Exchange Capacity (meq/100g)**	**Organic Matter Content (%)**
Wurno-Newbern-Faywood	27.1	54.4	18.5	5.1-7.8	3.0-22.0	0-3
Lowell	26.5	53.5	20.0	4.5-7.8	5.0-15.0	0-3

The Wurno-Newbern-Faywood and Lowell loam soils have similar particle size distributions and organic matter content. The cation exchange capacity for the Lowell is more narrowly defined than the Wurno-Newbern-Faywood and the pH range is greater. Soil augering done by William (Luke) Joyce at eight sites overlying James Cave suggest that the soil depth ranges from 0.70-2.6 meters.

1.3.3 Climate

Pulaski County is in a temperate climate zone with an approximate mean annual temperature of 11.4°C (The Southeast Regional Climate Center 2012). The county receives on average 38.91 inches of precipitation per year (The Southeast Regional Climate Center 2012). Analysis of precipitation records shows that there is no strong seasonality to precipitation. Evapotranspiration (ET), estimated by Gerst (2010) using the Penman-Moneith equation, is highest in the summer.

1.4 INSTRUMENTATION AND SAMPLING REGIME

A portion of James Cave has been instrumented with monitoring stations in eight locations. In the subsurface, there are three sites to measure epikarst drips and one site to measure discharge of the cave stream which flows eastward. On the surface, there is a precipitation station and three tension lysimeters in the vadose zone. Two of the lysimeters are at the approximate surface projections of two of the drip sites; the third is near the cave entrance. Figure 1.10 shows the site survey and monitoring station locations. The instrumentation and sampling regime at each of these monitoring stations has changed over time and as such, it is worthwhile to describe the methods for data collection.

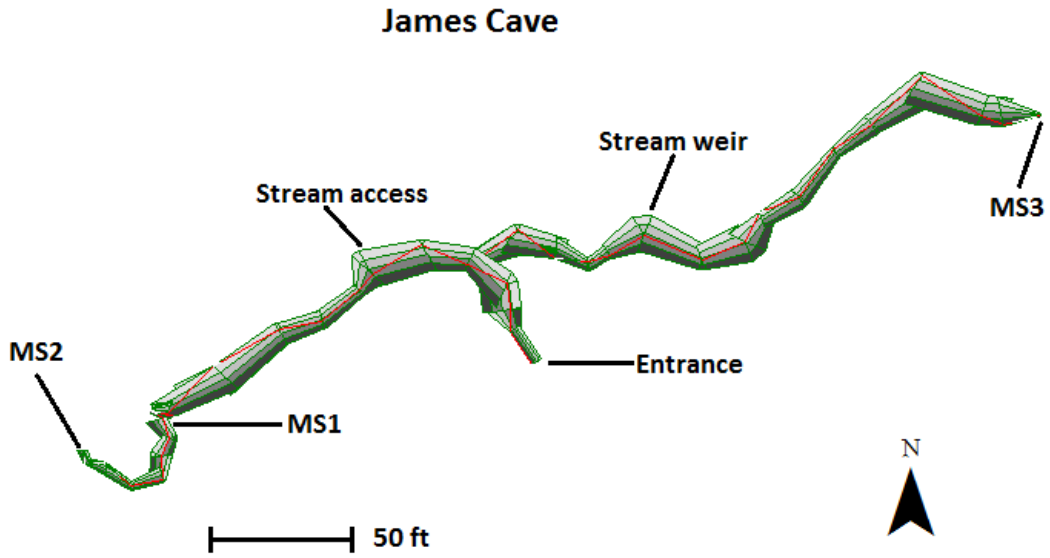

Figure 1.10. Survey of James Cave with monitoring stations. Survey produced using data collected by Tom Malabad. Highlighted in figure 1.6 is the section of study in relation to the full cave survey.

1.4.1 Current Instrumentation

The instrumentation of James Cave began in Summer 2007. Table 1.2 describes the instrumented monitoring stations and associated data collection for the overall James Cave project. Note that there have been changes to the instrumentation made since the start of the project; those are outlined in subsequent tables.

Table 1.2. Instrumentation by monitoring station. Elevation data from Gerst (2010).

Station Name	Physical Location of Station	Air Measure-ments	Hydrologic Measure-ments	Geochemical Measure-ments	Composite Sample Collection
Surface	Near cave entrance, ~605m AMSL	Air temp., relative humidity	Precip.	--	X
Soil Entrance	Near cave entrance, ~604m AMSL	--	--	--	X
Soil 2	Surface projection of MS2, ~605.8m AMSL	--	--	--	X
Soil 3	Surface projection of MS3, ~600m AMSL	--	--	--	X
MS1	Subsurface, 597m AMSL	Air temp.	Drip discharge	Water temp, specific conductance	X
MS2	Subsurface, 595.1m AMSL	Air temp.	Drip discharge	Water temp, specific conductance	X
MS3	Subsurface, 593m AMSL	Air temp.	Drip discharge	Water temp, specific conductance	X
Cave Stream	Subsurface, ~592m AMSL	--	Discharge (V-notch weir with pressure transducers)	Water temp, specific conductance	X

As noted in Table 1.2, samples of precipitation, soil water, drip water, and stream water were collected for geochemical analyses (anions, cations, alkalinity, as well as isotopes of the water molecule (^{18}O and ^{2}H) and of organic and inorganic carbon). Precipitation samples were collected using a dual precipitation collector; one collector was used for composite sample collection; the other collector was used as an isotopic control to determine the influence of evaporation on isotope fractionation.

As noted above, instrumentation of the drip sites has changed over time. Since the project's inception, drips have been consolidated on a suspended tarp (2.43m^2, 3.07m^2, and 3.51m^2, for MS1, MS2, and, MS3, respectively). Prior to January 2011, drips were channeled directly into a tipping bucket rain gauge to measure drip rate.

Currently (since January 2011), the drips are channeled into a small reservoir instrumented with a conductivity logger that measures water temperature and specific conductance. The outflow of this reservoir goes into the tipping bucket rain gauge that measures drip rate. From the rain gauge, drips are then funneled into a sample collection vessel instrumented with an airlock to prevent interaction of the sample with the cave atmosphere. Figure 1.11 shows the schematic set-up of drip site instrumentation and figure 1.12 shows a picture of the set-up in situ. It should be noted that prior to 2012, rain gauge failure was common, due to corrosion of exposed electronics. To fix this problem, the rain gauges were retrofitted in July 2012 with a reed switch and pulse adapter combination with a data logger microstation.

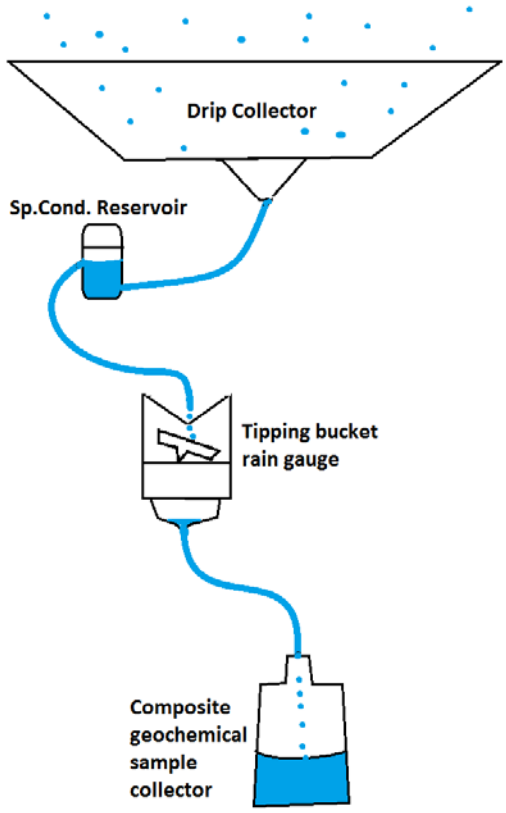

Figure 1.11. Schematic of current drip site instrumentation as of January 2011.

Figure 1.12. Instrumentation at MS3 with author (Sarah Eagle) in background. Photo taken in January 2013 by Wil Orndorff.

The cave stream is instrumented with a v-notch weir and pressure transducer and a Hobo conductivity logger. Figure 1.13 shows the cave stream v-notch weir with the location of the stilling well for the pressure transducer. The v-notch weir in conjunction with pressure transducers allows for calculation of stream discharge. Similar to the rain gauges, the weir has experienced several failures over the course of the project, due to leakage around the sides. In January 2011, the weir was re-constructed by Wil Orndorff using concrete, wood, and plastic sheeting to prevent leakage around the sides.

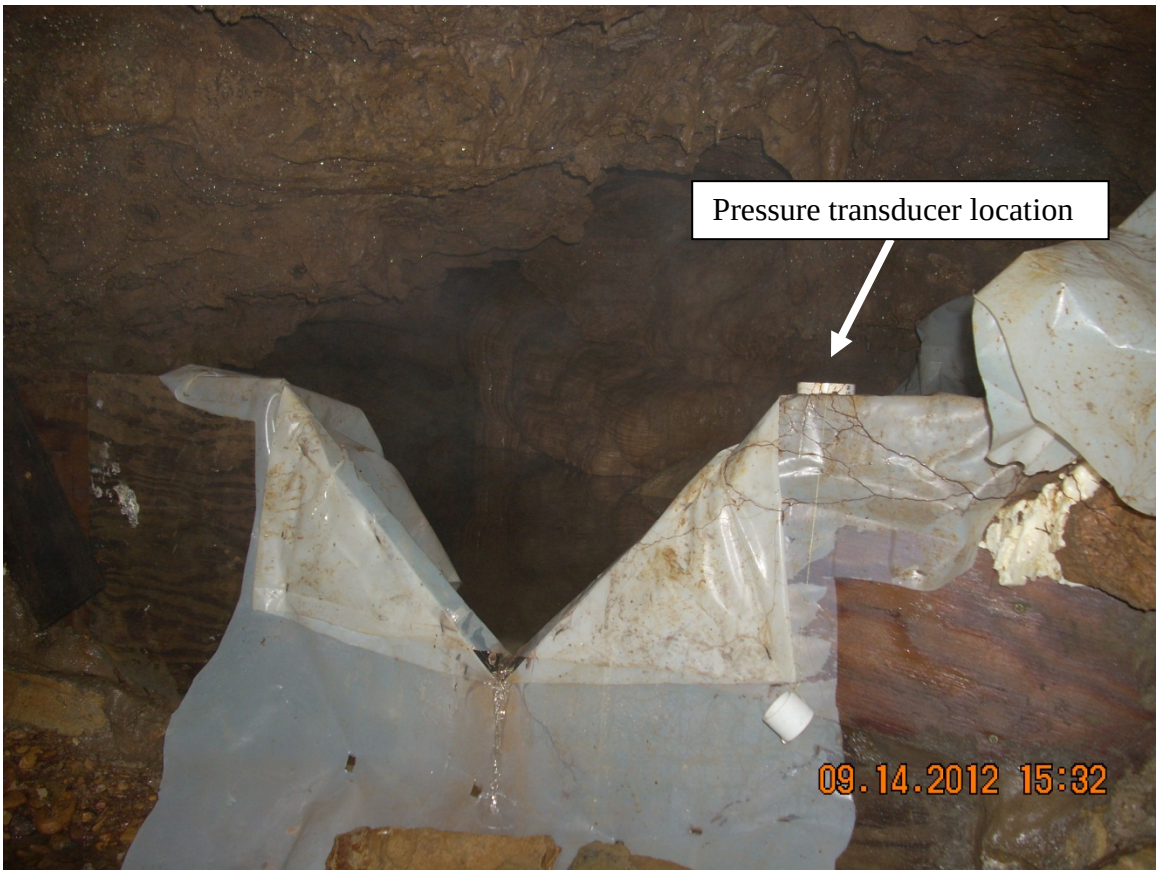

Figure 1.13. James Cave stream weir with location of stilling well and pressure transducer noted.

1.4.2 Chronology of James Cave Instrumentation and Sampling

The initial instrumentation of James Cave began in summer 2007 with the installation of monitoring equipment at the surface and at two drip sites (MS1, MS2). Each site was instrumented with a tipping bucket rain gauge to measure precipitation or drip rate, and a temperature/relative humidity sensor. Data were logged and stored using microstation data logger. At the drip sites, drip samples were collected from 10-15 stalactites. To collect the drip

samples, latex balloons were secured to the stalactites on one end with cable ties and attached to tubing on the other end; the tubing drained into a collection vessel. The vessel was instrumented with a multiparameter sonde (HI 9828) which measured pH, temperature, DO, ORP, and specific conductance of the inflow drips. Samples flowed out an overflow tube and into another vessel, which was fitted with an airlock and looped outflow tube to prevent interaction of the collected sample with the atmosphere (Gerst, unpublished). This sample was collected monthly and analyzed for geochemical parameters of interest. Biological samples of epikarstic fauna were also collected until January 2012.

Over time, the instrumentation and sampling regime have changed. Table 1.3 details the chronology of the project. Table 1.4 details the instrumentation specifics.

Table 1.3. Chronology of instrumentation changes at James Cave. Information gathered from field notes and downloaded data.

Date	Site(s) Impacted	Description
09/2007	Surface	Rain gauge with temperature, relative humidity sensor installed
09/2007	MS1, MS2	Suspended tarps and rain gauges installed; HANNA multiparameter sondes installed.
02/2008	MS3	Suspended tarp and rain gauge installed; HANNA multiparameter sonde installed.
08/2008	Surface	Precipitation collector installed
03/2009	Stream weir	Stream weir installed
03/2009	Stream weir	Solinst pressure transducers (level and barometric loggers) installed
06-07/2009	Soil2, Soil3, Soil Entrance	Tension lysimeters installed at 3ft depth
04/2010	Stream	HANNA multiparameter sonde installed
01/2011	Stream	HANNA moved upstream from weir to near entrance
01/2011	MS1, MS2, MS3	Sondes removed; specific conductance loggers installed
01/2011	Stream weir	Stream weir replaced with concrete V-notch weir
06/2011	Stream	Sonde removed; specific conductance logger installed
02/2012	All sites	Cease composite geochemical sampling
05/2012	MS1, MS2, MS3	Replaced microstation and smart sensor rain gauge with reed switch and pendant logger combination
05/2012	Stream weir	Replaced Solinst level and baro loggers with Onset
06/2012	Surface	Replace smart sensor rain gauge with reed switch and pendant logger combination
07/2012	MS1, MS2, MS3	Replaced pendant logger with pulse adaptor and microstation combination

Table 1.4. Instrumentation information for James Cave.

Item	Manufacturer	Part/Model Number
HANNA multiparameter sonde	HANNA Instruments	HI9828
Smart sensor rain gauge	Onset	RGB-M002
Microstation data logger	Onset HOBO	H21-002
Level logger	Solinst	3001
Barometric pressure logger	Solinst	3001
Water level logger	Onset HOBO	U20-001-01
Barometric pressure logger	Onset HOBO	U20-001-01
Specific conductance logger	Onset HOBO	U24-001
Reed switch	Texas Electronics	120-0018
Terminal Block	Texas Electronics	009-0059
Pendant logger	Onset HOBO	UA-003-64
Pulse adaptor	Onset HOBO	S-UCD-M001

1.5 METHODS

1.5.1 Sample Collection

Between June 2008 and January 2012 water samples were collected on a monthly or bimonthly interval from each of the sites described in Table 1.2. Samples of the precipitation and cave drips were composite samples of the discharge since last collection, or the discharge since last collection summing to one liter. Samples of soil water and the cave stream were grab samples of one liter or less depending on the volume available. Upon collection, samples were labeled and stored in a cooler with ice packs for transport back to the laboratory. Upon arrival at the laboratory water samples were filtered to 0.22µm and aliquoted into the following subsamples:

1) cation analysis: samples were collected in 60 ml acid-washed HDPE bottles and acidified with HNO3;

2) anion analysis: samples were collected in 30 ml HDPE bottles without preservation;

3) water isotopic analysis: samples were collected without headspace in 11mL polyseal glass vial and without preservation;

4) dissolved organic carbon analysis: samples were collected in 20 ml amber glass vials and acidified with HCl;

5) for inorganic and organic carbon isotope analysis: samples were collected without headspace in 20 ml amber glass vials with butyl rubber septa (inorganic) and teflon septa (organic) and were preserved with copper sulfate (inorganic) and phosphoric acid (organic);

6) pH and alkalinity analysis: samples were collected in 125 mL HDPE bottles.

After collection, all samples were stored at approximately 4ºC until analysis. The standard operating procedure for sample collection and geochemical sample preservation is provided in Appendix A.

In November of 2010 William Joyce conducted soil sampling and descriptions of the James Cave field site from hand augered soil cores. There were a total of eight soil cores done: two above MS1, three above MS2, and three above MS3. Soils were labeled based on horizons identified by W. Joyce.

1.5.2 Laboratory Analysis

Cations (Al, Ca, K, Mg, Na, Si, and Sr) were analyzed using Inductively Coupled Plasma Atomic Emission Spectrometry (Spectro ARCOS SOP) by the VT Soil and Plant Analysis Lab. Anions were analyzed for Cl, NO_3, and SO_4 using Ion Chromatography (Dionex DX-120). Alkalinity was measured using gran titration (Radtke, Wilde et al. 2012). Soil samples collected by W. Joyce were analyzed for water pH, buffer pH, nutrients (P, K, Ca, Mg, Zn, Mn, Cu, Fe, B), soluble salts, organic matter content, and cation exchange capacity by the Virginia Tech Soil Testing Laboratory. Analytical method details for soils are presented in Maguire and Heckendorn (2011).

Water isotopes were analyzed at Texas State University by co-PI Benjamin Schwartz. The carbon isotope samples were analyzed by co-PI Daniel Doctor at the USGS-Reston. As the isotope data are not discussed in this thesis, the analytical methods are not presented.

1.5.3 Data Collection and Management

Continuous time series data were offloaded from sites on a monthly or bimonthly basis. These data were stored on a variety of hard and virtual data storage locations and were aggregated for this project starting in fall of 2011. For preprocessing all time-series data were imported, preprocessed, corrected for drift, and resampled, where necessary, with AQUARIUS Workstation (Aquatic Informatics 2011). Additional information on data management and preprocessing can be found in Appendix B.

1.6 REFERENCES

Aquatic Informatics (2011). AQUARIUS 3.0 R3. 1032. Vancouver, British Columbia.

Aquilina, L., B. Ladouche, et al. (2006). "Water storage and transfer in the epikarst of karstic systems during high flow periods." Journal of Hydrology **327**(3-4): 472-485.

Bailly-Comte, V., J. B. Martin, et al. (2010). "Water exchange and pressure transfer between conduits and matrix and their influence on hydrodynamics of two karst aquifers with sinking streams." Journal of Hydrology **386**(1-4): 55-66.

Bakalowicz, M. J. (2004). The epikarst, the skin of karst. Epikarst: Special Publication 9., Charles Town, WV, Karst Waters Institute.

Baker, A. and C. Brunsdon (2003). "Non-linearities in drip water hydrology: an example from Stump Cross Caverns, Yorkshire." Journal of Hydrology **277**(3–4): 151-163.

Baker, A., D. Genty, et al. (2000). "Hydrological characterisation of stalagmite dripwaters at Grotte de Villars, Dordogne, by the analysis of inorganic species and luminescent organic matter." Hydrology and Earth System Sciences **4**(3): 439-449.

Baldini, J. U. L., F. McDermott, et al. (2012). "Identifying short-term and seasonal trends in cave drip water trace element concentrations based on a daily-scale automatically collected drip water dataset." Chemical Geology **330–331**(0): 1-16.

Bartholomew, M. J. (1987). "Structural evolution of the Pulaski thrust system, southwestern Virginia." Geological Society of America bulletin **99**(4): 491.

Bureau of the Census and NRCS (2002). NRCS Counties by State. United States Census Bureau and Department of Agriculture-Natural Resources Conservation Service.

Choquette, P. W. and L. C. Pray (1970). "Geologic nomenclature and classification of porosity in sedimentary carbonates." AAPG bulletin **54**(2): 207.

Curti, E. (1999). "Coprecipitation of radionuclides with calcite: estimation of partition coefficients based on a review of laboratory investigations and geochemical data." Applied Geochemistry **14**(4): 433-445.

El-Kadi, A. I., L. N. Plummer, et al. (2011). "NETPATH-WIN: An Interactive User Version of the Mass-Balance Model, NETPATH." Ground water **49**(4): 593-599.

Fairchild, I. J., A. Borsato, et al. (2000). "Controls on trace element (Sr–Mg) compositions of carbonate cave waters: implications for speleothem climatic records." Chemical Geology **166**(3–4): 255-269.

Genty, D. and G. Deflandre (1998). "Drip flow variations under a stalactite of the Père Noël cave (Belgium). Evidence of seasonal variations and air pressure constraints." Journal of Hydrology **211**(1–4): 208-232.

Gerst, J. D. (2010). Epikarst control on flow and storage at James Cave, VA: an analog for water resource characterization in the Shenandoah Valley karst. Geosciences. Blacksburg, VA, Virginia Polytechnic Institute and State University. **Master of Science**.

Grant, D. M. and B. D. Dawson (2001). Isco Open Channel Flow Measurement Handbook. Lincoln, Nebraska, Isco, Inc.

Gregory, L., B. Wilcox, et al. (2009). "Large-scale rainfall simulation over shallow caves on karst shrublands." ECOHYDROLOGY **2**: 72-80.

Hergenroder, J. D. (1957). Geology of the Radford Area, Virginia. Geology. Blacksburg, VA, Virginia Polytechnic Institute. **Master of Sciences**.

Klimchouk, A. (2003). Towards defining, delimiting and classifying epikarst: its origin, processes and variants of geomorphic evolution. Epikarst, Shephardstown, West Virginia, Karst Waters Institute, Inc.

KWI (2006). "What is Karst (and why is it important)?". Retrieved December 1, 2011, from http://www.karstwaters.org/aboutkarst/index.php.

Maguire, R. O. and S. E. Heckendorn (2011). Laboratory Procedures, Publication 452-881. Blacksburg, VA, Virginia Polytechnic Institute and State University.

McDonald, J. and R. Drysdale (2007). "Hydrology of cave drip waters at varying bedrock depths from a karst system in southeastern Australia." Hydrological Processes **21**(13): 1737-1748.

McDonald, J., R. Drysdale, et al. (2007). "The hydrochemical response of cave drip waters to sub-annual and inter-annual climate variability, Wombeyan Caves, SE Australia." Chemical Geology **244**(3-4): 605-623.

MRLC (2006). National Land Cover Dataset. Environmental Protection Agency- Multi-Resolution Land Characteristics Consortium, http://datagateway.nrcs.usda.gov.

Mylroie, J. E., J. W. Jenson, et al. (2003). Epikarst on Eogenetic Rocks. Epikarst, Shephardstown, West Virginia, Karst Waters Institute, Inc.

Perrin, J., P.-Y. Jeannin, et al. (2003). "Epikarst storage in a karst aquifer: a conceptual model based on isotopic data, Milandre test site, Switzerland." Journal of Hydrology **279**(1–4): 106-124.

Radtke, D. B., F. D. Wilde, et al. (2012). Alkalinity and Acid Neutralizing Capacity (version 4.0). National Field Manual for the Collection of Water-Quality Data: U.S. Geological Survey Techniques of Water-Resources Investigations. S. A. Rounds, U.S. Geological Survey. **9**.

Schultz, A. P. and M. J. Bartholomew (2009). Geologic Map of the Radford North Quadrangle, Virginia. A. Cross and E. V. M. Campbell, Virginia Division of Mineral Resources.

Sheffer, N. A., M. Cohen, et al. (2011). "Integrated cave drip monitoring for epikarst recharge estimation in a dry Mediterranean area, Sif Cave, Israel." Hydrological Processes **25**(18): 2837-2845.

Sherwin, C. M. and J. U. L. Baldini (2011). "Cave air and hydrological controls on prior calcite precipitation and stalagmite growth rates: Implications for palaeoclimate reconstructions using speleothems." Geochimica Et Cosmochimica Acta **75**(14): 3915-3929.

The Southeast Regional Climate Center (2012). "Historical Climate Summaries for Virginia." 2012, from http://www.sercc.com/climateinfo/historical/historical_va.html.

Tooth, A. F. and I. J. Fairchild (2003). "Soil and karst aquifer hydrological controls on the geochemical evolution of speleothem-forming drip waters, Crag Cave, southwest Ireland." Journal of Hydrology **273**(1–4): 51-68.

USDA-NRCS (2010). Soil Survey Tabular Database. United States Department of Agriculture-Natural Resources Conservation Service.

USGS-Mineral Resources Program (2005). USGS Geologic Map of Conterminous United States. United States Geological Survey.

Virginia Agricultural Experiment Station (2012). "Weather Data." Retrieved January 30, 2013, from http://www.vaes.vt.edu/college-farm/weather/2012/weather2012.html.

Williams, P. (2008). "The role of the epikarst in karst and cave hydrogeology: a review." International Journal of Speleology (Edizione Italiana) **37**(1): 1-10.

Williams, P. W. (1983). "The role of the subcutaneous zone in karst hydrology." Journal of Hydrology **61**(1–3): 45-67.

Yang, R., Z. Liu, et al. (2012). "Response of epikarst hydrochemical changes to soil CO2 and weather conditions at Chenqi, Puding, SW China." Journal of Hydrology **468–469**(0): 151-158.

CHAPTER 2
Investigation of Epikarst Seasonality through Geochemical and Hydrologic Time Series Data

2.1 INTRODUCTION

The epikarst, also known as the subcutaneous zone, is the recharge controlling portion of a karst aquifer. It is a region of highly weathered rock in the vadose zone of a karst aquifer and is an interface between the transmission zone, where conduits are frequent, and the soil overburden (Williams 2008). In the epikarst, hydraulic conductivity and degree of weathering and therefore transmissivity decrease with depth creating the potential for transient storage of infiltrating water in a leaky, perched aquifer (Williams 1983; Klimchouk 2003; Bakalowicz 2004; Aquilina, Ladouche et al. 2006; Williams 2008). This zone of storage may allow for hydrologic and geochemical attenuation of recharge and hence indicates the considerable potential influence of the epikarst.

Despite the importance of this feature, studying the epikarst has been historically difficult due to inherent heterogeneity and complexity (Williams 2008). Over the past two decades, improvements in instrumentation and data logging have allowed for direct measurements of drip rates in caves (Genty and Deflandre 1998; Baker and Brunsdon 2003; McDonald and Drysdale 2007; Gregory, Wilcox et al. 2009; Sheffer, Cohen et al. 2011). Many of these drip studies were designed to address controls on speleothem growth for extrapolation to paleoclimate studies. However, some of the results have been used to infer flow routes and geochemical processes in epikarst (Genty and Deflandre 1998; Tooth and Fairchild 2003). For example, Tooth and Fairchild (2003) described the influence of the soil zone on drip water geochemistry and documented the existence of prior calcite precipitation deduced from Sr/Ca ratios. Other studies have elucidated some of the causal or correlative variables on drip water geochemistry through the use of trace elements, organic matter luminescence, and P_{CO2} (Baker, Genty et al. 2000; McDonald, Drysdale et al. 2007; Sherwin and Baldini 2011; Baldini, McDermott et al. 2012). Many of these previous studies have limited monitoring periods, and few studies have been able to combine high resolution monitoring of both hydrology and geochemistry, which are both key elements for elucidating the function of the epikarst.

This study utilizes long term, high resolution time series data from a cave in southwestern Virginia to examine spatial and temporal variability in hydrology and geochemistry of epikarst discharge (cave drips). These data address concerns on the significance of seasonal variability in the epikarst. We have combined the hydrologic and geochemical datasets to deduce a conceptual model of physical and chemical interactions in the epikarst over five hydrologic seasons (2008-2013). Results of this study can be extended to karst systems in other temperate climates where the infiltration into the epikarst and therefore processes in the epikarst are expected to be similar.

2.2 SITE DESCRIPTION

James Cave is located in Pulaski County, Virginia. The land use in the vicinity of the cave is agricultural pasture land. The region is in a temperate climate zone and experiences an approximate mean annual temperature of 11.4°C (The Southeast Regional Climate Center 2012). The county receives on average 38.91 inches of precipitation per year (The Southeast Regional Climate Center 2012).

The study region is located within the Valley and Ridge physiographic province. The Pulaski Fault system dominates the structural geology in this region. As described by Bartholomew (1987) the Pulaski Fault system is a series of Alleghanian thrust faults responsible for more than 100 km of westward displacement of the Pulaski thrust sheet over units as young as Mississippian age. James Cave formed within the carbonate Cambro-Ordovician age Conococheague formation. The proximity of secondary faults likely played a role in the development of this cave as well as current flow paths in the region. As shown in Figure 2.1, the cave is oriented parallel to a major fault which is also the contact between the Conococheague and Elbrook formations in the northeastern part of the county.

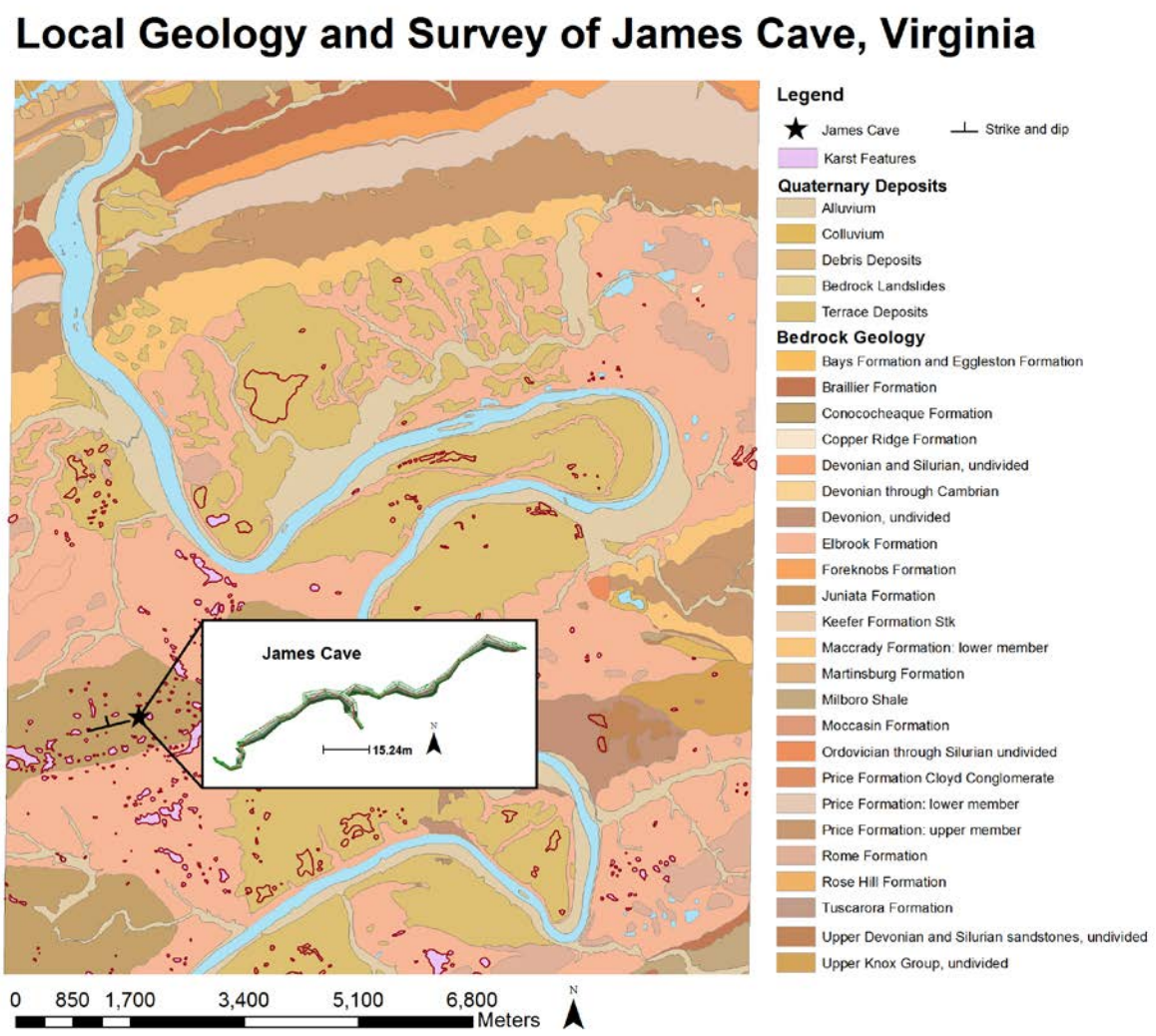

Figure 2.1. Geologic map of area surrounding James Cave. Geologic data from Schultz and Bartholomew (2009). Data for the cave survey (inset) collected by Tom Malabad.

The Conococheague formation has been described in this area as a fine-grained bluish-gray limestone (Hergenroder 1957). The Conococheague also contains thin laminations of argillaceous material, dolomite in varying proportions with the limestone, as well as shale and calcareous sandstone interbeds (Hergenroder 1957). The Elbrook is described as a thin-bedded to shaly dolomite that also contains dolomitic to pure calcareous limestone as well as some shale interbeds (Hergenroder 1957). The site of study is overlain by silt loam soils as well as carbonate regolith.

2.3 METHODS

2.3.1 Sampling Regime

Monitoring sites. James Cave is instrumented with monitoring stations at different depths. On the surface, there is a precipitation station and three tension lysimeters in the vadose zone, two of which are at the approximate surface projections of two of the drip sites and one of which is near the cave entrance, at the base of a sinkhole. In the subsurface, there are three sites instrumented to measure epikarst drips as well as two locations for cave stream monitoring. Locations of monitoring sites are shown in Figure 2.2.

Continuous monitoring. Continuous (10 minute interval) monitoring of cave drip rate and precipitation was conducted from late summer 2007 to winter 2013 using HOBO® tipping bucket rain gauges and multi-station data loggers. At the subsurface sites, drips were collected using tarps with areas of 2.43m^2, 3.07m^2, and 3.51m^2 for MS1, MS2, and MS3, respectively. Figure 2.3 shows the continuous monitoring set up for the drip sites. Precipitation was measured at the surface near the cave entrance. These data are supplemented with data from the nearby Kentland Farms (Virginia Agricultural Experiment Station 2012) during periods of equipment failure. Specific conductance of drip water was also measured from winter 2011 to winter 2013 using HOBO® conductivity loggers. Multi-point drift correction of the specific conductance was done via a linear adjustment in AQUARIUS Workstation (Aquatic Informatics 2011) and were based on field measurements conducted with an Oakton conductivity meter. Time-series data were imported, preprocessed, corrected for drift, and resampled, where necessary, with AQUARIUS Workstation (Aquatic Informatics 2011).

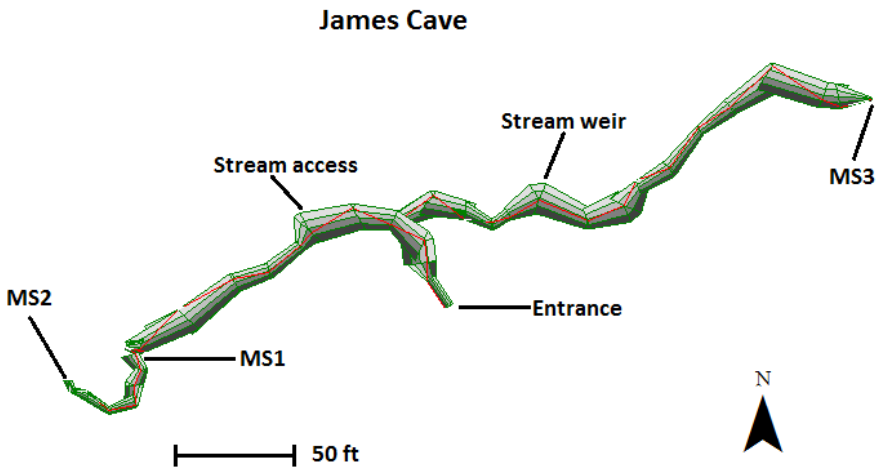

Figure 2.2. Survey of James Cave with monitoring stations. Survey produced courtesy of Tom Malabad). Highlighted in figure 1.6 is the section of study in relation to the full cave survey.

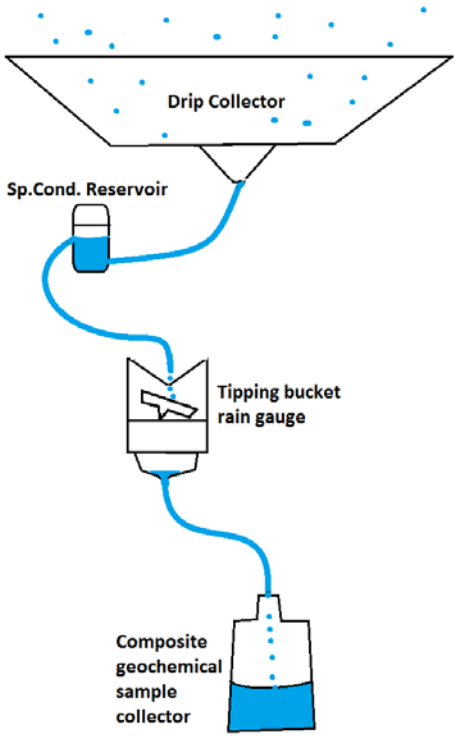

Figure 2.3. Instrumental set-up for drip monitoring and sampling. Specific conductance reservoir is ~ 300mL and the composite geochemical sample collector is ~ 1L.

Composite samples. In addition to continuous monitoring, discrete and integrated samples of precipitation, soil water and drip water were collected for geochemical analysis (major cations, anions, DOC, water isotopes, carbon isotopes). Soil water samples were collected from tension lysimeters by generation of a vacuum by attachment and suction from a hand pump. Cave drip waters were continuously collected over the month using composite sample containers (see Figure 2.3 above for the drip set up). Precipitation was also collected over the month using a composite sample container located near the rain gauge.

Soil samples. Soil samples were collected by William Joyce in November 2010 using a bucket auger. There were a total of eight soil cores done: two above MS1, three above MS2, and three above MS3. Soils were labeled based on horizons identified by W. Joyce and include horizons A and B from all sites, and C, D, and E observed at some sites.

Cave stream. The cave stream in James Cave was instrumented with a v-notch weir in January of 2011. At the time of weir construction two pressure transducers were deployed. A pressure transducer at the stream weir and a nearby barometric pressure transducer allow for the calculation of stream discharge. Barometric pressure and actual water level measurement corrections are applied and the corrected water level (in feet) is then used to determine the stream discharge based on the following equation from Grant and Dawson (2001) for 90 degree v-weirs where Q is the discharge in cubic feet per second and h is the corrected head in feet:

$$Q = 2.5 * h^{2.5} \quad (2.1)$$

In the fall of 2011, the cave stream was instrumented with a conductivity logger and grab samples were also collected monthly for geochemical analysis.

2.3.2 Laboratory Analysis of Geochemical Samples

After collection and upon arrival at the laboratory water samples were filtered to 0.22µm and aliquoted into the following subsamples:

1) cation analysis: samples were collected in 60 ml acid-washed HDPE bottles and acidified with HNO3;

2) anion analysis: samples were collected in 30 ml HDPE bottles without preservation;

3) pH and alkalinity analysis: samples were collected in 125 mL HDPE bottles.

Upon division, samples were stored at approximately 4^{o}C until analysis.

Filtered, non-chemically preserved samples were analyzed for major anions (Cl, NO_3, and SO_4) via Ion Chromatography (Dionex DX-120). Filtered, acidified samples were analyzed for cations (Al, Ca, K, Mg, Na, Si, and Sr) via Inductively Coupled Plasma Atomic Emission Spectrometry (Spectro ARCOS SOP). Alkalinity was measured using gran titration (Radtke, Wilde et al. 2012).

Soil samples were analyzed for water pH, buffer pH, extractable nutrients (P, K, Ca, Mg, Zn, Mn, Cu, Fe, B), soluble salts, organic matter content, and cation exchange capacity by the Virginia Tech Soil Testing Laboratory. Analytical methods for soil analysis are presented in Maguire and Heckendorn (2011).

2.3.3 NETPATH

Using the data from geochemical analysis of precipitation, soil water and drip water, a mass balance analysis was conducted using NETPATH-WIN modeling software (El-Kadi, Plummer et al. 2011). NETPATH is a code for modeling net geochemical reactions along a flow path. The NETPATH model was designed to consider the mixture of two waters, soil water and precipitation, then rock reaction in terms of dissolution and potentially precipitation. This mixing model is shown in figure 2.4.

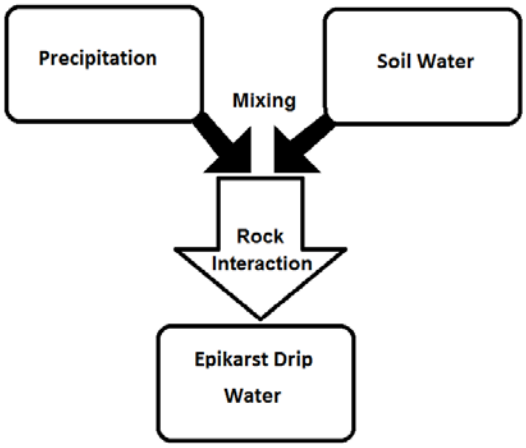

Figure 2.4. Geochemical mixing and interaction model.

The inputs for this model were the geometric mean concentrations of Ca, Mg, and Na for each site. The outputs of NETPATH are molar proportions of mixing based on an element and molar contributions from dissolution based on mineral stoichiometry. In the NETPATH model for this

project, Na was used as the element to determine mixing between soil water and precipitation and water-rock interaction with calcite and dolomite solid phases were based on Ca and Mg concentrations.

2.4 RESULTS

2.4.1 Soils

Results of the chemical analyses of soils reveal many similarities in pH, organic matter content, and selected extractable metals (Appendix C). The pH of the A horizon for all sampled sites is between 4.4 and 5.3 and increases with depth. The pH of the B horizon is consistently above pH 6 for all but one observation. The cation exchange capacity measured (3.0-9.8 meq/100g) is in the lower range observed in the USDA soil survey (3.0-22.0 meq/100g) and the organic matter content is higher at the soils above MS3 (5.5-6.6% in the A horizon) than observed by the USDA soil survey (0-3%) (USDA-NRCS 2010).

Despite some similarities, there are notable differences in soil chemistry between the sites. For example, concentrations of extractable Ca and P were similar in the soils above MS1 and MS2, but higher (statistically significant; α=0.10) in the soils above MS3. Figure 2.5 shows the concentration of several nutrients by site and soil horizon as well as significant differences. Results of the soil analyses can be found in Appendix C.

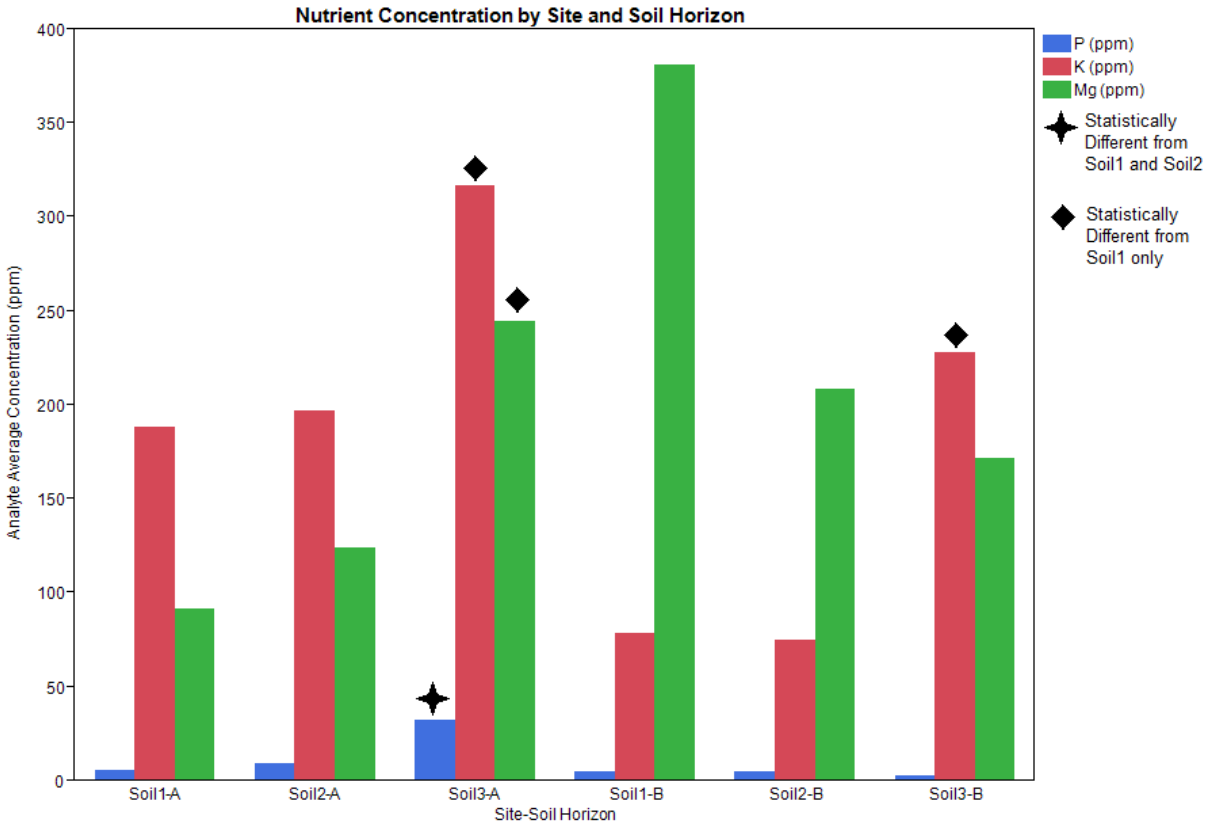

Figure 2.5. Soil concentrations of P, K and Mg by site and soil horizon. The location of Soil 1, Soil 2, and Soil 3 are at the approximate surface projections of drip sites MS1, MS2, and MS3, respectively. A and B refer to soil horizons.

2.4.2 Hydrology

Drips. Figure 2.6 shows an overview of the cave drip hydrographs through time from late 2007 to early 2013; additional figures are presented in Appendix D. As can be seen on Figure 2.6, breakthrough of the recharge season, defined as the time when significant drip rates commence, begins between November and January. The duration of the recharge period ranges from approximately three to six months. Table 2.1 summarizes the approximate details of the recharge season for the monitored time period (2007-2013).

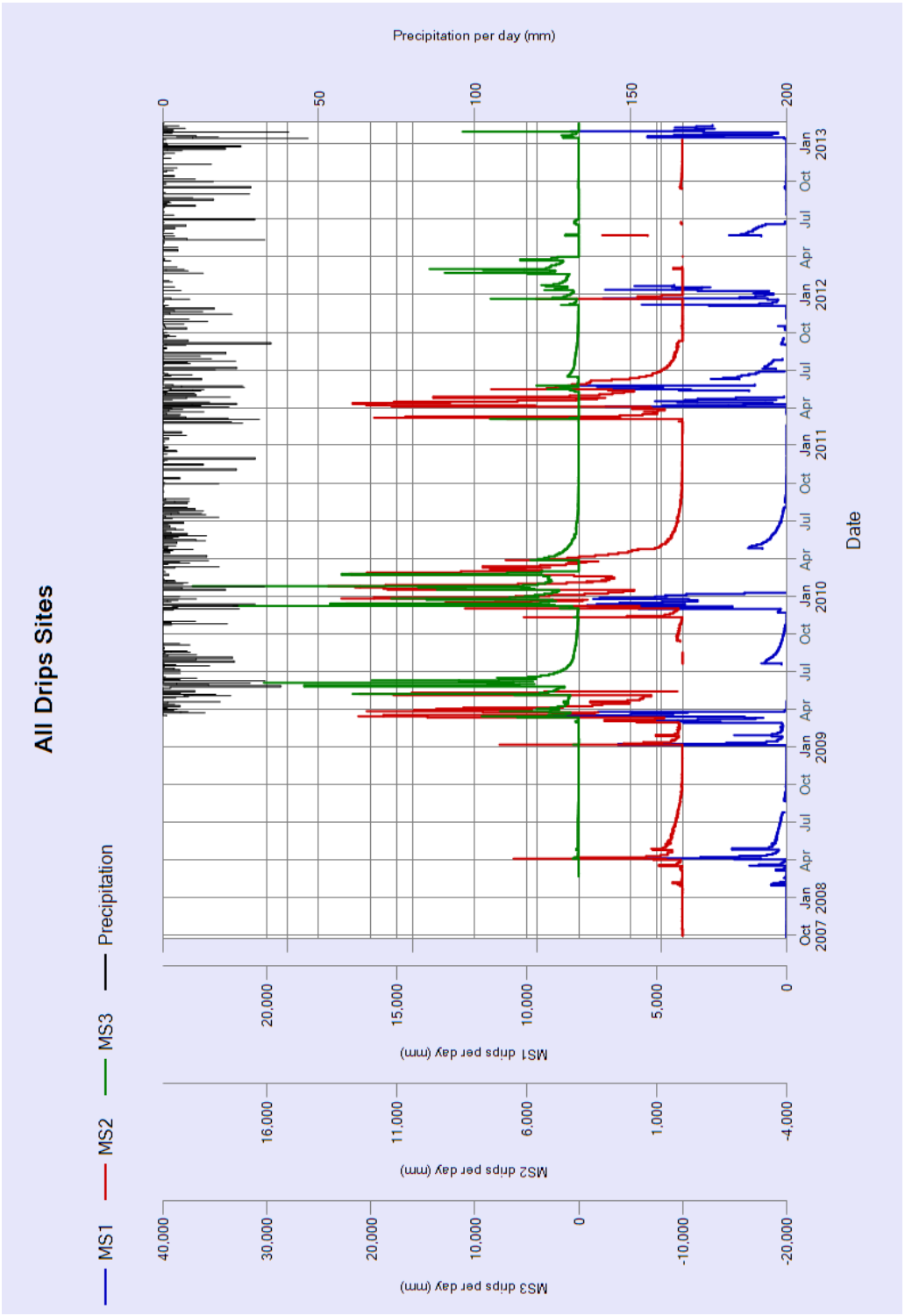

Figure 2.6. James Cave drip hydrographs between late 2007 and 2013. Note the offset scale of drip rates for the three sites—scales for MS1 and MS2 have the same magnitude, MS3 is a half scale. Missing drip periods indicate equipment failure. Precipitation data supplemented with data from Kentland Farms during times of rain gauge failure (Virginia Agricultural Experiment Station 2012).

Table 2.1. Summary of recharge timeline and maximum discharge based on cave drip data. "NA" is given for periods of equipment failure. Note that MS3 was not instrumented until Feb 2008 and thus the recharge start could not be determined for that year.

Drip Site	Recharge Start	Recharge End	Recharge Duration (months)	Maximum Discharge Observed (mm/day)
MS1	Feb 2008	May 2008	3	5000
MS2	Feb 2008	May 2008	3	7000
MS1	Jan 2009	NA	NA	10500
MS2	Jan 2009	NA	NA	12500
MS3	Mar 2009	June 2009	4	30000
MS1	NA	May 2009	NA	12300
MS2	Nov 2009	May 2010	5	13500
MS3	Nov 2009	May 2010	5	36000
MS1	NA	June 2011	NA	8000
MS2	Mar 2011	June 2011	4	13000
MS3	Mar 2011	June 2011	4	7000
MS1	Dec 2011	May 2012	6	7000
MS2	Dec 2011	NA	NA	5500
MS3	Dec 2011	NA	NA	14500
MS1	Jan 2013	NA	NA	8000
MS3	Jan 2013	NA	NA	11500

Overall, the beginning of the recharge season is generally the same for each of the drip sites, with the exception of MS3 in 2009. Based on the record, the beginning of the recharge season is the dominant predictor of the duration of the recharge season as there is notable similarity of the end of the recharge season (May or June) for each year observed.

Precipitation. Figure 2.7 shows the daily sum of precipitation for the recorded period at the James Cave monitoring site. The precipitation data do not show any strong seasonal component.

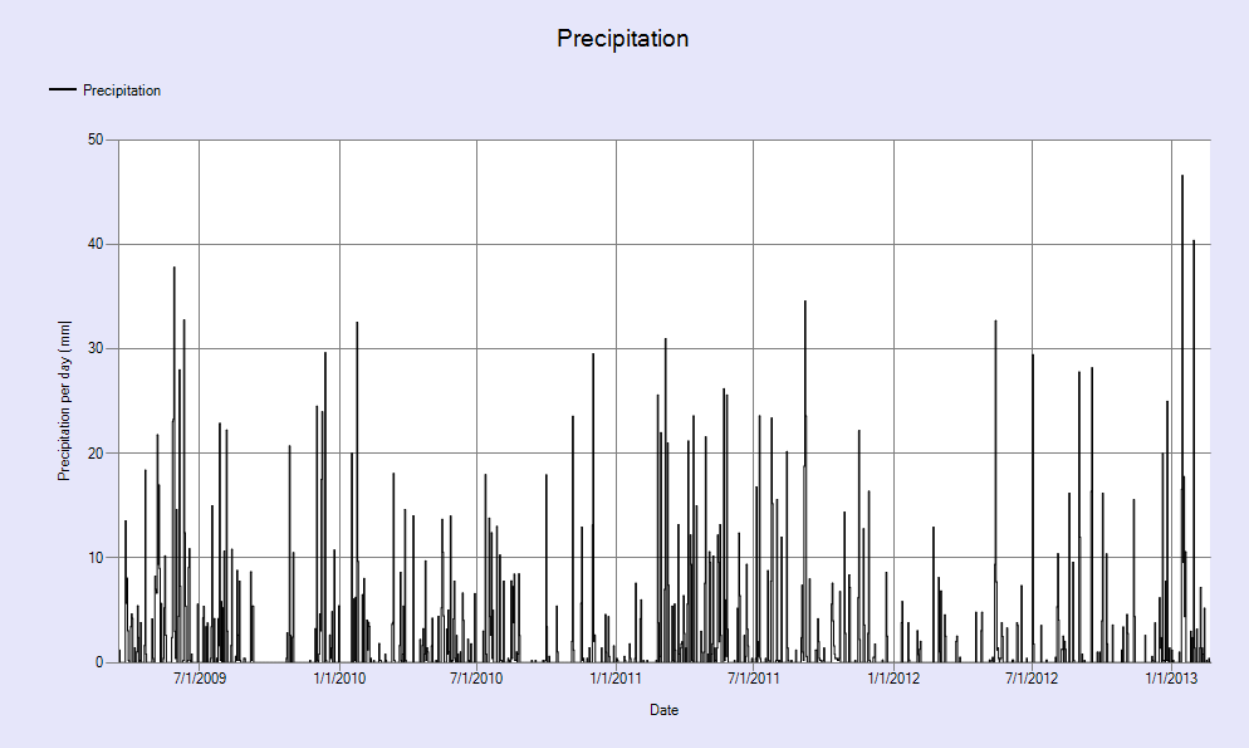

Figure 2.7. Daily precipitation totals from March 2009 to February 2013. Dataset supplemented with data from Kentland Farms from November 2011 through August 2012 (Virginia Agricultural Experiment Station 2012). The period of no precipitation in late 2009 is due to equipment failure.

2.4.3 Discrete/Composite Hydrogeochemistry

The discrete (soil water, stream) and composite (drips, precipitation) geochemical samples at the James Cave monitoring site were collected based on availability and analyzed based on volume and priority. As such, some locations have more numerous observations and some analytes are analyzed more frequently than others. Of the samples discussed in this thesis 94% of the collected cave water (drips and cave stream) samples have a charge balance error of 20% or less. Tabular data for discrete and composite samples are presented in Appendix E.

Concentrations of several analytes (Ca, Sr, HCO_3) increase along the flow path (from precipitation to soil water to drip water), as shown in figure 2.8. For Na and SO_4, the concentration patterns show analyte enrichment from precipitation water to soil water and then dilution from soil water to drip water. The boxplot for sodium is shown in figure 2.8 and the boxplot for sulfate and other analytes are in Appendix F.

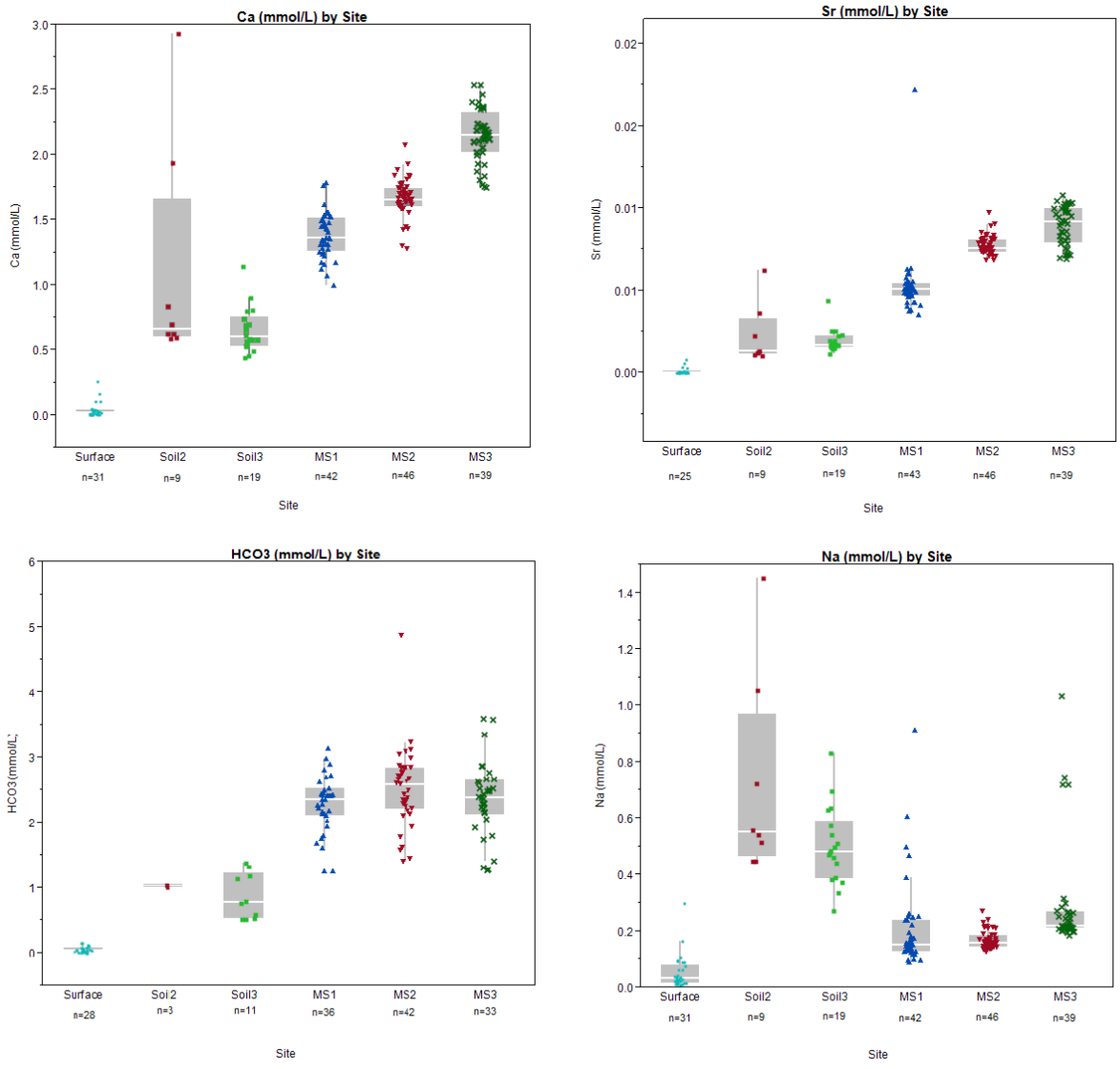

Figure 2.8. Boxplots of Ca, Sr, HCO_3, and Na. Soil2 and Soil3 are soil water samples.

In addition to variation in the concentrations of analytes by sampling horizon, there are also differences of concentrations through time. For Ca, there is a pattern of seasonal variability, as shown in figure 2.9, particularly at MS3. For other analytes, such as Si, concentrations do not appears to have a predictable temporal pattern. Additional figures depicting the analyte concentration by site and through time can be found in Appendix G.

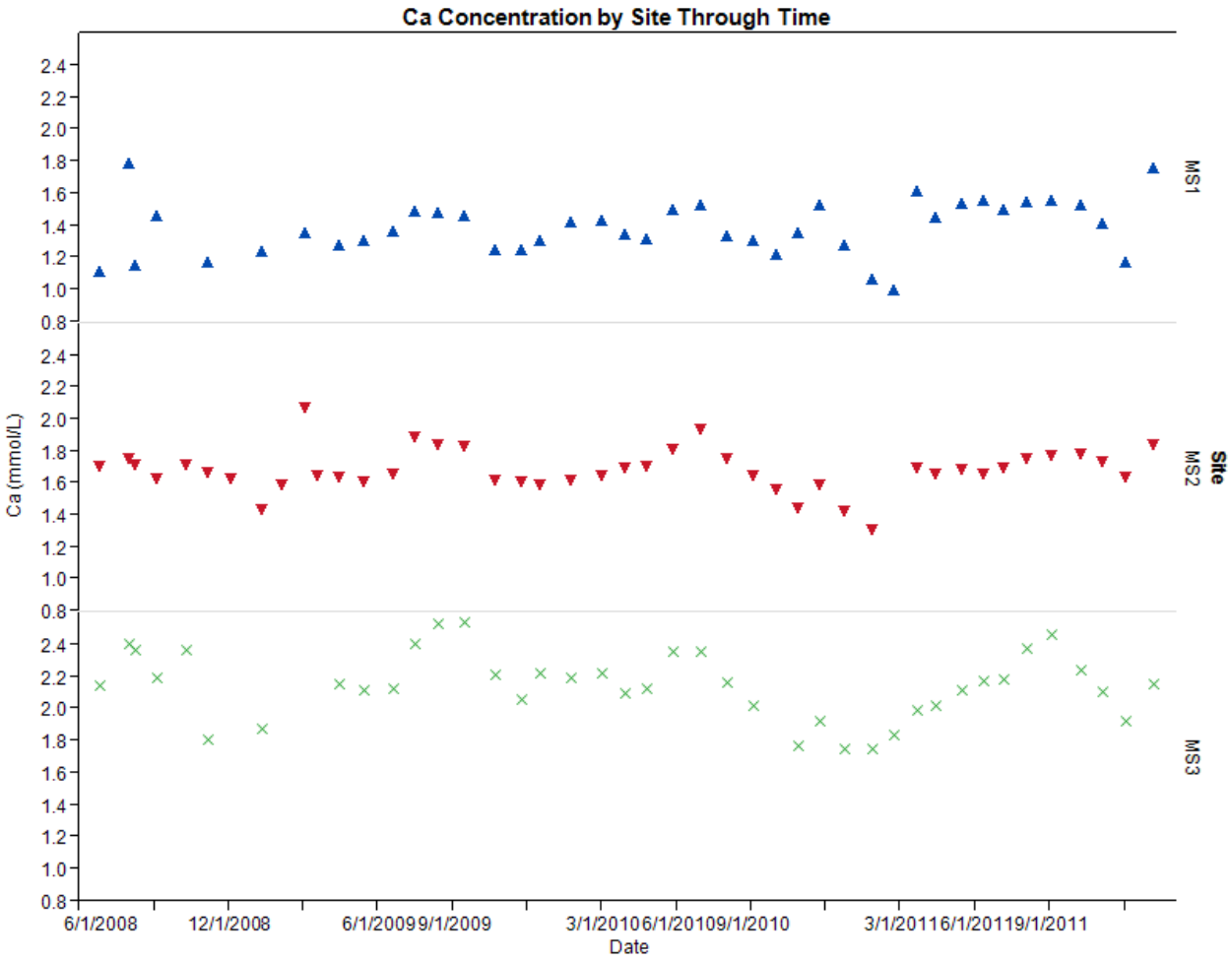

Figure 2.9. Concentration of calcium (mM) for the drip sites over time.

Interesting patterns of correlation are also found between analytes. Figure 2.10 shows a graph of the Mg concentration versus the Ca concentration of precipitation, soil water, drip water, and the cave stream. The biplot indicates the distinct differences between the sampling horizons and due the differences between the slope of the regression lines suggests that Mg and/or Ca have more than one source. Figure 2.11 shows significant correlation between strontium and calcium. As observed in figures 2.10 and 2.11, the drips show proportional trends between Ca and Mg and Ca and Sr, indicating similar ratios in the carbonate rock.

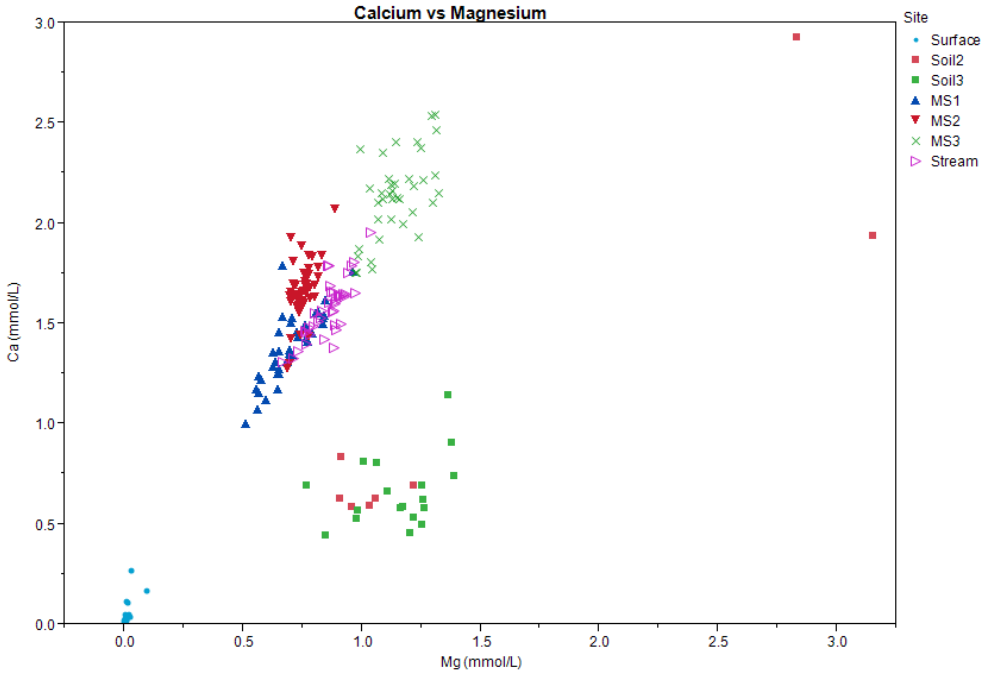

Figure 2.10. Magnesium versus calcium concentration by site. Slope of regression line for drips reveals a Ca:Mg ratio of 1.5, r-squared= 0.79; slope of the regression line for precipitation and soil water reveals a Ca:Mg ratio of 0.67, r-squared=0.87.

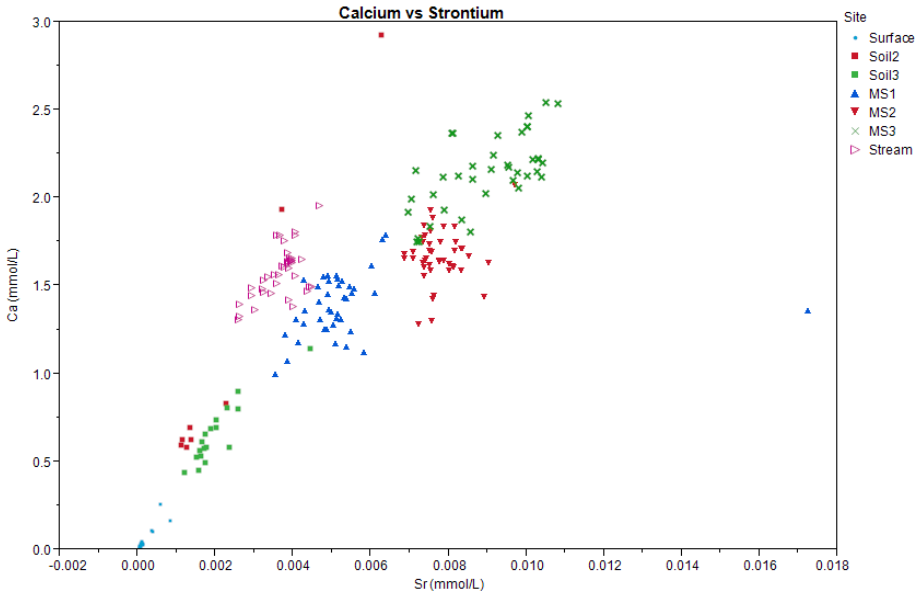

Figure 2.11. Strontium versus calcium concentration by site. Slope of regression line for drips reveals a Ca:Sr ratio of 124.3, r-squared=0.50.

More graphs are presented in Appendix H, which contains a scatterplot matrix of Ca, K, Mg, Na, Si, Sr, Cl, NO_3, SO_4, and HCO_3.

Figure 2.12 shows the geometric mean concentrations of the major ions. Geometric mean was used because the data best fit a log normal distribution. There are differences in mean concentrations between the sites and between sampling horizons along the flow path—from precipitation to soil water to cave drip to cave stream. The figure is divided into four groups (A, B, C, and D). Group A includes analytes which increase over the flow path (Ca, Sr, and HCO_3). Group B includes analytes which undergo enrichment from precipitation to soil water, but dilution from soil water to drip water (Na and SO_4). Group C includes analytes which are more similar by site than horizon (Cl and NO_3); in other words, the concentration of nitrate at MS3 is more similar to soil 3 than any other sample, just as the concentration of nitrate at MS2 is most similar to soil 2. Group D includes the analytes K, Mg, and Si, which have more complex geochemistry and/or multiple sources or sinks.

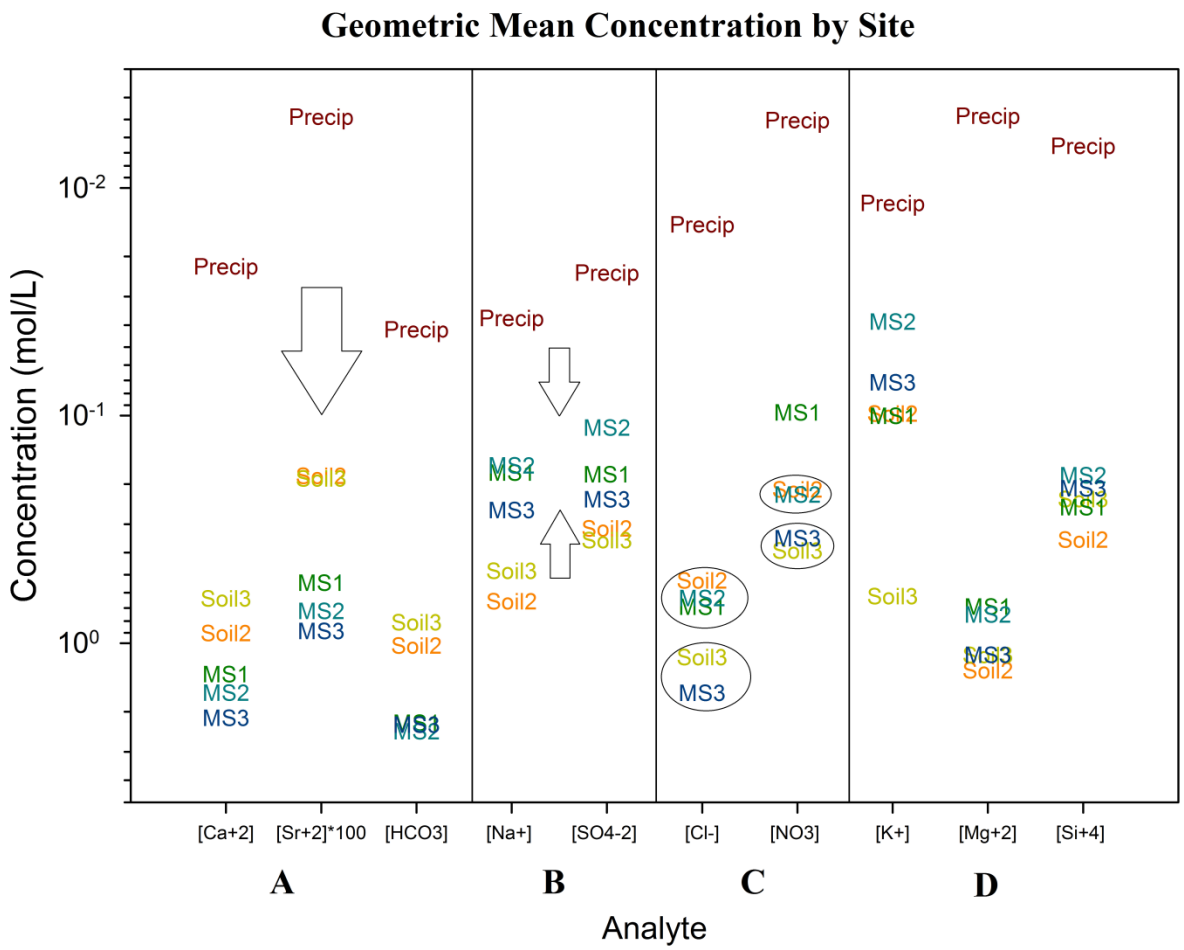

Figure 2.12. Geometric mean concentrations of selected analytes by site. Note the reverse order of concentration on the y axis. A shows the analytes whose concentrations increase over the flow path; B shows the analyte which are enriched in the soil water, then diluted in the drip water; C shows the analytes that have more similarity by site (soil water similar to drip water); D shows the analytes that have more complex geochemistry or that have multiple sources in this system.

2.4.4 Time Series of Specific Conductance

Time series data of specific conductance from January 2011 until February 2013 are shown in Figure 2.13.

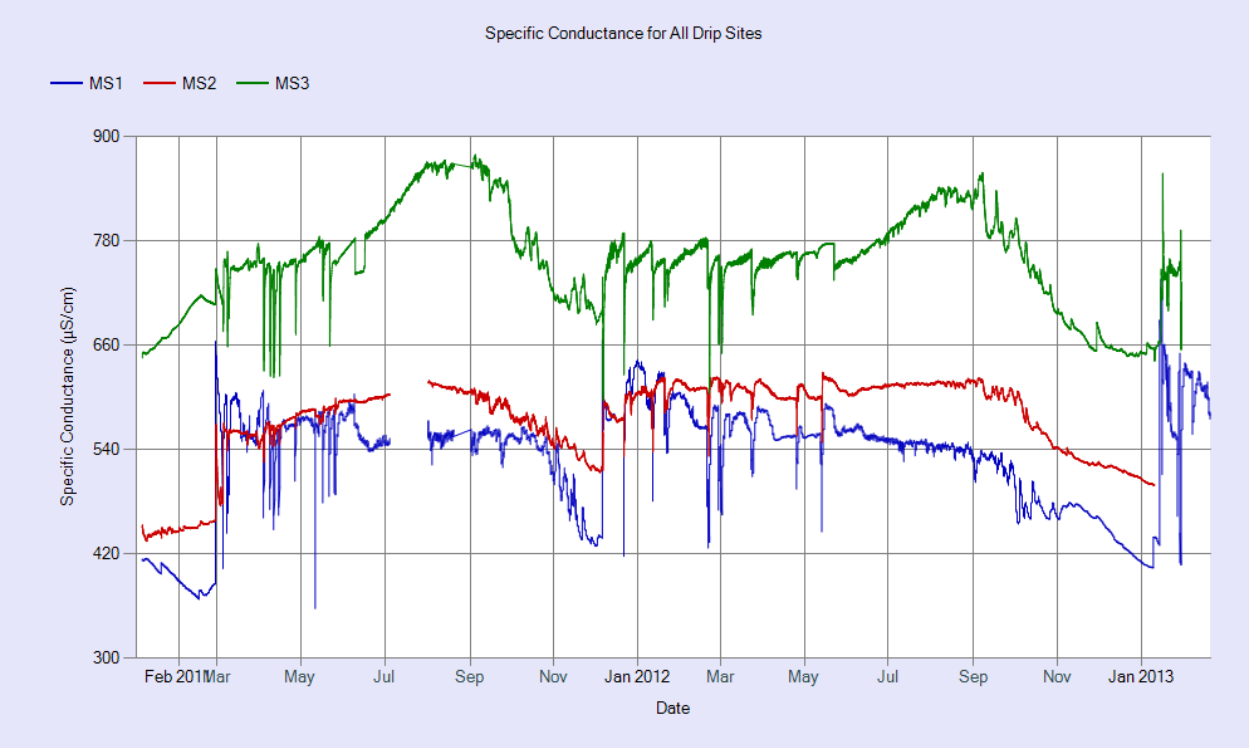

Figure 2.13. Specific conductance for each drip site. Note period of missing data in summer 2011.

Figure 2.13 shows significant variation in specific conductance over the period of record with short term perturbations and longer term (multiple month) trends. MS3 has consistently higher conductivity while MS1 and MS2 generally have similar and lower conductivity values. Worth noting is the decline in conductivity in the Fall of both 2011 and 2012 as well as the increase (more prominent at MS3) from Spring to Summer.

Figure 2.14 shows the response in specific conductance to initiation of the recharge season and high flow events at MS3. At the beginning of drips (Dec 2011) there is a small but measurable increase in conductivity, followed by a sudden drop, then gradual increase. For subsequent fluxes in drip discharge, only the sudden drop in conductivity and gradual increase are observed. MS1 and MS2 show similar responses to flow influx.

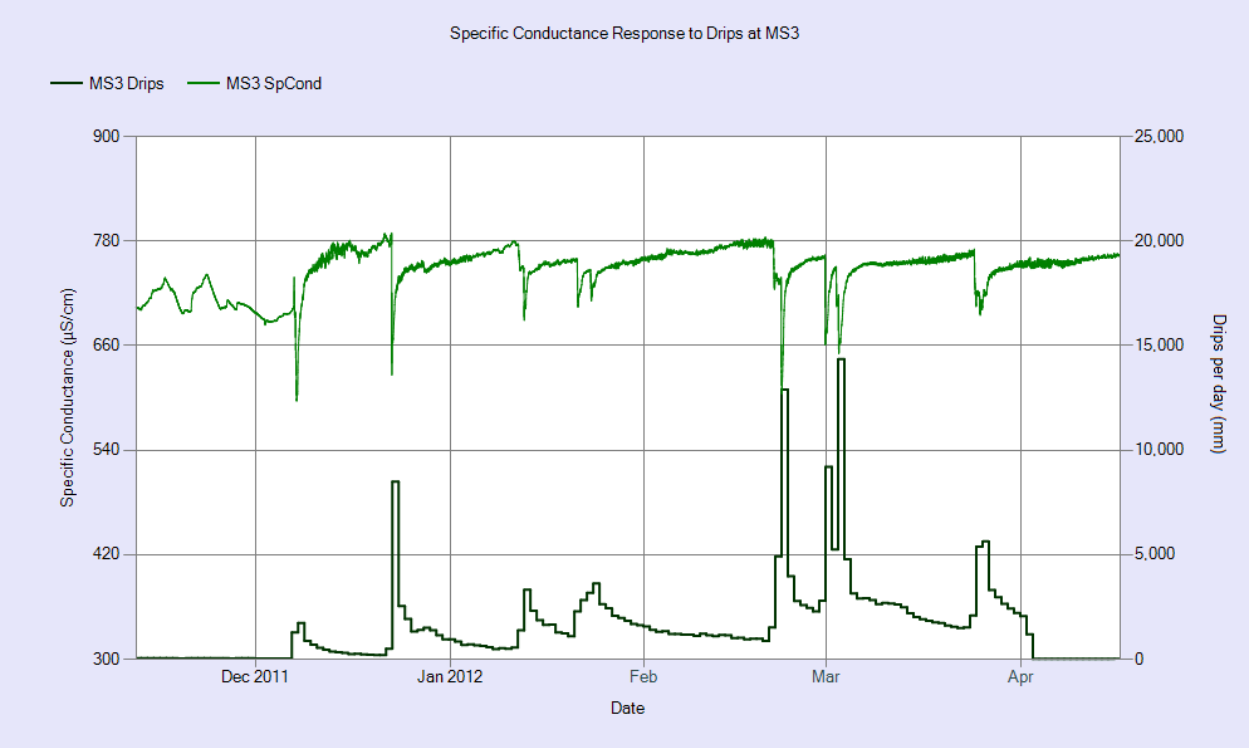

Figure 2.14. Specific conductance response to drips at MS3 from Nov 2011 to April 2012

2.4.5 Mass Balance Calculations

In the NETPATH model, Na was used as the element to determine mixing between soil water and precipitation and calcite and dolomite were the solid phases available for water-rock interaction. The output of NETPATH includes the molar proportions of end-member mixing and molar contributions from dissolution based on mineral stoichiometry. Soil waters were selected based on their spatial proximity to the drip site of interest; i.e. soil 2 water was mixed with precipitation to create MS1 and MS2 water, and soil 3 water was mixed with precipitation to create MS3 water. Precipitation was chosen to represent as the dilute water component which mixes with soil water prior to rock interaction. Table 2.2 outlines the output of NETPATH for each drip site.

Table 2.2. NETPATH-predicted mixing proportions of precipitation and soil water and the extent of dissolution of calcite and dolomite to create drip water chemistry at MS1, MS2 and MS3.

Drip site	Proportion Precipitation	Proportion Soil Water	Millimoles Calcite Dissolution	Millimoles Dolomite Dissolution
MS1	0.73	0.27	0.78	0.33
MS2	0.75	0.25	0.99	0.41
MS3	0.46	0.54	1.26	0.52

As can be seen in the NETPATH results, MS1 and MS2 are similar in terms of mineral dissolution and mixing proportions, while MS3 shows differences in both mixing and mineral dissolution. The mixing model proportions were used in conjunction with the geometric means of various analytes to back calculate the concentration of the drip site based on the concentration of precipitation and soil water. The mixing model best predicts the concentration of SO_4; the predicted concentrations are less than 20% different for MS2 and MS3. The mixing model does not predict well for MS1 likely due to the lack of a soil water sample at the surface projection for that specific site.

2.4.6 Cave Stream

Despite the limited record of observations for discharge at the cave stream, two hydrologic years are observed in figure 2.15. Similar to the drip hydrologic record, the stream exhibits periods of high flow, recession, and base flow. However, in contrast to the drip hydrologic record, the recession periods are more frequent and may be observed following each high flow event in early 2011.

The specific conductance record is also limited at the cave stream site, however, the relationship between discharge rate and conductivity observed in the cave drips may also be seen in the cave stream conductivity record as shown in figure 2.16 where an increase in the discharge overlaps with a sudden decrease in conductivity.

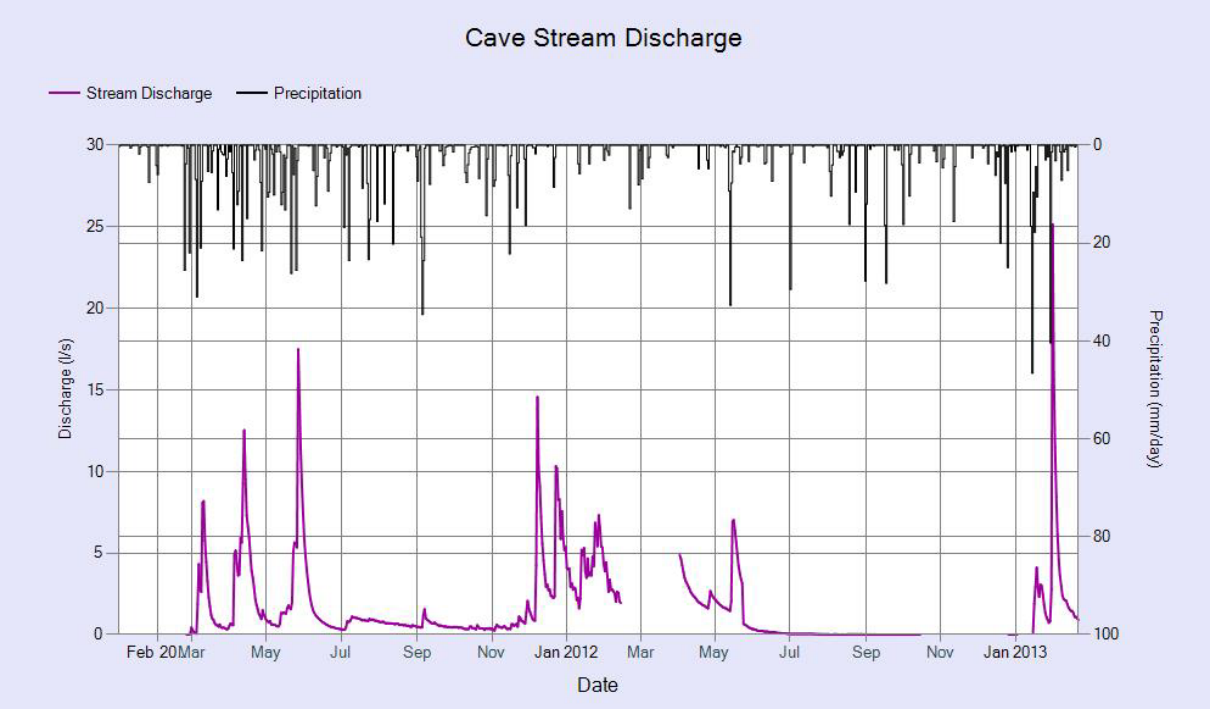

Figure 2.15. Daily average cave stream discharge and precipitation. The lack of discharge data during early 2012 is due to equipment failure. Precipitation data have been supplemented with data from Kentland Farms (Virginia Agricultural Experiment Station 2012).

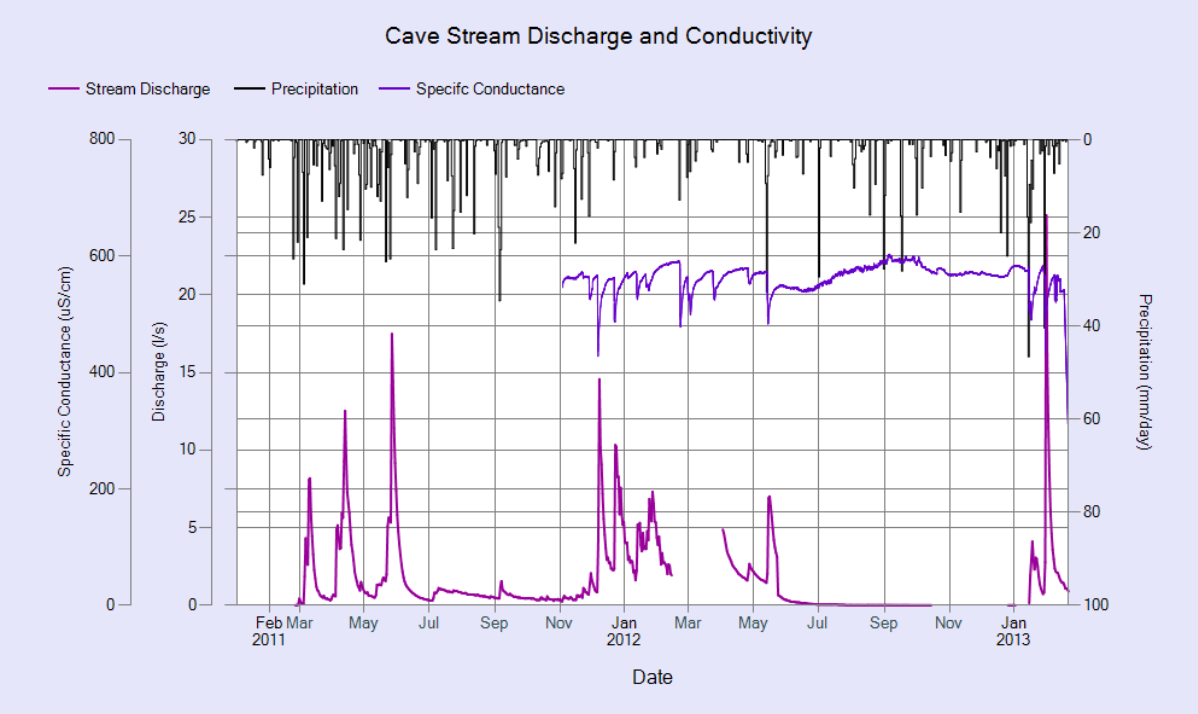

Figure 2.16. Cave stream specific conductance, discharge, and surface precipitation. Precipitation data have been supplemented with data from Kentland Farms (Virginia Agricultural Experiment Station 2012).

Geochemical data and figures for the cave stream are included in Appendices E, F, G and H. The Sr and Ca relationship in the cave stream water is different than what is observed in the cave drips. The fact that the cave stream falls on a regression line with the soils rather than the cave drips may indicate a greater influence of soil water in the overall cave stream geochemistry, but further analysis is needed to support that interpretation.

2.5 DISCUSSION

2.5.1 Temporal and Spatial Patterns of the Hydrologic Record

The hydrologic record can be divided into seasons based on the hydrographs from figure 2.6 and Appendix D. The predominant divisions in the hydrologic record are as follows: 1) a recharge period which is characterized by high drip rates and marked response to precipitation events; 2) a recession period showing the transition between the recharge period and low flow which typically has the characteristic pattern of a recession curve; and 3) a low flow period during which there is virtually no response to precipitation events and the flow rate is at a minimum. Figure 2.17 shows the full hydrographic record for the James Cave site with the hydrologic divisions marked on the x-axis.

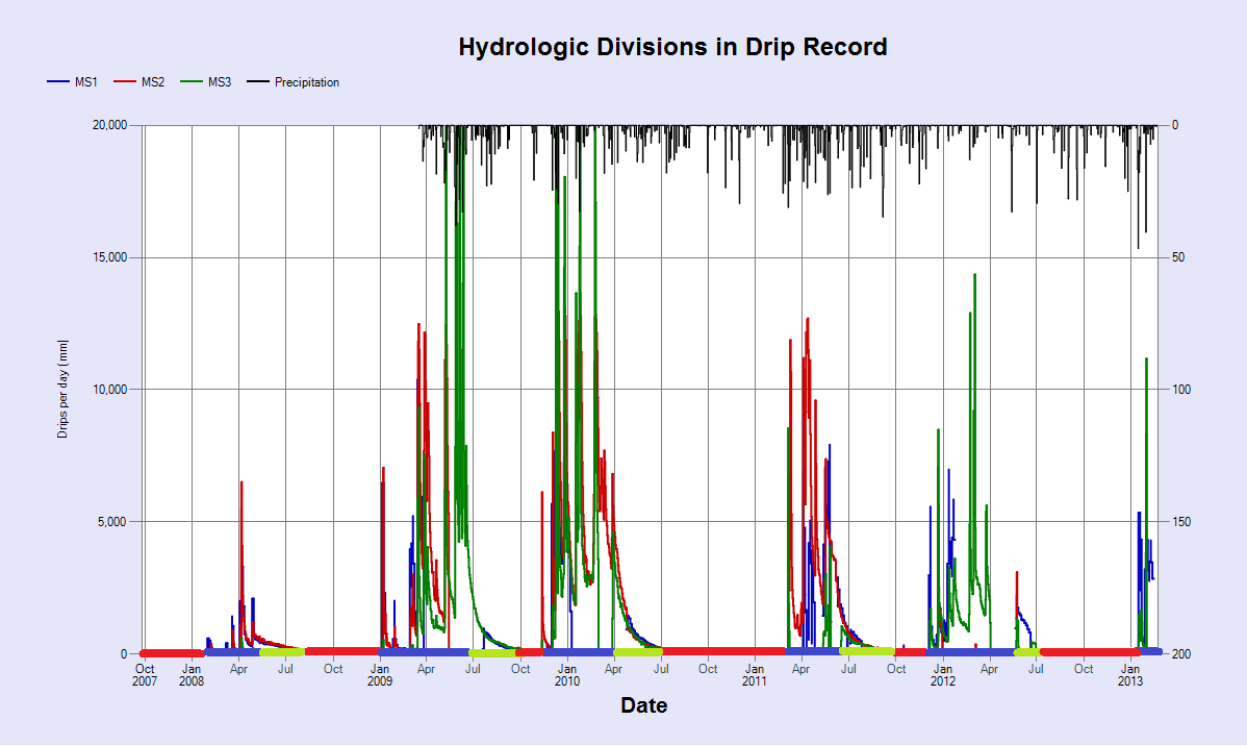

Figure 2.17. Hydrologic divisions in the drip record indicated by color coding on the x-axis. Red indicates low flow, blue indicates recharge, and green indicates the recession period. The precipitation record begins in March 2009. Missing data indicate periods of instrument failure. Although it appears that MS3 has higher drip rate than MS1 and MS2, this observation is obscured by the different areas of the collection tarps. Normalize to the tarp area, the sites have similar discharge rates.

Temporal variations in cave drip rates are well documented in the literature (Baker, Genty et al. 2000; Fairchild, Borsato et al. 2000; Perrin, Jeannin et al. 2003; Sheffer, Cohen et al. 2011). For this study, the hydrologic divisions (recharge, recession, and baseflow) are functional definitions used to characterize seasonality of recharge through the epikarst rather than how these seasons relate to speleothem growth, for example.

2.5.2. Temporal and Spatial Patterns of the Geochemical Record

Results from this study document spatial variability in geochemistry between drip sites as well as between different sampling horizons (i.e. surface, soil water, drips). For all analytes the most notable change in geochemistry along the flow path is the increase in concentration from precipitation water to soil water. Analytes attributed to rock-water interaction (i.e. Ca, Sr) and soil mineral constituents (i.e. Na, K), as well as anthropogenic inputs (i.e. NO_3) all increase in

concentration. From the soil water horizon to the drip water, there is further enrichment of rock derived analytes and dilution of some, but not all, extractable soil nutrients (i.e Na, K) and human-sourced analytes (i.e. NO_3).

Drip sites MS1 and MS2 are more consistent in their chemical constituents and are typically more dilute with respect to nearly all analytes than drip site MS3. Of particular importance, MS3 has the highest specific conductance during all seasons and the highest NO_3— an indicator of direct surficial connection. However, as this study focuses on the overall seasonal trends, the geochemistry at these sites will be considered collectively rather than individually for the remainder of this discussion due to their similar temporal trends.

All three drip water sites show temporal variations but not consistent trends in concentration with respect to several analytes including NO_3, Na, K, and SO_4—generally those components attributed to surface and soil water influence. Magnesium also does not show marked seasonality as compared to trends observed in Baldini, McDermott et al. (2012) where a seasonality was observed in Mg concentration in their period of study. However, as shown in the soil water samples there are multiple sources of Mg in this study system inferred from enrichment from precipitation water to soil water and again from soil water to drip water. In contrast, Ca concentrations as well as specific conductance, which can be seen in figures 2.9 and 2.13, respectively, both show seasonal oscillations at each site. The highest concentrations of Ca are observed in the late summer (August-September) and the lowest concentrations are observed in late fall and early winter (November-January). For the specific conductance record, as shown in figure 2.18, three periods may be identified: 1) period A, January through May, a time when the conductivity is the most variable and has sharp decreases and recover; 2) period B, May through August, characterized by a steady increase or leveling off of conductivity; and 3) period C, September to January, characterized by a gradual and consistent decrease in conductivity.

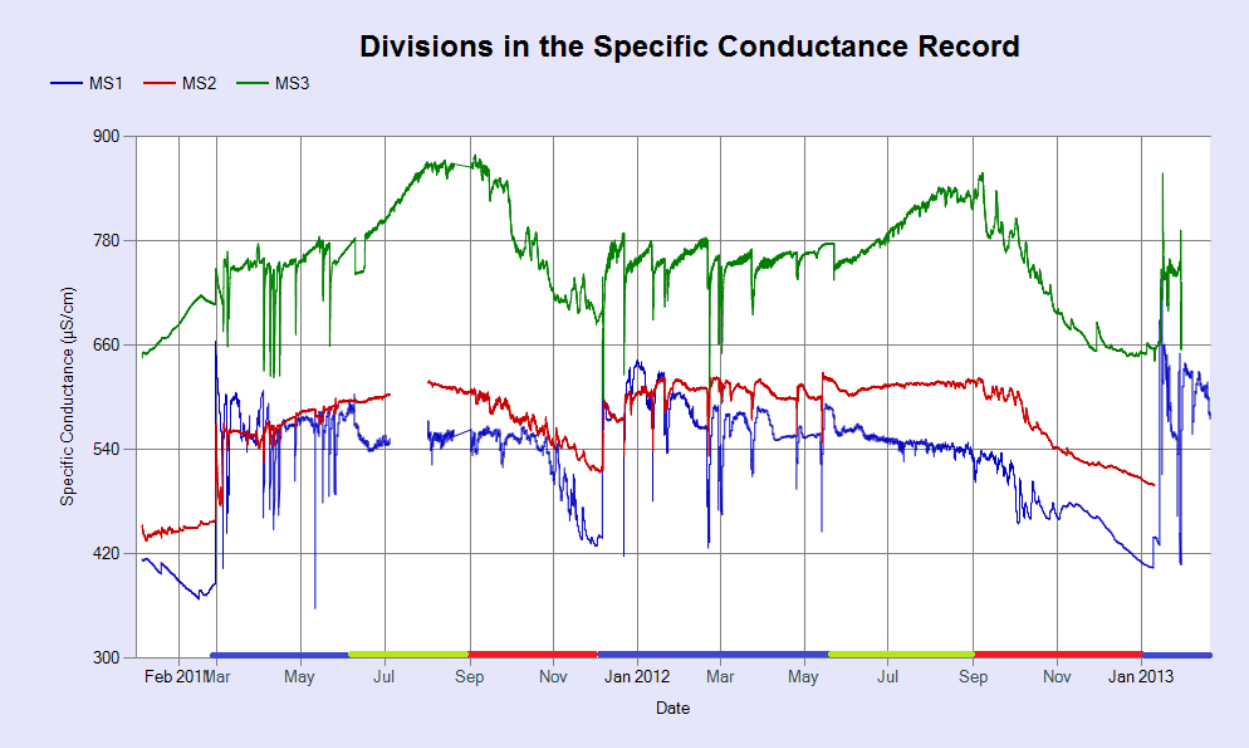

Figure 2.18. Divisions in the specific conductance record indicated by color coding on the x-axis. Blue indicates period A, green indicates period B, and red indicates period C.

Previous studies have also observed variation in conductivity in cave drip waters; however in these previous studies the period of record has either only covered a single hydrologic season (Baker, Genty et al. 2000) or does not have the resolution necessary to observe the rapid conductivity response to drips during high flow (Genty and Deflandre 1998). The two long term trends (period B and period C) in the specific conductance record are observed in the Ca concentration record: Ca concentration increases with specific conductance (period B) followed by Ca concentration decrease with specific conductance (period C). Period A is not observed in the Ca concentration record; this is likely due to the composite sampling method which loses the high resolution variation in period A of the conductivity record.

2.5.3 Composite Hydrogeochemical Model

Comparison of the records for the hydrologic and geochemical data show that the large-scale divisions overlap. Figure 2.19 shows the conductivity for all sites, the combination of drips for all sites, and the precipitation record for the period.

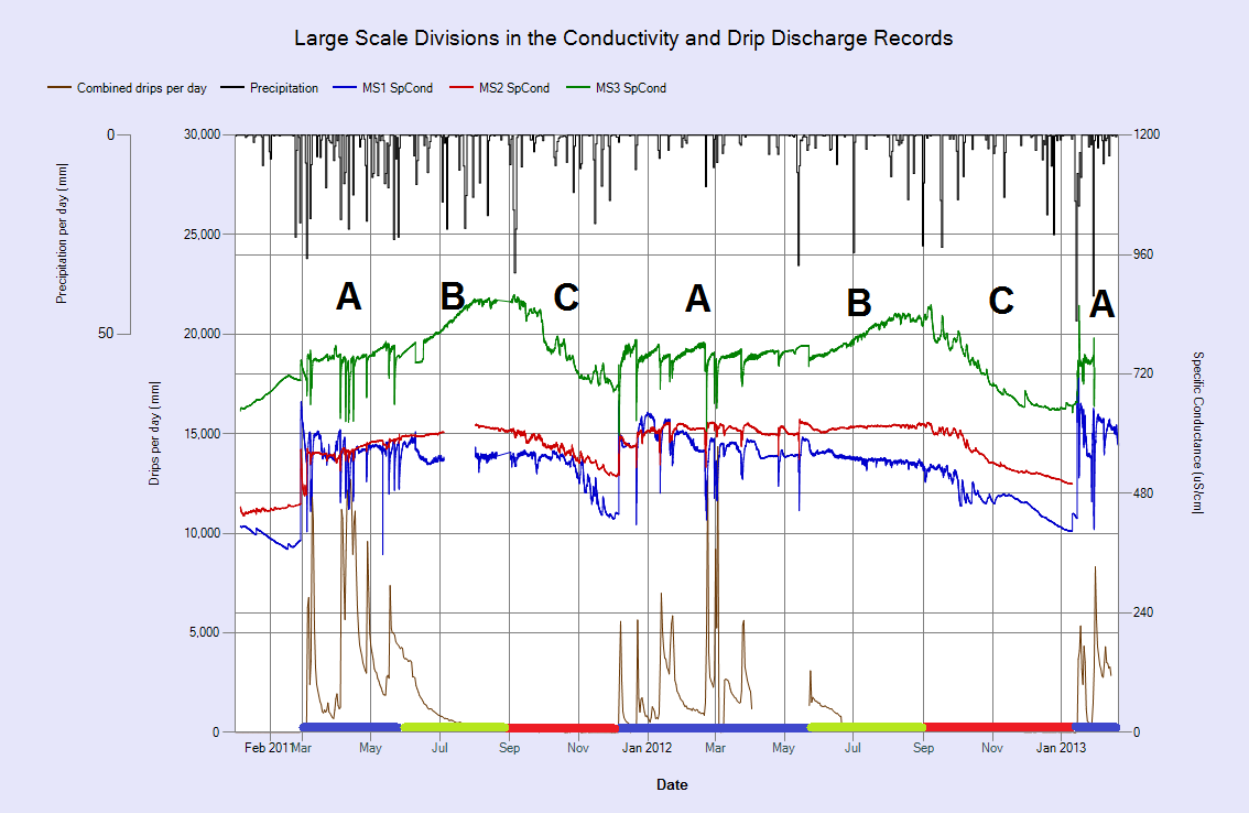

Figure 2.19. Large scale divisions in the conductivity and drip discharge records indicated by color coding on the x-axis. Colors indicate the division in the time series record: 1) blue indicates the hydrologic recharge season and the conductivity period A; 2) green indicates the hydrologic recession period and the conductivity period B; and 3) red indicates the hydrologic low flow period and conductivity period C.

As shown in figure 2.19, conductivity period A overlaps with the hydrologic recharge season. During the recharge season, sudden increases in drips are correlated with sudden decreases in conductivity, suggesting a rapid influx of dilute water. For conductivity period B, the gradual increase in conductivity coincides with the hydrologic recession period, indicative of more rock-water interaction. During conductivity period C, the gradual decline of conductivity coincides with the lowest flow period in the hydrologic record, indicating that although the duration of rock-water interaction is high, the further dissolution of rock is not observed.

A close up of the recharge season and conductivity period A from Winter 2011/2012 is shown in figure 2.20. This figure shows the relationship between the sudden decreases in conductivity and the increased drip discharge and the spike in conductivity at the onset of the recharge season—approximately on December 10, 2011. Sudden responses in conductivity to

drip events are only observed in the recharge period and are not observed during recession or low flow (see figure 2.19).

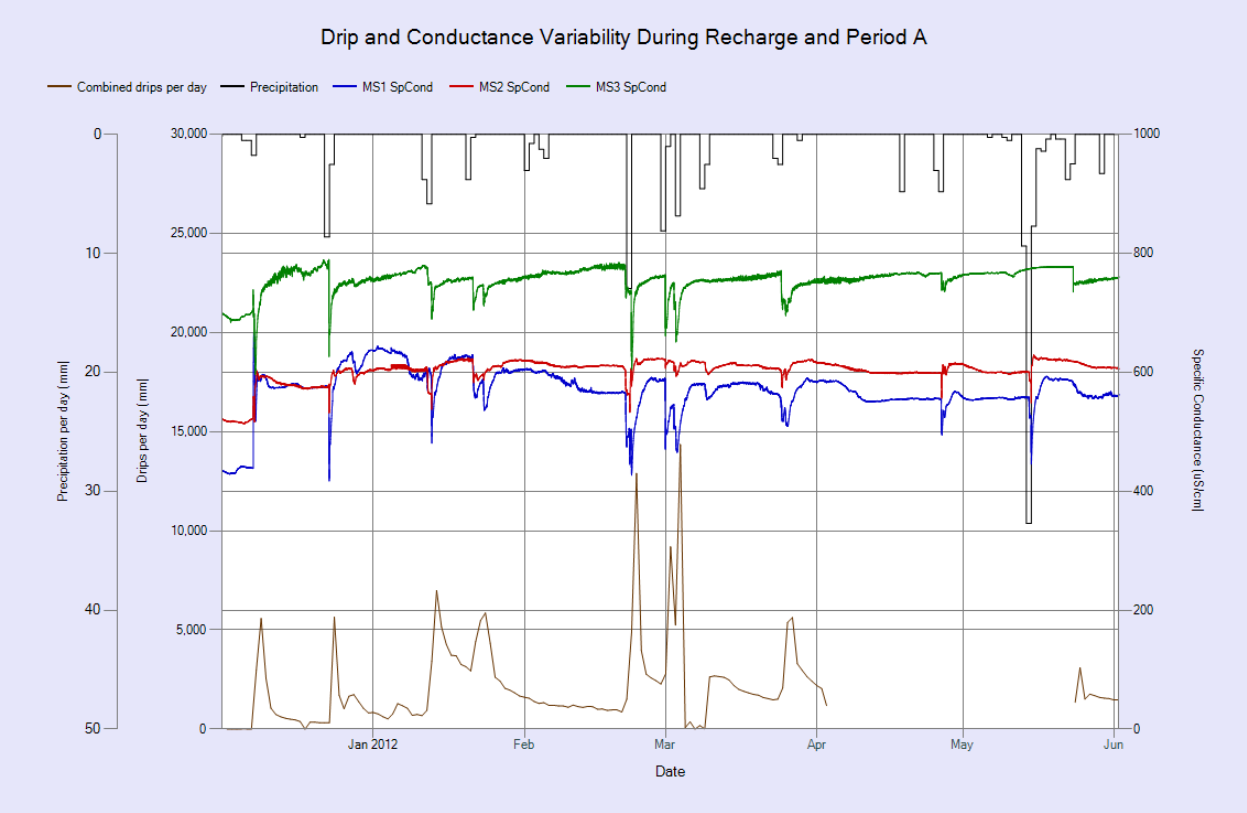

Figure 2.20. Drip and conductance variability during recharge and conductivity period A.

The conductivity pattern observed during the recharge season can be explained by two processes. First, the sudden decline in response to a drip and precipitation event can be explained by rapid infiltration of precipitation which increases the precipitation contribution and causing overall geochemical dilution. This interpretation is supported by results of the mixing model, which suggest that drip water geochemistry can be explained by mixing of precipitation and soil water with subsequent water-rock interaction. Our mixing model is further supported by Tooth and Fairchild (2003) in that rapid macropore and epikarst piston flow allow for dilute water to bypass storage as demonstrated in their plumbing model. Second, we saw sharp increases of conductivity at the onset of the recharge season and after the sudden decline for each drip and precipitation event. A similar pattern was reported by Genty and Deflandre (1998) with the explanation of highly mineralized water being flushed out due to hydraulic pressure. Genty

and Deflandre (1998) also noted a similar pattern of increased conductivity associated with recharge, however, they observed that the conductivity remains elevated during the recharge season, in contrast to this study, where the conductivity increase occurs at the outset of the recharge season but is followed by rapid decreases in conductivity.

Elucidation of the cause of the sudden, seasonal influence of dilute water during the recharge season along with the occasional influx of more mineralized water requires additional consideration of conductivity periods B and C. Conductivity period B coincides with both the hydrologic recession period as well as the regional climatic summer. During summer evapotranspiration is highest, which removes most precipitation before it can infiltrate into the soil. However, deep soil water above the epikarst surface is expected to remain due to limited root penetration. This deep soil water can slowly drain from the soil into the epikarst, generating cave drips, even in summer. The pattern of increasing conductivity during this recession period is related to water-rock interaction. During summer increased biological activity will produce higher CO_2 partial pressures of at depth (Yang, Liu et al. 2012) and therefore increase calcite dissolution. This increased pCO_2 results in higher concentrations of Ca, Sr, and HCO_3, solutes associated with calcite dissolution, and a higher specific conductance of drip water.

For conductivity period C in the Fall, the gradual decline in conductivity coincides with the drastically reduced drip rate—a relationship also observed by Genty and Deflandre (1998). These patterns can be explained by prior calcite precipitation. Prior calcite precipitation is the loss of calcite components (Ca, HCO_3, CO_3, or alkalinity) prior to the sampling location (i.e. in the epikarst) due to changes in the local environment impacting the solubility of calcite. Indicators of prior calcite precipitation include ratios of analytes which indicate preferential precipitation in agreement with partitioning coefficients. For example, there is a specific Sr/Ca ratio in solution that reflects the Sr/Ca ratio of the dissolving rock. When prior calcite precipitation occurs, the ratio of Sr/Ca in drip waters will increase due to the preferential incorporation of Ca in precipitated calcite relative to Sr (Curti 1999). Figure 2.21 demonstrates that as the concentration of Ca in drip water decreases, the water becomes more enriched with Sr relative to Ca. Previous literature supports the use of Sr/Ca to infer prior calcite precipitation and has also been observed in cave drip waters (Fairchild, Borsato et al. 2000; Tooth and Fairchild 2003).

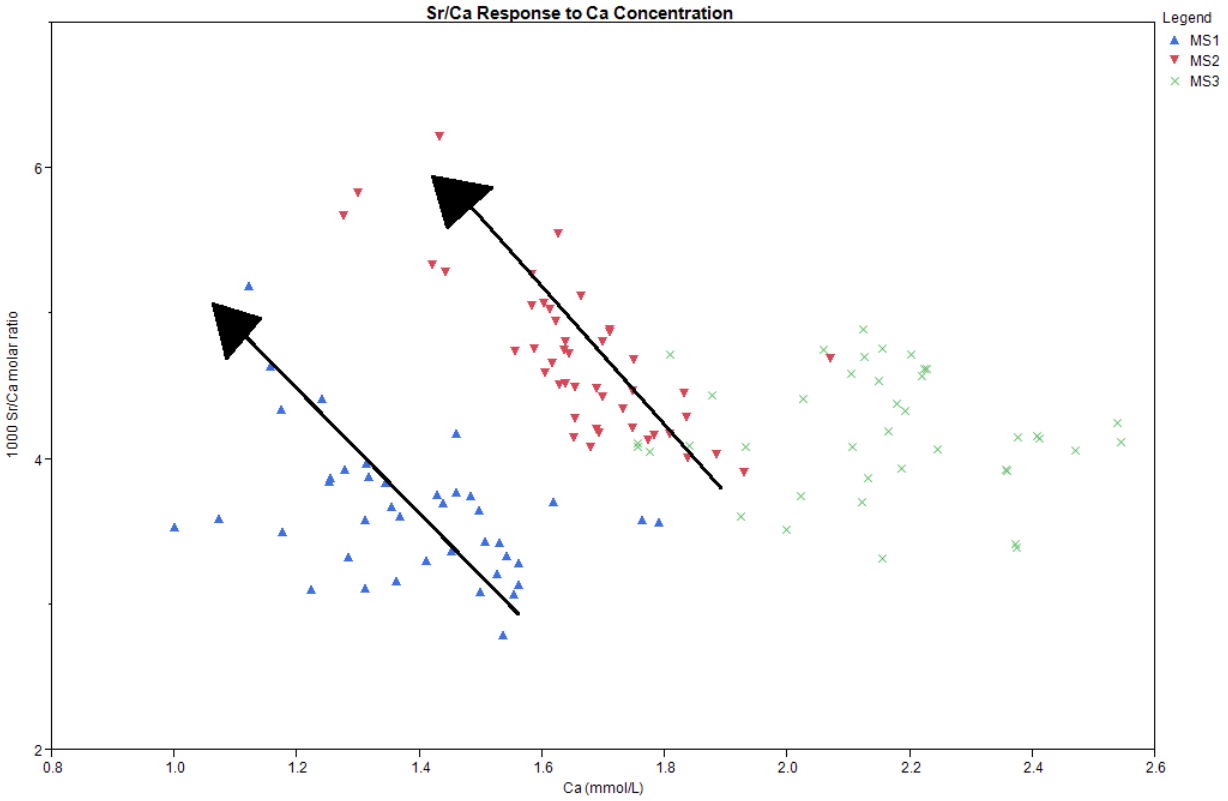

Figure 2.21. Sr/Ca response to Ca concentration in drip waters. Arrows indicate the relationship between a declining Ca concentration and increasing Sr/Ca, indicating prior calciate precipitation.

Figure 2.22 shows the discrete geochemical record divided into three sections which clearly show an oscillation in the Sr/Ca molar ratio, especially at MS2. Periods of increasing Sr/Ca (late summer through early winter) indicate increasing calcite precipitation and periods of decreasing Sr/Ca (winter through late summer) indicate increasing calcite dissolution.

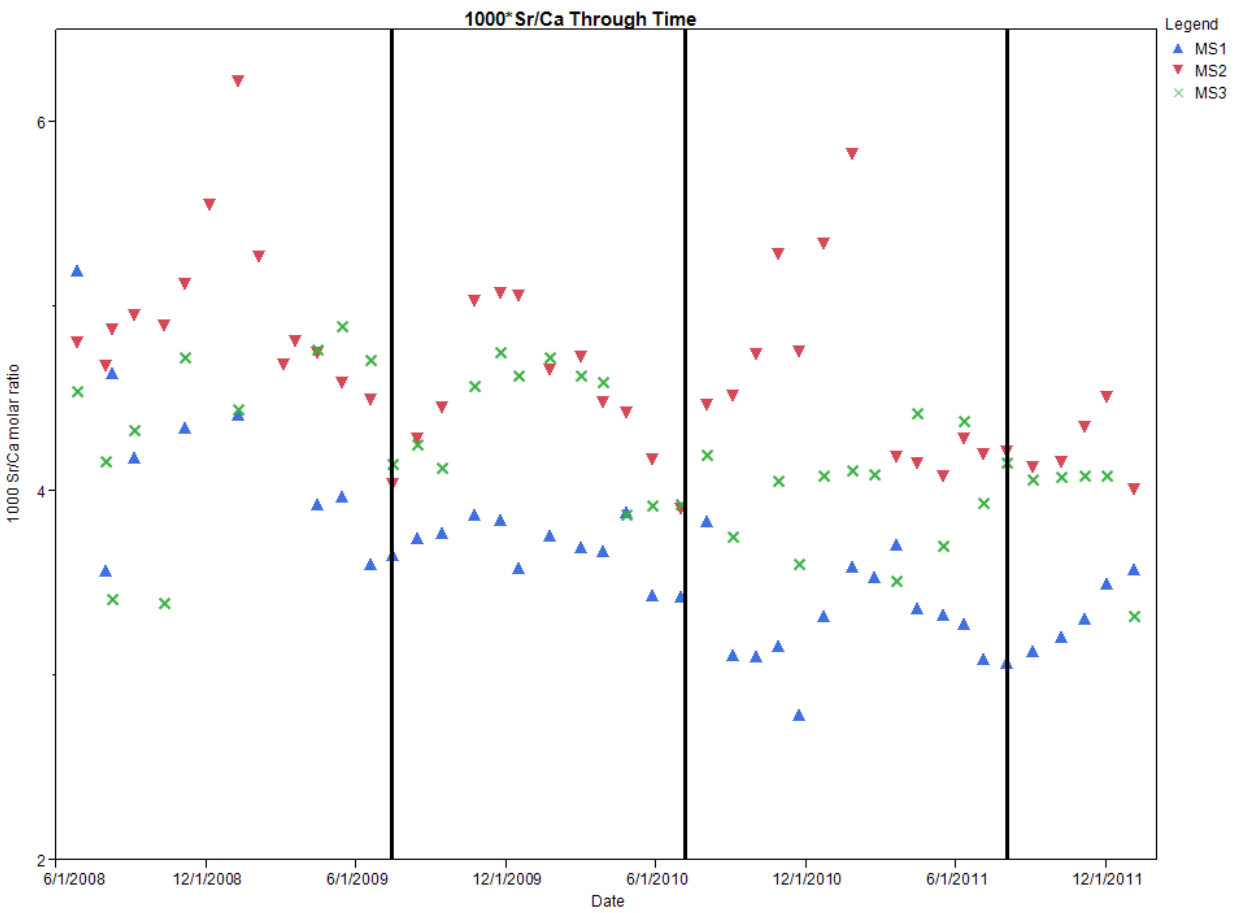

Figure 2.22. Sr/Ca through time. Vertical lines separate observable periods of Sr enrichment and depletion relative to Ca.

Conceptual model of the Epikarst

We propose the following conceptual model to describe the role of the epikarst in influencing the hydrology and geochemistry of recharge. The conceptual model describes the epikarst filling, draining, and local atmospheric connectivity presented in figure 2.23 A through C. Panel X shows the hypothetical scenario where the epikarst is completely dry—this is not expected at the James Cave field site but possible in arid regions where equilibration with soil gases would be expected.

Recharge (winter-spring): Panel A depicts the fully saturated epikarst which occurs during conductivity period A and hydrologic recharge season. During this period significant recharge to the underlying karst aquifer occurs and there is consistency of P_{CO2} throughout the system due to the lack of opportunity for gaseous diffusion. The initial flush of drip water has high specific

conductance due to interaction of epikarst water with rock during the baseflow (epikarst filling) season (panel C). However, as discharge continues, fully saturated macropores in the soil and fractures in the epikarst allow dilute precipitation to bypass storage and flow directly through the epikarst and into the cave. As a result, after the first flush, subsequent drip water has lower conductance due to mixing of precipitation with epikarst water.

Recession (summer). Panel B (conductivity period B and hydrologic recession season) illustrates the scenario of reduced input where the ET exceeds precipitation. Near surface moisture is lost and deep soil moisture continues to enter the epikarst while the declining pressure head leads to progressively lower drip rates. Gas exchange is limited to the deep soil zone and therefore P_{CO2} is expected to increase, along with calcite dissolution and as a result, specific conductance of drip water also increases. This period is observed in the hydrologic record as recession.

Baseflow (fall). Panel C shows that during the fall, the epikarst continues to drain, reflected by low to negligible drip discharge. This draining results in the drying of the upper epikarst, which increases permeability for gas flow and allows for degassing of CO_2. Loss of CO_2 results in calcite precipitation in the epikarst, which is reflected in the decreased Ca concentrations, increased Sr/Ca ratios, and decreased specific conductance in drips. However, as evapotranspiration tapers off during the fall, precipitation infiltrates into soils and this water eventually fills the epikarst. The duration of this season depends on the quantity of precipitation received after precipitation exceeds PET (See Gerst (2010) for additional explanation). Once the epikarst is filled, the recharge period begins (Panel A).

Duration of the seasons described above rely heavily on inputs. As mentioned above and alluded to in Gerst (2010), the length of the recharge season is dependent on when the recharge season begins. As shown in panel C of figure 2.23, once precipitation starts to exceed evapotranspiration, infiltration of water is reinitiated and the epikarst begins to fill. After the volume of infiltrated water has reached storage capacity of the epikarst, breakthrough of recharge (cave drips) begins. If there is reduced precipitation in the fall and early winter, baseflow will be extended and the recharge season will start later, resulting in an overall shorter recharge season

because recession begins in the late spring/early summer when ET exceeds precipitation regardless of antecedent conditions. Duration of the recession period is not as variable since cessation of input is a necessary precursor for the commencement of this season—in this dataset this is observable since recession consistently begins in May or June. Therefore, the main control on duration of recession is the storage capacity of the epikarst—which is relatively stable.

The physical basis for the conceptual model is supported by Williams (2008) in terms of porosity, permeability, and occurrence of conduit and fracture features being reduced with depth. Furthermore, the plumbing diagrams from Tooth and Fairchild (2003) support the cascading notion of preferentially filled pores in this model, the piston effect that this has on the overall system, and the varying equilibration with the gas phase in different epikarst conditions (i.e. seasons).

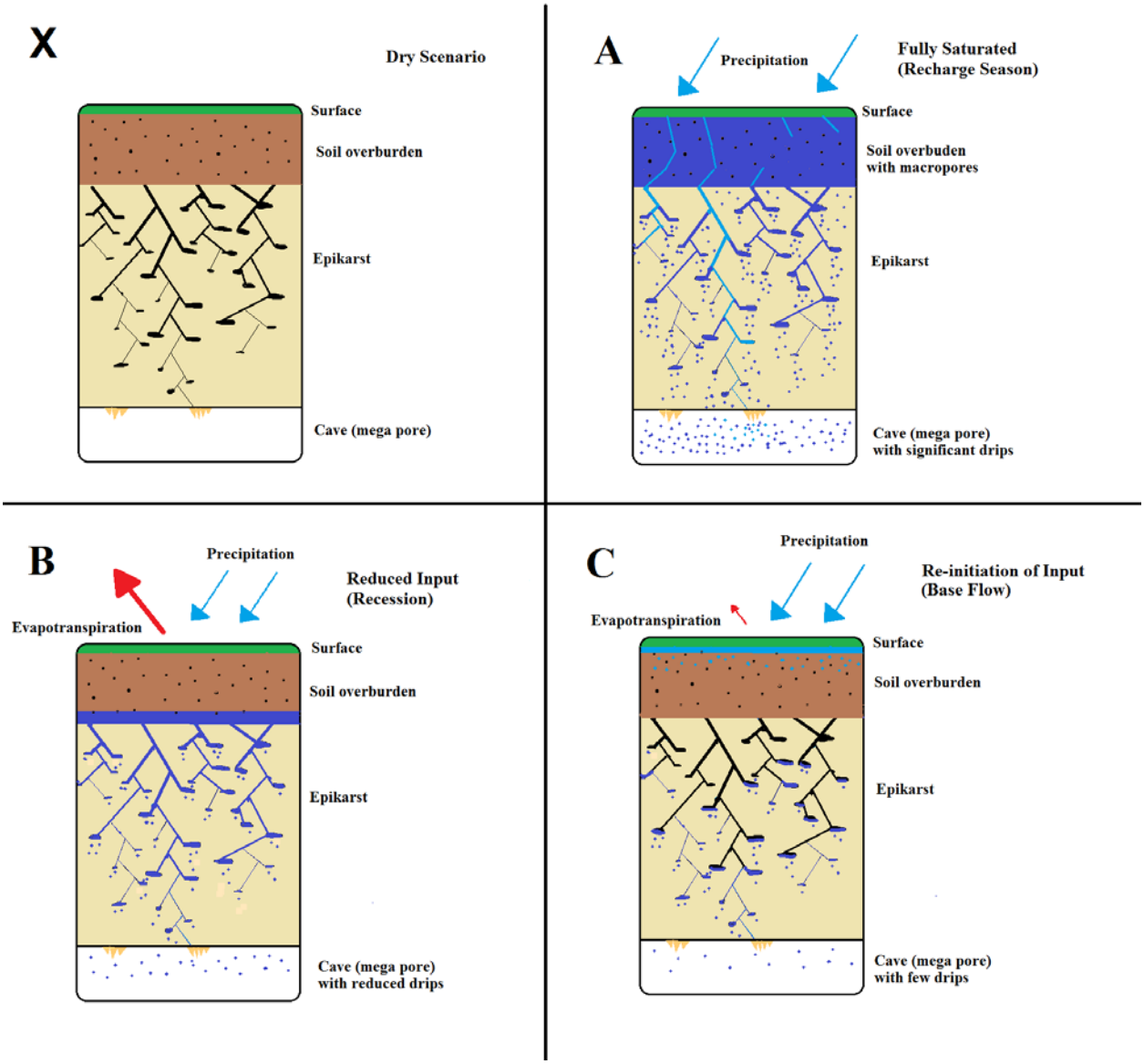

Figure 2.23. Conceptual model of the epikarst at James Cave. Panel X depicts the hypothetical scenario where the epikarst is dry; panel A depicts the full saturated epikarst; panel B depicts reduced hydrologic input; and panel C depicts the re-initiation of input. Lines in the epikarst reflect a function rather than a feature and may be shown in the field as fractures, conduits, etc.

2.6 IMPLICATIONS

The seasonality of epikarst storage documented in this project has implications for attenuation of both flow and chemical constituents through the epikarst. These implications include the following:

1) During the recharge period (winter-spring), hydrologic connectivity to the surface is greatest, as is the potential for surface contamination to reach the underlying karst aquifer.
2) During recession (summer), the average residence time of water in the epikarst appears to be greater than during the recharge period, which can enhance attenuation of surface-derived contaminants. This can have a positive impact if attenuation is the goal, however, if dilution or removal is the goal, the effect may be negative.
3) During baseflow (fall) due to drying in the upper epikarst, there is release of CO_2 and a subsequent precipitation of calcite. Although there is likely increased residence time of water (and contaminants) during this period, the complex rock-water interactions occurring during baseflow preclude a simple explanation of the extent of contaminant attenuation.

Finally, while this study allows for the above implications which have potential to impact hydrologic policy, perhaps the most significant outcome is recognition of both annual and seasonal variability in epikarst monitoring which requires long term, high resolution monitoring.

2.7 REFERENCES

Aquatic Informatics (2011). AQUARIUS 3.0 R3. 1032. Vancouver, British Columbia.

Aquilina, L., B. Ladouche, et al. (2006). "Water storage and transfer in the epikarst of karstic systems during high flow periods." Journal of Hydrology **327**(3-4): 472-485.

Bailly-Comte, V., J. B. Martin, et al. (2010). "Water exchange and pressure transfer between conduits and matrix and their influence on hydrodynamics of two karst aquifers with sinking streams." Journal of Hydrology **386**(1-4): 55-66.

Bakalowicz, M. J. (2004). The epikarst, the skin of karst. Epikarst: Special Publication 9., Charles Town, WV, Karst Waters Institute.

Baker, A. and C. Brunsdon (2003). "Non-linearities in drip water hydrology: an example from Stump Cross Caverns, Yorkshire." Journal of Hydrology **277**(3–4): 151-163.

Baker, A., D. Genty, et al. (2000). "Hydrological characterisation of stalagmite dripwaters at Grotte de Villars, Dordogne, by the analysis of inorganic species and luminescent organic matter." Hydrology and Earth System Sciences **4**(3): 439-449.

Baldini, J. U. L., F. McDermott, et al. (2012). "Identifying short-term and seasonal trends in cave drip water trace element concentrations based on a daily-scale automatically collected drip water dataset." Chemical Geology **330–331**(0): 1-16.

Bartholomew, M. J. (1987). "Structural evolution of the Pulaski thrust system, southwestern Virginia." Geological Society of America bulletin **99**(4): 491.

Bureau of the Census and NRCS (2002). NRCS Counties by State. United States Census Bureau and Department of Agriculture-Natural Resources Conservation Service.

Choquette, P. W. and L. C. Pray (1970). "Geologic nomenclature and classification of porosity in sedimentary carbonates." AAPG bulletin **54**(2): 207.

Curti, E. (1999). "Coprecipitation of radionuclides with calcite: estimation of partition coefficients based on a review of laboratory investigations and geochemical data." Applied Geochemistry **14**(4): 433-445.

El-Kadi, A. I., L. N. Plummer, et al. (2011). "NETPATH-WIN: An Interactive User Version of the Mass-Balance Model, NETPATH." Ground water **49**(4): 593-599.

Fairchild, I. J., A. Borsato, et al. (2000). "Controls on trace element (Sr–Mg) compositions of carbonate cave waters: implications for speleothem climatic records." Chemical Geology **166**(3–4): 255-269.

Genty, D. and G. Deflandre (1998). "Drip flow variations under a stalactite of the Père Noël cave (Belgium). Evidence of seasonal variations and air pressure constraints." Journal of Hydrology **211**(1–4): 208-232.

Gerst, J. D. (2010). Epikarst control on flow and storage at James Cave, VA: an analog for water resource characterization in the Shenandoah Valley karst. Geosciences. Blacksburg, VA, Virginia Polytechnic Institute and State University. **Master of Science**.

Grant, D. M. and B. D. Dawson (2001). Isco Open Channel Flow Measurement Handbook. Lincoln, Nebraska, Isco, Inc.

Gregory, L., B. Wilcox, et al. (2009). "Large-scale rainfall simulation over shallow caves on karst shrublands." ECOHYDROLOGY **2**: 72-80.

Hergenroder, J. D. (1957). Geology of the Radford Area, Virginia. Geology. Blacksburg, VA, Virginia Polytechnic Institute. **Master of Sciences**.

Klimchouk, A. (2003). Towards defining, delimiting and classifying epikarst: its origin, processes and variants of geomorphic evolution. Epikarst, Shephardstown, West Virginia, Karst Waters Institute, Inc.

KWI (2006). "What is Karst (and why is it important)?". Retrieved December 1, 2011, from http://www.karstwaters.org/aboutkarst/index.php.

Maguire, R. O. and S. E. Heckendorn (2011). Laboratory Procedures, Publication 452-881. Blacksburg, VA, Virginia Polytechnic Institute and State University.

McDonald, J. and R. Drysdale (2007). "Hydrology of cave drip waters at varying bedrock depths from a karst system in southeastern Australia." Hydrological Processes **21**(13): 1737-1748.

McDonald, J., R. Drysdale, et al. (2007). "The hydrochemical response of cave drip waters to sub-annual and inter-annual climate variability, Wombeyan Caves, SE Australia." Chemical Geology **244**(3-4): 605-623.

MRLC (2006). National Land Cover Dataset. Environmental Protection Agency- Multi-Resolution Land Characteristics Consortium, http://datagateway.nrcs.usda.gov.

Mylroie, J. E., J. W. Jenson, et al. (2003). Epikarst on Eogenetic Rocks. Epikarst, Shephardstown, West Virginia, Karst Waters Institute, Inc.

Perrin, J., P.-Y. Jeannin, et al. (2003). "Epikarst storage in a karst aquifer: a conceptual model based on isotopic data, Milandre test site, Switzerland." Journal of Hydrology **279**(1–4): 106-124.

Radtke, D. B., F. D. Wilde, et al. (2012). Alkalinity and Acid Neutralizing Capacity (version 4.0). National Field Manual for the Collection of Water-Quality Data: U.S. Geological Survey Techniques of Water-Resources Investigations. S. A. Rounds, U.S. Geological Survey. **9**.

Schultz, A. P. and M. J. Bartholomew (2009). Geologic Map of the Radford North Quadrangle, Virginia. A. Cross and E. V. M. Campbell, Virginia Division of Mineral Resources.

Sheffer, N. A., M. Cohen, et al. (2011). "Integrated cave drip monitoring for epikarst recharge estimation in a dry Mediterranean area, Sif Cave, Israel." Hydrological Processes **25**(18): 2837-2845.

Sherwin, C. M. and J. U. L. Baldini (2011). "Cave air and hydrological controls on prior calcite precipitation and stalagmite growth rates: Implications for palaeoclimate reconstructions using speleothems." Geochimica Et Cosmochimica Acta **75**(14): 3915-3929.

The Southeast Regional Climate Center (2012). "Historical Climate Summaries for Virginia." 2012, from http://www.sercc.com/climateinfo/historical/historical_va.html.

Tooth, A. F. and I. J. Fairchild (2003). "Soil and karst aquifer hydrological controls on the geochemical evolution of speleothem-forming drip waters, Crag Cave, southwest Ireland." Journal of Hydrology **273**(1–4): 51-68.

USDA-NRCS (2010). Soil Survey Tabular Database. United States Department of Agriculture-Natural Resources Conservation Service.

USGS-Mineral Resources Program (2005). USGS Geologic Map of Conterminous United States. United States Geological Survey.

Virginia Agricultural Experiment Station (2012). "Weather Data." Retrieved January 30, 2013, from http://www.vaes.vt.edu/college-farm/weather/2012/weather2012.html.

Williams, P. (2008). "The role of the epikarst in karst and cave hydrogeology: a review." International Journal of Speleology (Edizione Italiana) **37**(1): 1-10.

Williams, P. W. (1983). "The role of the subcutaneous zone in karst hydrology." Journal of Hydrology **61**(1–3): 45-67.

Yang, R., Z. Liu, et al. (2012). "Response of epikarst hydrochemical changes to soil CO2 and weather conditions at Chenqi, Puding, SW China." Journal of Hydrology **468–469**(0): 151-158.

APPENDICES

Appendix A. Standard Operating Procedures for Sample Collection and Preservation

STANDARD OPERATING PROCEDURES
For Monitoring of Epikarst Parameters in James Cave, Pulaski County, VA

Prepared by: Jonathan Gerst
Modified by: Madeline Schreiber and others

Summary:
The following instructions should be utilized in order to collect data and maintain sampling equipment for the James Cave Epikarst Research Project in Pulaski County, VA.

- One surface station, just outside the cave entrance, has been equipped with the following instruments: precipitation collector, precipitation gauge, Temperature (T) logger, and Relative Humidity (RH) logger.
- Three lysimeters have been installed at the surface to sample soil water (Soil Entrance, Soil 2, Soil 3)
- Three drip monitoring stations (MS1, MS2, MS3) have been equipped with the following instruments: drip tarp, biological strainer, rain gauge to measure drip rate, Hanna probes to measure continuous pH/T/DO/SC/ORP, and an overflow bottle to collect water for composite geochemistry.
- The stream station has a weir with pressure transducer/barologger to measure discharge. There is also a Hanna probe to measure continuous geochem.

Timing:
Monitoring should be performed at least once monthly in order to ensure that monitoring equipment has adequate battery power. One monitoring event (i.e. Data collection from all four monitoring stations) normally takes approximately 5 hours.

Equipment requirements:
The following pieces of equipment are to be compiled before going into the field:
- Asus laptop with fully charged batteries (keep charged in office when not in use)
- Connector cable from laptop to Hobo logger (earphone jack cable)
- Connector cable for laptop to Hanna Probe
- Connector cable for laptop to Hobo U-Shuttle (mini-B to USB)
- 16 fully charged 6 V lead battery cells (Model No.: LC-R0612P) for Hanna Probes in Pelican cases (four per case => total of 4 cases). *See end of this document for directions on charging.*
- Eight rechargeable AA batteries for Hobo loggers
- Tools: flathead screw driver, pocket knife, zip ties, Sharpie, duct tape
- Cave equipment: helmet, headlamp + a backup, coveralls, elbow and knee packs, boots, gloves
- backpack (dry bag)

- Desiccant packs for microstations
- Field book
- Cooler with bottles, and some ice bricks from freezer in 5044

Before you go: Bottle Preparation and Labeling

Bottles you will need

- 4 x wide mouth 125 mL
- 9 x empty 1 L
- 1 x 1 L filled with DI
- 1 x 500 mL

DI:

- Use DI from system next to sink in Maddy's lab.
- Fill 1L bottle with 500 mL of DI. (can use volumetric or Erlenmeyer, it needs to be close, but not exact)
- Take split for O/H isotopes in 11 ml square glass vial (label Precip Control Initial with date), put in box in cabinet with James Cave O/H isotope samples.

Labeling:

- Use a different color labeling tape than the past few samplings (check fridge).
- Use sharpie to write sample name and sampling date on label tape.
- 125 mL
    - Biosample 1
    - Biosample 2
    - Biosample 3
    - (unlabeled extra bottle)
- Empty 1 L
    - Precip control final
    - Precip
    - Site 1
    - Site 2
    - Site 3
    - Stream
    - Soil 2
    - Soil 3
    - (unlabeled extra bottle)
- 1 L filled with DI
    - Precip control initial
- 500 mL
    - Soil Entrance

Packing:

- Put bottles in a box or cooler.
- Put box on or next to equipment cart.

Once you are in the field:

Surface Monitoring

1- Inspect all in situ monitoring equipment, and note any oddities, equipment malfunctions, site changes, and any evidence of tampering.
2- Rain gauge download: Connect the laptop to the Hobo logger via serial port. Connection to the hobo logger is found by removing the nickel sized white plastic cap (Use flat headed screwdriver) from the logger's protective casing.
3- Open HOBOware Pro software on laptop and click "Readout Device". Follow naming mechanism currently in use on field laptop, and convert data to Microsoft Excel format.
4- Change Hobo logger batteries only if necessary (Red light= functioning battery).
5- Collect precipitation control sample: Extract precip control sample (i.e. the PVC cylinder closest to the rain gauge) by first removing the plug on the top of the PVC cylinder (allows air flow). The clear plastic tube should be suspended/fixed behind zipties at this point (it should not be connected to the funnel as we don't want rain to get into the control!) Dislodge the plastic tubing from the zipties, and empty sample from the plastic tubing into 1L bottled labeled "Precipitation Control Final"
6 - Upon completion of sampling the control, reconnect tubing to the funnel bottom, and fill the PVC precip control cylinder with 500 mL of fresh DI water (labeled Precipitation Control Initial). The fresh water serves as the Precip Control initial sample for the next month's event. After you are finished filling with DI water, replug the top of the PVC cylinder. Also (IMPORTANT), remember to remove the tubing from the funnel so that no precipitation gets into the precip control cylinder.
7 – Collect precipitation sample: Extract precip sample by (i.e. far left PVC cylinder) removing tubing and directing flow from rain collection cylinder to the 1L bottle labeled "precipitation". When finished, reconnect tubing between funnel and PVC cylinder for additional rainwater collection.

NOTE: Maintenance of DPAD

Although it hasn't been a problem recently, in 2008 and early 2009, DOC showed abnormally high concentrations that were probably the result of bacterial growth or bug guts becoming dissolved in the sample after getting stuck inside the collection cylinder.

One thing to watch for: critters (probably groundhogs) have previously chewed through the clear plastic tubing (near base of collection cylinders) for a drink from the water contained in the PVC cylinders. It's important to check the tubing each time for chew marks and leaks.

Last, leaks may also occur because freeze-thaw in the winter breaks the seals between the pvc cylinder and the pipe ends. Jonathan reglued back in January 2010, but seals may have re-broken. To check, simply twist the bottom pipe end, and if it spins freely about the PVC cylinder, then apply more glue.

Lysimeter Sampling

Using hand vacuum pump, put ~20 inHG pressure on the soil lysimeters. Put the vacuum on the extraction tube (one with short duct tape). The other line should remain crimped. This will suck water into the lysimeter for you during the field event. Commence subsurface sampling, but don't forget to extract/pump out the samples at the end of the day. When you return, place the extraction line into your container. Then put the bike pump on the purge line. When you're done, recrimp both lines.

Subsurface Monitoring for Sites 1-3 and Stream:

1- Inspect all insitu monitoring equipment, and note any oddities, equipment malfunctions, site changes, and any evidence of tampering.
2- Download rain gauges: Connect the laptop to the Hobo logger via serial port. Connection to the hobo logger is found by removing the nickel sized white plastic cap (Use flat headed screwdriver) from the logger's protective casing. Open HOBOware Pro software on laptop and click "Readout Device". Follow naming mechanism currently in use on field laptop, and convert data to Microsoft Excel format.
4- Change Hobo logger batteries once per month. Use rechargeable AAs.
5- Collect water from overflow container using 1L container (these should have been previously labeled for site name). Label with date.
6- Collect biosample using 125 mL container. Label container with the site location and date, if needed.
7- Stop and turn off the Hanna Probe (Stored in Pelican Case) and then connect it to the laptop via the laptop's USB port.
8- Open Hanna Probe software (HI 92000 -4.9.1) on laptop, turn on Hanna Probe (Hanna Probe should read "PC Connection"), and click "Connect" on laptop. Click "Get Lot" on laptop (Select lot according to the date of the previous monitoring event). Click "Save" on laptop, and save as single monitoring date. Note: The Hanna software won't allow long names to be saved, so you must rename the file according to the naming mechanism already in use on the laptop. Data should already be in Excel format.
9- Turn off the Hanna Probe again, disconnect from the laptop, and reconnect to the monitoring system in order to replace batteries. Make sure replacement batteries are fully charged 6 volt lead batteries (see instructions below for charging).
10- After the Hanna Probe has been reconnected to the monitoring system and the batteries have been replaced, turn the Hanna Probe back on. Using the hand-held Hanna Probe select "Log", "Options", "Continuous", "New Lot", and then name the lot according to the date of the monitoring event (e.g., 7-18-08). When prompted to "Add Remark", click "No". When prompted to "Touch the tag with tag reader", click "Skip."
11- Make sure to secure the Hanna Probe and batteries in the in-situ Pelican Case.

Geochemical Sample Collection

Use 1L Nalgenes to collect overflow at all subsurface monitoring stations. Directions on how to process those samples when back in the lab are later in this document.

Stream Discharge Data Download (1 download per every 4 months)

Retrieve pressure transducer from PVC pipe on weir and download data using optical reader to laptop using Levelogger Pro. Do the same for the barometric logger that is positioned in the cave ceiling above the HI9828 stream case. Measure the water level above the weir with ruler for calibration purposes...make sure to measure from bottom of V-notch weir to the top of the overall pool elevation.

Back at the car

1 – Put samples in the cooler with ice bricks

Back in the Office

Immediately:
1- Biosamples should be treated with formalin (15 ml - use graduated cylinder). Biosamples should be put in ziploc bags labeled "James Cave Bio Samples" with the date. The bag should be put in the bottom shelf of the fridge in 5044.
2 – Geochem samples should be put in the fridge – alert Maddy that the samples are there. Instructions for processing are below.
3 – Take laptop out of case and plug into plug strip in 5046.
4- Take batteries off cart and put on benchtop in 5046 for charging. Put first set of batteries on charger. The battery charger currently used for this project can charge up to four 6V batteries at once (i.e. Two 6V batteries per output). There are two recharge outputs on the battery charger. Connect two batteries to one recharge output making sure of the following: the red recharger electrode must be connected to one of the battery's red electrodes, the black recharger electrode must be connected to the other battery's black electrode, the two batteries will be connected together using extra wiring so that the first batteries black electrode is connected to the second batteries red electrode. When finished, the batteries should be connected in 'series' (As opposed to 'parallel'). Repeat abovementioned process for the second set of batteries. After proper connection has been established with the batteries, a yellow light will appear on the recharger to indicate that the battery is charging. If there is a short in the circuit, or the batteries have expired then a red light will appear on the recharger. Once the batteries are charged, a green light will appear, indicating that the battery is ready.
5 – When batteries are charged, put them back on cart.
6 – Recharge the AA batteries by putting in charger on plug strip
7- Data collected in the field should be converted to excel format and then uploaded to Scholar.

Preparing samples for geochemical analysis

1. Check volume of your sample.
If you have 225 ml or greater, you can do all samples.
If you have < 225 ml, need to make some decisions. I recommend collecting the following samples in order of importance:

- 20 ml cations (best to have 25 ml, but we can get away with 20)
- 5 ml anions (at a minimum, best to have more)
- 25 ml alkalinity (at minimum, best to have 100 ml for precip and 50 ml for drip/stream samples)
- 11 ml O/H isotopes
- 25 ml DOC
- 25 ml organic C isotopes (best to have 50 ml so can fill up 2 vials)
- 25 ml inorganic C isotopes (best to have 50 ml so can fill up 2 vials)

2. Labeling bottles. Its best to label bottles before filling with sample and then double-checking the label when you filter into the bottle.

Label bottle with Site name, date, the analyte (e.g. cations, anions, DOC, etc, 0.22 um, and the preservative, if any. Examples:

Cations	Site name, date, "cations, 0.22 um, HNO3"
Anions	Site name, date, "anions, 0.22 um"
Alkalinity	Site name, date, "alkalinity, 0.22 um"
DIC isotopes	Site name, date, "DIC isotopes, 0.22 um, CuSO4"
DOC	Site name, date, "DOC, 0.22 um, HCl"
DOC isotopes	Site name, date, "DOC isotopes, 0.22 um; H3PO4"
O/H isotopes	Site name, O/H isotopes, 0.22 um"

3. CAREFUL Syringe Filtration for DIC/DOC and alkalinity (DO NOT AGITATE WATER)
Use 20 or 60ml syringe with 0.22 um Polysulfone GD/X syringe filter. Attach syringe filter to syringe, pour water smoothly into syringe, filter into the labeled sample bottle. Follow directions below for further preservation and bottle storage.

4 Regular Syringe Filtration filtration for everything else.
You can use take off the filter and use the syringe to pull up water from the sample, then attach the filter and push sample through.

5 Specific directions for individual analytes
<u>Cations</u>
Use 30 ml clear bottle
Put 20-25 ml (20 ml minimum) filtered sample into bottle.
Add 3 drops of concentrated HNO3 (in fume hood, use dropper, wear gloves and face mask)

Keep refrigerated until analysis (6 month holding time)
Analyze using ICP-AES at Soil Testing Lab

Anions

15-30 ml clear bottle (whatever is available, just make sure these haven't been acid washed)
Put 5-10 ml (5 ml is minimum) filtered sample into bottle
DO NOT PRESERVE
Keep refrigerated until analysis (2 week holding time)
Analyze using ion chromatograph

Alkalinity

Put 25-100 ml (25 ml minimum, 50 ml or 100 ml is best if you have it) filtered sample into bottle
DO NOT PRESERVE
Keep refrigerated until analysis (24 hour holding time)
Analyze using revised gran titration method (see Denise's instructions)

Dissolved Inorganic Carbon (DIC) Isotopes

Need two 20 mL **clear** EPA VOC vials with **black butyl rubber** septa.
Add about 5 mg of blue copper sulfate solid to the vials **prior** to adding sample. To do this, tare empty bottle on balance, add 0.005 g of powder. Don't need to be exact, its just used as a bacteriocide.
Fill vials all the water with filtered water, until positive meniscus formed.
Screw on cap (they may be some spillage) but don't overtighten. Check septa to make sure not creased.
Keep refrigerated until analysis
Holding time is several months
Send samples to Dan Doctor at USGS

Dissolved Organic Carbon (DOC)

Need one 20 mL amber glass vial with regular Teflon (white) septa
Add 1 drop of concentrated HCl to vial (acid in dropper bottle in fume hood, make sure to use gloves and wear face mask)
Fill vials all the water with sample, until positive meniscus formed.
Screw on cap (they're be some spillage) but don't overtighten. Septa should not be creased.
Keep refrigerated until analysis
Holding time is several months
Analyze DOC using Carbon Analyzer

Dissolved Organic Carbon (DOC) Isotopes

Need two 20 mL amber glass vials with regular Teflon (white) septa
Add small drop of 85% phosphoric acid to vial (acid in fume hood, use plastic transfer pipet in beaker next to acid bottle. Make sure to use gloves and wear face mask)
Fill vials all the water with sample, until positive meniscus formed.
Screw on cap (they're be some spillage) but don't overtighten. Septa should not be creased.
Keep refrigerated until analysis
Holding time is several months
Send DOC isotopes to Dan Doctor

Oxygen and Deuterium Isotopes

Use 11 mL polyseal glass vials.
Fill all the way to top if possible
Store samples at room temperature and in the dark (in the box is great). Store them cap-side down.
Before sending to Benjamin, fill a 2 ml vial to the top, screw on cap. Keep these upside down in the box.
Label according to Benjamin's instructions.

Cleaning and Washing Instructions

Bottles

All bottles must be cleaned after use.
If doing by hand, fill plastic bin with soapy water. Soak bottles. Use scrub brushes to get off crusty stuff. Wash with MilliQ from wall, then do final rinse with NanoPure. Dry in drying rack.
If doing by dishwasher, follow dishwasher instructions.

Bottles should be completely dry before being used.

Other special cleaning procedures:
Amber glass vials should be triple rinsed in Nanopure OR baked in muffle furnace at 450 C for at least 4 hours.

Clear vials with black septa should be tripled rinsed in DI and carefully dried (put foil over to prevent particle contamination).

Appendix B. Data Management Plan and Preprocessing as of April 2013

James Cave, Virginia Monitoring Site
Data Management Plan and Preprocessing as of April 2013

Prepared and written by Sarah Eagle

I. **Definitions**
- A. Programs of import
  - i. HOBOware
    1. By Onset, for data loggers and some preprocessing
    2. File type supported: **DTF**
  - ii. Excel
    1. Microsoft spreadsheet manipulation and editing product
    2. File type supported: **CSV**
  - iii. AQUARIUS workstation
    1. Time series aggregation, manipulation, and preprocessing
    2. File type supported: **AQW**
  - iv. Solinst Level Logger
    1. Pressure transducer software for managing loggers and some preprocessing
    2. File type supported: **LEV**
- B. Data types
  - i. Drip/precip data
    1. Collected via Onset tipping bucket rain gauges in conjunction with Onset microstations
    2. Recorded in millimeters or inches
       a. Recorded as counts (one count=0.1mm) at MS3 through 110512
    3. Raw data as DTF files, exported data as CSV
  - ii. Relative humidity
    1. Previously collected via Onset sensor and logged on microstation
    2. Recorded as %; raw data as DTF files, exported as CSV
  - iii. Air temperature
    1. Collected in one of two ways:
       a. In conjunction with drips as a single DTF on a Onset microstation (previous)
       b. On their own on an Onset pendant logger (recent)
    2. Recorded in celsius or fahrenheit
    3. Raw data as DTF files, exported data as CSV

iv. Specific conductance/water temperature
    1. Collected together via Onset conductivity loggers
    2. Specific conductance measured in uS/cm
    3. Temperature in Celsius or Fahrenheit
    4. Raw data as DTF files, exported data as CSV
v. Stream discharge
    1. Previously collected via Solinst pressure transducers
    2. Currently collected via Onset pressure transducers
    3. Recorded in two separate loggers—one of water pressure the other for barometric pressure
        a. Onset transducers record in pressures—must convert to length measurement in HOBOware
        b. Solinst transducers report in length upon uploading
    4. Raw data as solinst files or DTF, both exported as CSV

II. Preprocessing as of April 2013—for S. Eagle thesis

A. Drip data (includes drips, RH, air temp)

i. Review dates in data files for discrepancies between DTFs and CSVs—supplement straight from DTF data for periods of questionable CSV data.

ii. Organize each subset (MS1, MS2, MS3, and precip) into the same CSV structure:
    1. MS1 by comma separated value: Observation number, date and time (MM/DD/YYYY HH:MM), drips (in), drips (mm), temp (F), RH (%), temp (C).
    2. MS2 by comma separated value: Observation number, date and time (MM/DD/YYYY HH:MM), drips (in), drips (mm), temp (F), RH (%), temp (C).
    3. MS3 by comma separated value: Observation number, date and time (MM/DD/YYYY HH:MM), counts (#), temp (F), RH (%), temp (C), drips (in), drips (mm).
    4. Surface by comma separated value: Observation number, date and time (MM/DD/YYYY HH:MM), temp (F), RH (%), precip (in), precip (mm), temp (C).

iii. Import each subset of data in AQUARIUS using the Import From File Toolbox
    1. Be sure to specify the CSV structure while importing
    2. For all raw data, be consistent about the Parameter setting and the Interpolation Type especially for Precip/Drip data
        a. S. Eagle used Precip parameter with “1-Ins Values” as the interpolation type

3. Combine data files during import for each site

iv. Preprocessing for each data type
    1. Use Signal Trimming Toolbox to remove erroneous values (-888.88)
    2. Use Signal Joining Toolbox to join signals with different units (i.e. combine mm and in drip data, combine C and F temp data)

v. Export
    1. Use Export to File Toolbox to export the combined and minimally preprocessed data as a CSV

vi. Additional note for S. Eagle data
    1. After steps i-v, data were re-imported into AQUARIUS and the Descriptive Statistics Toolbox was used to create a daily sum of drips and precipitation for use in thesis

B. Specific Conductance and Water Temp

i. Open each DTF file in HOBOware and temperature correct using the HOBOware Conductivity Assistant and the linear temperature compensation option.
    1. Create new series for the temperature corrected conductivity and export data to CSV

ii. Organize each subset (MS1, MS2, MS3, or stream) into the same CSV structure:
    1. The same comma separated value for each site: observation number (#), date and time (MM/DD/YYYY HH:MM), Full range uncorrected conductivity (uS/cm), temperature (C), specific conductance (uS/cm)

iii. Import each subset of data into AQUARIUS using Import from File toolbox
    1. Be sure to specify the CSV structure while importing
    2. For all raw data, be consistent about the Parameter setting and the Interpolation Type
    3. Combine data files during import for each site

iv. Preprocessing for each data type
    1. For periods of missing DTFs for conductivity, the CSVs were imported without a temperature correction and were corrected using the Math Toolbox and a linear correction
    2. Using the Signal Trimming Toolbox, trim conductivity values below 100—these are values measured while the logger is dry or being offloaded.
    3. Combined data using the Signal Joining Toolbox where necessary.

v. Drift correction

1. Import discrete calibration data via Import from File toolbox
2. Combine continuous and discrete data using Data Correction Toolbox
3. Correct for drift by using Multi-Point Drift Correction feature

vi. Export
1. Use Export to File Toolbox to export the combined and minimally preprocessed data as a CSV

C. Stream data
i. For solinst data files
1. Once exported from Level logger software as CSVs, import both barometric and level logger CSVs into AQUARIUS using Import from File toolbox.
a. This data should all be in feet.
2. Using the Math toolbox, correct do the barometric pressure correction by subtracting the baro "length" from the level "length"
a. "length" is calculated in Solinst Level Logger software

ii. For HOBO pressure transducers
1. Open DTF files in HOBOware
2. Using the Barometric Compensation Assistant correct for barometric pressure using the baro file for the same time period.
3. Export data with new "Sensor Depth" column in feet to CSV
4. Import new CSVs into AQUARIUS using Import from File toobox

iii. Combine and calculate
1. Combine solinst and HOBO baro-corrected data using the Signal Joining toolbox.
a. All of these data should be in feet now
2. Correct the baro-corrected data with the 'water level above v-notch' measurement taken in the field by using the Math toolbox to subtract this value
a. The following was used for S. Eagle thesis:
i. Date: 7/5/11
ii. Measured water level in stream: 0.1122 ft
iii. Water level logged on pressure transducer: 0.5774 ft
iv. Difference: 0.4652 ft
b. This value should be measured and updated via field measurements from time to time
3. Use the Math toolbox and the following equation to determine discharge in cubic feet per second: ((water level)^2.48)*4.28
4. Note on S. Eagle thesis

a. Prior to calculation of discharge, the water level was averaged to a single daily value and therefore the discharge is reported as a daily average cubic feet per second

III. Data Management Plan

A. Naming conventions

i. All drip/precip data files (CSV, DTF) should follow this naming formula: YYMMDD(start)_YYMMDD(end)_Datatype_Site.Filetype

1. An example: 120621_120630_driprate_T_site3.csv

ii. All conductivity data files (CSV, DTF) should follow this naming formula: YYMMDD(start)_YYMMDD(end)_Site_Cond_LoggerID.Filetype

1. An example: 120402_120511_Site1_Cond_9792786.dtf
2. For temperature corrected CSVs the suffix Tcorr will be added after the logger ID
    a. An example: 120402_120511_Site1_Cond_9792786_Tcorr.csv

iii. Stream discharge—All HOBO pressure transducer files (CSV, DTF) should follow this naming formula: YYMMDD(start)_YYMMDD(end)_LoggerType_LoggerID.Filetype

1. An example: 120523_120816_Baro_9917852.dtf
2. For baro corrected files, the exported CSV will have the same naming convention with the LoggerType being replaced with LevelCorr
    a. An example: 120523_120816_LevelCorr_9917858

iv. General notes

1. Start and end dates refer to the data available—NOT to when the sensor was deployed/offloaded
    a. During periods of data loss (i.e. low battery), the end date will reflect the last measurement taken
2. Acceptable shorthand notation
    a. For rain gauge data: precip, drips, driprate
    b. For temperature data: temp, T
    c. For conductivity data: Cond
    d. For relative humidity: RH
    e. For stream discharge: Baro, Level
    f. For sites: MS1, site1, MS2, site2, MS3, site3, stream, surface

B. Categorization structure of data

i. Data will be primarily divided into data type. Acceptable primary sections are as follows:

1. Conductivity
2. Drip data—includes all data measured with rain gauges
3. Stream—includes all discharge data from stream

ii. Data will be secondarily divided into raw data files (DTF, LEV) and exported data (CSV)
    1. Exported data can be equivalent to raw data or have corrections made in HOBOware or Solinst Level Logger only

iii. Subsections for Conductivity
    1. Raw data files (DTF)
        a. Subsections: MS1, MS2, MS3, Stream
    2. Temperature Corrected (CSV)
        a. Subsections: MS1, MS2, MS3, Stream
    3. No DTF
        a. For CSV files where the DTF was lost and the temperature correction for conductivity is conducted outside of HOBOware
    4. Conductivity Calibration
        a. For CSV files of discrete conductivity calibration data (measured in field with Cond meter)

iv. Subsections for drip data
    1. Raw data files (DTF)
        a. Subsections: MS1, MS3, MS3, Surface
    2. Exported data files (CSV)
        a. Subsections: MS1, MS2, MS3, Surface
        b. These data should not have undergone any preprocessing as of yet

v. Subsections for Stream data
    1. Raw data files (DTF, LEV)
    2. Exported data files (CSV)
        a. Subsections: Baro corrected through HOBOware, exported CSVs from Solinst

C. Categorization of processed and aggregated data
    i. Two subsections: AQUARIUS files, Consolidated data
    ii. AQUARIUS files (AQW)
        1. Sectioned into Conductivity and Drip files
        2. Holds information on preprocessing done in AQUARIUS
    iii. Consolidated data
        1. Output of aggregation done in AQUARIUS
        2. Same file naming conventions as mentioned above with the addition of resolution

a. Examples: full equals full resolution available (i.e. 10 minute intervals), daily equals daily sum for drips

D. Back-up, storage, and publication
   i. Scholar
      1. Recommended for backup of raw data
      2. Under resources subsection, divided into similar categories as detailed above
      3. Subsections currently applied may continue for future data
      4. This should be considered a temporary sharing location; not for long term storage or easy accessibility
   ii. VTech Works
      1. Recommended for publication and storage of annually aggregated data
      2. Long term storage ability and accessibility outside of institution
   iii. Dropbox
      1. Recommended for short term storage of data and easy accessibility between collaborators
      2. Not for long term storage or for primary copies of data
      3. Additional note—once you delete the file on the hosting/connecting PC, the file is deleted on drop box as well. In other words—do not delete any files from your computer that may be connected to dropbox until the files are backed up elsewhere
   iv. External hard drive
      1. Recommended for primary raw data storage
      2. Subsections outlined above should be utilized for organization
      3. External hard drive should reside with person primarily responsible for data management
   v. CUAHSI Hydroserver
      1. Recommended for final phase publication of minimally preprocessed data
      2. Metadata required and use of Observations Data Model (ODM) language
      3. Will meet requirements for future data dissemination

E. General outline (for sampling days and data offloads upon return from sampling)
   i. Offload data and backup
      1. Offload data from both shuttles
      2. Save and rename DTF files as defined above
      3. Move DTF files directly to external hard drive, or temporarily place in dropbox until files can be move to external hard drive
         a. *Temporary storage on dropbox should not exceed 1 week!

ii. Preprocessing of drip/air temp/RH data
    1. Open each DTF in HOBOware, check for errors
    2. Export as CSV and follow naming convention outline above
        a. Save copy of CSV on external hard drive and to scholar
        b. Temporary storage on dropbox is ok, but should not exceed 1 week
    3. Repeat steps 1 and 2 as necessary for temperature data
iii. Preprocessing of conductivity data and water temp
    1. Open each DTF in HOBOware
    2. Using Conductivity Assistant in HOBOware, do temp correction on conductivity
    3. Follow naming convention outlined above and export temperature corrected data with Tcorr suffix as CSV
        a. Save copy of CSV on external hard drive and to scholar
        b. Temporary storage on dropbox is ok, but should not exceed 1 week
iv. Preprocessing of stream data
    1. Open each water pressure transducer DTF in HOBOware
    2. Using the Barometric Compensation Assistant, correct the level file for barometric pressure
    3. Follow the naming convention above and export the baro corrected pressure transducer data as a CSV
        a. Save a copy of CSV on external hard drive and to scholar
        b. Temporary storage on dropbox is ok, but should not exceed 1 week
v. Overview of files generated for each sampling trip
    1. DTF files (~13 files)
        a. Drips: MS1, MS2, MS3, Surface
        b. Air Temp: MS1, MS2, MS3, Surface
            i. Surface temperature will likely be included in the drip/precip file
        c. Conductivity, Water temp: MS1, MS2, MS3, Stream
        d. Discharge: Stream level and baro
    2. CSV files (~12 files)
        a. Drips: MS1, MS2, MS3, Surface
        b. Air temp: MS1, MS2, MS3, Surface
            i. Surface temperature will likely be included in the drip/precip file
        c. Conductivity, water temp: MS1, MS2, MS3, Stream

i. Conductivity should be temperature corrected at this point, but temperature should remain in the exported file

d. Discharge: Stream baro corrected

F. Preprocessing for annual data dump
   i. Follow preprocessing as outlined in II above
   ii. Export a single year using the Export to File toolbox
   iii. Add to scholar compiled data as well as VTech works

Appendix C. Soil Analyses

Table A.1. Tabular chemical data from solid soil samples.

Sample ID	pH	Buffer pH	P (ppm)	K (ppm)	Ca (ppm)	Mg (ppm)	Zn (ppm)	Mn (ppm)	Cu (ppm)	Fe (ppm)	B (ppm)	Organic Matter Content %	Soluble Salts (ppm)	Cation Exchange Capacity (meq/100g)	% Acidity	% Base Saturation
S11A	5.31	6.19	8	181	390	98	1.4	8.9	0.4	11.4	0.3	3	294	4.5	28.0	72
S11B	6.16	6.39	7	91	369	320	0.6	5.4	0.2	7.1	0.1	1.2	64	4.8	1.3	98.7
S12A	4.96	6.22	3	196	388	86	1.6	11	0.6	13	0.3	3	269	4.2	25.4	74.6
S12B2	6.43	6.38	3	66	418	443	0.5	9.2	0.3	7.2	0.1	1.3	51	6	2.0	98
S22A	4.37	5.98	15	322	469	132	2.8	26.8	0.4	17	0.3	5	845	6.7	37.0	63
S22B	6.22	6.39	8	107	528	266	0.5	12.2	0.4	12.1	0.2	1.6	205	5.2	1.2	98.8
S23A	5.22	6.23	4	72	325	117	0.9	12.2	0.5	13.3	0.2	2	141	3.8	26.7	73.3
S23B	6.59	6.42	2	43	318	152	0.3	6.7	0.4	11.1	0.2	1	51	3	1.7	98.3
S23BB	7.14	N/A	40	45	645	389	0.4	14.2	0.3	18.4	0.1	1.1	38	6.5	N/A	100
S23BD	6.57	6.42	8	35	324	160	0.3	4.8	0.3	11.5	0.1	1	51	3.1	1.6	98.4
S23E	5.86	6.04	5	190	357	204	0.5	5.7	0.3	12.4	0.1	1.3	90	6.1	35.1	64.9
S31A	5.15	6.09	33	319	956	289	3.4	10.9	0.5	17	0.6	6.6	947	9.8	18.8	81.2
S31B	5.37	6.31	3	296	271	127	0.4	3.7	0.5	6.5	0.2	1.4	179	3.7	14.5	85.5
S31CB	7.58	N/A	169	37	1135	264	0.3	14.8	0.2	19.1	0.1	0.7	102	7.9	N/A	100
S32A	4.93	6.08	32	315	701	200	3.1	8.1	0.5	12.5	0.4	5.5	666	7.8	24.2	75.8
S32B1	6.45	6.48	3	160	282	216	0.4	1.1	0.5	5.3	0.2	1.8	128	3.6	1.1	98.9
S32BC	7.05	N/A	143	32	865	324	0.3	11.1	0.2	14.6	0.1	0.8	90	7.1	N/A	100

**Buffer pH and all elemental valuves are based on Mehlich-1 nutrient levels.

Appendix D. Site Specific Hydrographs

Data used to create these figures will be available on VTech Works (http://vtechworks.lib.vt.edu/) in May 2013.

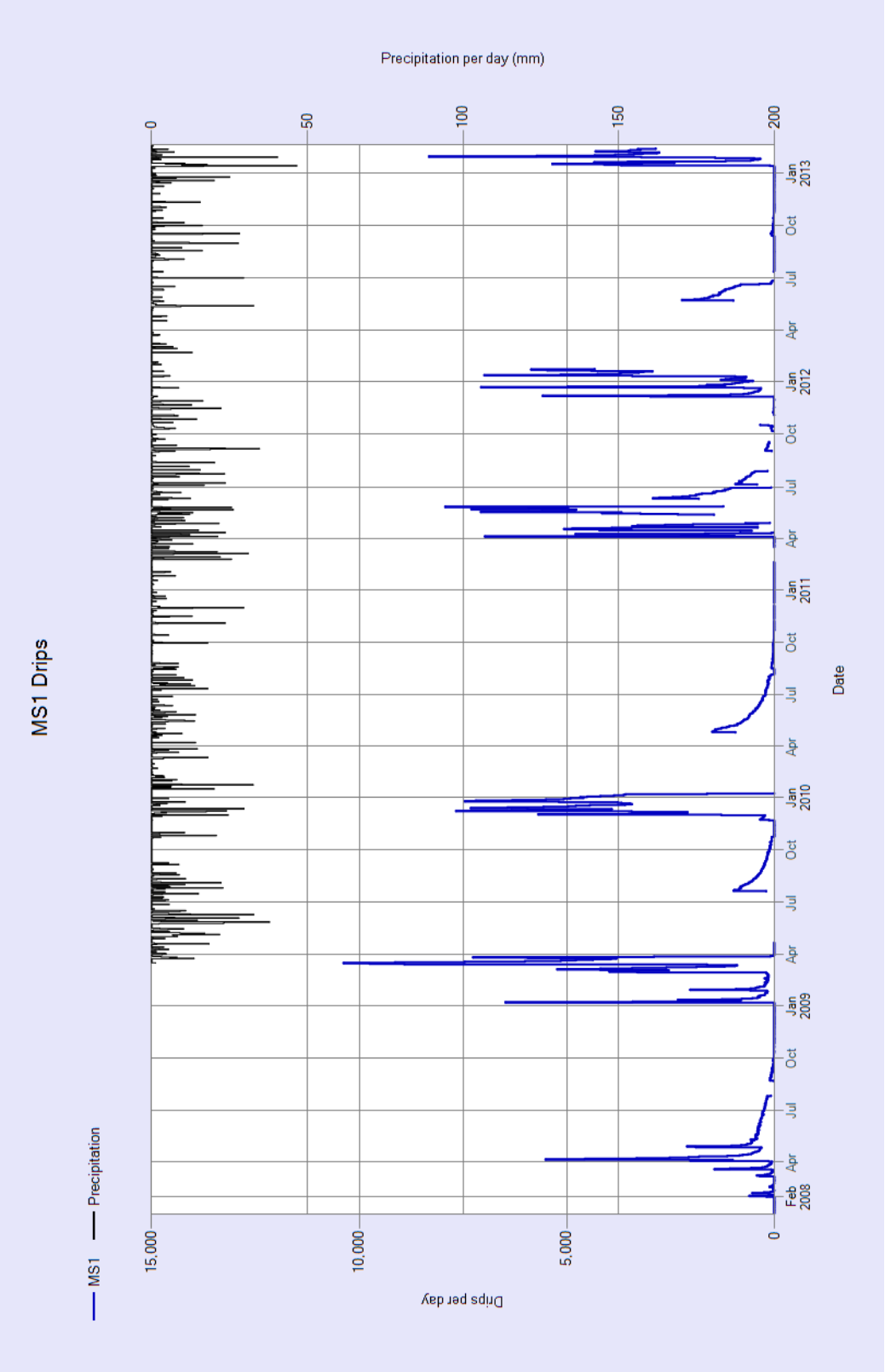

Figure A.1. Cave drip hydrograph for MS1.

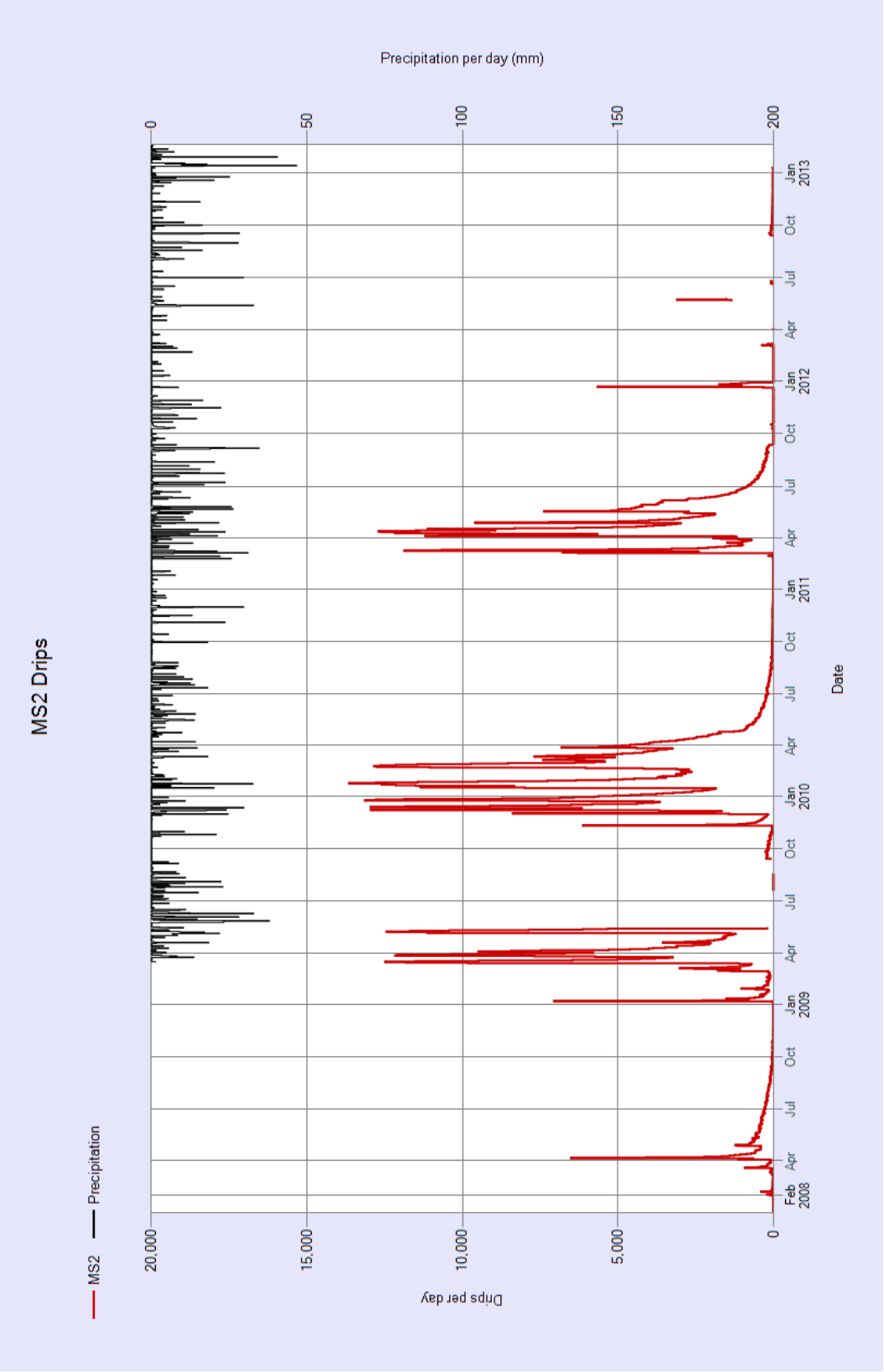

Figure A.2. Cave drip hydrograph for MS2.

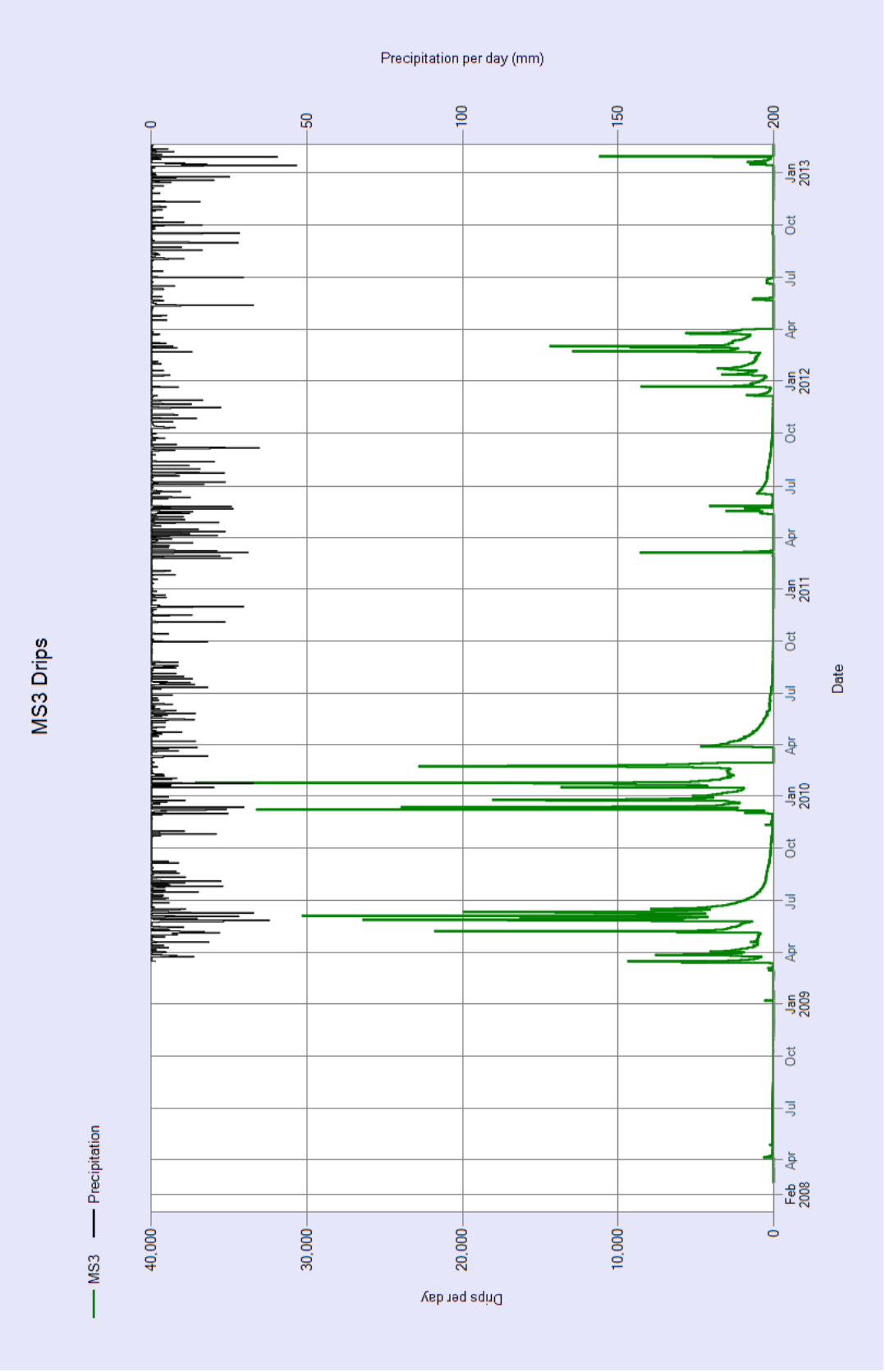

Figure A.3. Cave drip hydrograph for MS3.

Appendix E. Tabular Data for Discrete and Composite Geochemical Samples

Table A.2. Color coding for tabular data. These color codes pertain to highlighting in the other tables presented in this appendix.

Questionable Value
Missing Data
BDL: Below detection limit
NA: Not analyzed
No sample collected
Inflection point Method for ALK
BDL, approx at 1/2 MDL

Table A.3. Precipitation geochemical data.

	Cation concetrations					Anion concentrations				
Detection Limit	0.055	0.175	0.121	0.037	0.053	0.1	0.1	0.1		
Date	Ca+2 (mg/L)	K+ (mg/L)	Mg+2 (mg/L)	Na+ (mg/L)	Si+4 (mg/L)	Cl- (mg/L)	NO3 N (mg/L)	SO4-2 (mg/L)	Alk (HCO_3) (mg/L)	pH
06/26/08	1.380	0.310	0.194	0.626	0.077	0.561	0.391	1.734		
07/14/08	1.438	0.364	0.163	0.980	0.088	0.815	0.192	1.438	2.81	6.04
07/31/08	0.488	0.395	0.124	0.923	0.096	1.308	0.174	1.859	2.46	5.59
08/08/08	1.350	2.050	0.630	2.110	0.550					
09/04/08	0.446	0.376	0.081	0.519	0.114	0.480	0.167	2.924	0.56	6.22
10/10/08						2.200	0.900	4.400	4.22	5.81
11/04/08	6.654	8.257	2.270	6.904	1.809					
12/04/08									3.99	6.44
01/09/09	0.620	0.150	0.000	0.430	0.190	0.628	0.146	2.982	8.28	5.86
02/03/09										
03/04/09										
03/19/09										
04/14/09						0.398	0.335	2.957	4.93	5.60
05/14/09	0.347	1.650	0.090	1.504	0.067	0.398	0.156	2.433	6.77	6.67
06/19/09										
07/15/09										
08/14/09	1.607	0.263	0.394	2.176	0.219	0.202	0.120	0.985	1.04	5.75
09/14/09	4.243	0.542	0.366	0.827	0.267	0.567	0.282	3.142	9.52	6.87
10/23/09	0.518	0.435	0.127	0.666	0.336	0.299	0.124	1.959	2.67	5.90
11/23/09	0.322	0.181	0.122	0.554	0.189	0.298	0.109	2.772	4.93	5.45
12/15/09	0.198	0.106	0.049	0.471	0.137	0.110	0.055	1.017	4.93	5.73
01/23/10										
03/01/10	10.610	0.882	0.711	3.830	0.499					
03/29/10										
4/26/2010	0.587	0.398	0.148	2.265	0.141	0.599	0.267	2.064		
5/27/2010										
7/1/2010	1.849	3.309	0.463	0.719	0.210	0.529	1.856	3.795	2.22	5.36
8/2/2010										
8/16/2010	1.570	2.540	0.394	2.473	0.163				5.46	6.41
9/2/2010	0.727	4.837	0.203	0.392	0.206				3.59	5.59
9/30/2010	4.454	0.403	0.267	1.780	0.101	0.113	0.218	1.222	9.78	6.18
10/28/2010	1.385	0.493	0.195	0.767	0.089					
11/22/2010	1.041	0.173	0.217	1.508	0.175					
12/22/2010										
1/25/2011										
2/22/2011										
3/21/2011										
4/14/2011	1.905	0.294	0.101	0.880		1.012	0.814	4.739	0.18	4.39
5/16/2011						1.153	0.303	1.859	1.38	4.63
6/10/2011	0.950	0.357	0.090	0.339		0.745	0.402	2.176	2.31	4.58
7/5/2011	0.622	0.576	0.126	0.537		0.558	0.389	2.159	3.70	4.74
8/2/2011	1.126	0.265	0.113	2.096		0.543	0.206	2.003	2.96	4.37
9/2/2011	0.537	0.592	0.145	0.255		0.879	0.582	3.952	1.48	4.38
10/7/2011	0.286	0.293	0.058	0.338		0.756	0.649	2.547	1.66	5.03
11/4/2011	0.313	0.222	0.055	0.368		0.305	0.431	3.141	0.87	5.32
12/2/2011	0.215	0.131	0.039	0.278		0.628	0.590	2.165	1.39	4.67
1/4/2012	0.142	0.020	0.028	0.346		0.382	2.607	1.566	1.20	4.63
Min	0.14	0.02	0.00	0.26	0.07	0.11	0.06	0.99	0.18	4.37
Max	10.61	8.26	2.27	6.90	1.81	2.20	2.61	4.74	9.78	6.87
Mean	1.60	1.03	0.27	1.26	0.27	0.63	0.48	2.46	3.53	5.49
Median	0.84	0.39	0.14	0.74	0.18	0.56	0.29	2.17	2.81	5.59
Number of Analyses/detects	30.00	30.00	30.00	30.00	21.00	26.00	26.00	26.00	27.00	27.00
Standard Deviation	2.23	1.74	0.42	1.37	0.37	0.44	0.57	0.99	2.63	0.74
Coefficient of Variation	139.63	169.11	156.81	108.47	137.52	68.75	118.96	40.22	74.55	13.57

Table A.4. Soil entrance soil water geochemical data.

	Cation concentrations						Anion concentrations				
Detection Limit	0.055	0.175	0.121	0.037	0.053	0.004	0.1	0.1	0.1		
Date	Ca+2 (mg/L)	K+ (mg/L)	Mg+2 (mg/L)	Na+(mg/L)	Si+4(mg/L)	Sr+2(mg/L)	Cl- (mg/L)	NO3N (mg/L)	SO4-2 (mg/L)	Alk (HCO_3) (mg/L)	pH
08/14/09	29.297	71.065	13.587	12.204	16.138	0.250	39.663	17.318	59.526	34.31	6.80
10/23/09							53.172	6.260	90.244		
11/23/09	23.766	67.187	14.941	12.170	8.720	0.124	11.530	19.187	117.665	22.96	5.88
12/15/09	24.021	67.576	15.727	15.835	6.789	0.117	5.874	27.304	111.382	20.75	5.96
01/23/10	25.909	57.108	14.556	15.566	5.801	0.113	7.675	35.807	150.677		
03/29/10	16.897	51.989	10.144	13.116	5.337	0.069	5.594	25.426	126.973		
4/29/2010	17.034	53.679	9.711	11.643	7.497	0.072	11.718	28.144	133.512	19.24	6.04
2/22/2011	35.440	64.333	19.313	17.541		0.157	7.961	57.306	42.407		
3/21/2011											
4/14/2011	32.518	90.533	19.841	23.159		0.132	49.099	61.650	30.745		
5/16/2011	34.367	94.384	21.086	20.369		0.135	39.246	61.423	32.945		
6/10/2011	24.948	84.910	14.334	18.529		0.099	30.412	39.881	36.797		
1/4/2012	7.247	34.369	4.572	8.819	0.030		4.291	39.719	32.212	25.41	5.74
Min	7.25	34.37	4.57	8.82	0.03	0.07	4.29	6.26	30.74	19.24	5.74
Max	35.44	94.38	21.09	23.16	16.14	0.25	53.17	61.65	150.68	34.31	6.80
Mean	24.68	67.01	14.35	15.36	7.19	0.13	22.19	34.95	80.42	24.53	6.08
Median	24.95	67.19	14.56	15.57	6.79	0.12	11.62	31.98	74.89	22.96	5.96
Number of Analyses/detects	11.00	11.00	11.00	11.00	7.00	10.00	12.00	12.00	12.00	5.00	5.00
Standard Deviation	8.47	17.93	4.88	4.27	4.82	0.05	18.70	17.94	45.92	5.94	0.42
Coefficient of Variation	34.34	26.75	33.99	27.83	67.04	40.38	84.28	51.32	57.10	24.21	6.83

Table A.5. Soil 2 soil water geochemical data.

	Cation concentrations						Anion concentrations				
Detection Limit	0.06	0.18	0.12	0.04	0.05	0.00	0.10	0.10	0.10		
Date	Ca (mg/L)	K (mg/L)	Mg (mg/L)	Na (mg/L)	Si (mg/L)	Sr (mg/L)	Cl- (mg/L)	NO3N (mg/L)	SO4-2 (mg/L)	Alk (HCO_3) (mg/L)	pH
07/15/09	33.516	4.914	22.191	10.342	14.643	0.198	20.629	6.952	27.188	63.94	6.87
10/23/09							24.117	5.489	23.554		
12/15/09	23.607	2.072	23.295	10.294	8.549	0.108	13.433	0.512	90.632	61.68	6.88
01/23/10	25.160	2.880	21.978	12.504	7.739	0.117					
4/29/2010							13.010		33.665		
12/22/2010							24.923	7.565	21.768		
4/14/2011	27.920	2.604	29.638	16.681		0.115	18.096	30.955	29.660		
5/16/2011	25.174	1.923	25.627	12.893		0.099	15.039	12.980	28.786		
6/10/2011	23.877	1.978	25.110	11.866		0.095					
12/2/2011	117.462	25.056	68.747	33.367		0.547					
1/4/2012	77.661	6.646	76.561	24.235		0.322	27.635	1150.145	19.215		
Min	23.61	1.92	21.98	10.29	7.74	0.10	13.01	0.51	19.22	61.68	6.87
Max	117.46	25.06	76.56	33.37	14.64	0.55	27.64	1150.15	90.63	63.94	6.88
Mean	44.30	6.01	36.64	16.52	10.31	0.20	19.61	173.51	34.31	62.81	6.88
Median	26.55	2.74	25.37	12.70	8.55	0.12	19.36	7.56	27.99	62.81	6.88
Number of Analyses/detects	8.00	8.00	8.00	8.00	3.00	8.00	8.00	7.00	8.00	2.00	2.00
Standard Deviation	34.70	7.88	22.46	8.20	3.77	0.16	5.59	430.76	23.23	1.60	0.01
Coefficient of Variation	**78.33**	**131.07**	**61.28**	**49.66**	**36.60**	**79.93**	**28.52**	**248.26**	**67.70**	**2.54**	**0.10**

Table A.6. Soil 3 soil water geochemical data.

	Cation concentrations						Anion concentrations				
Detection Limit	0.055	0.175	0.121	0.037	0.053	0.004	0.1	0.1	0.1		
Date	Ca (mg/L)	K (mg/L)	Mg (mg/L)	Na (mg/L)	Si (mg/L)	Sr (mg/L)	Cl- (mg/L)	NO3 N (mg/L)	SO4 (mg/L)	Alk (HCO_3) (mg/L)	pH
07/15/09	45.904	27.872	33.157	14.472	12.904	0.386	55.196	16.797	41.237	80.81	6.40
08/14/09	23.389	19.859	30.678	8.627	9.672	0.204	47.425	12.154	36.645	48.85	6.53
09/14/09	19.897	17.259	30.471	7.733	7.450	0.149	47.773	13.877	34.341	35.96	6.88
10/23/09	18.371	16.220	29.179	6.252	6.841	0.135	47.692	13.450	27.743	46.64	6.46
11/23/09	32.221	18.318	25.830	8.819	7.558	0.223	36.602	11.040	46.574	69.53	6.69
12/15/09	23.368	26.987	28.228	10.118	4.439	0.148	45.814	22.694	31.268	31.72	6.49
01/23/10	23.556	22.764	28.495	11.466	3.259	0.152	63.995	33.038	46.579	30.99	6.32
4/29/2010	36.365	28.783	33.480	8.979	4.666	0.223	44.273	33.579	35.760	72.78	6.69
7/1/2010	24.843	25.387	30.514	11.165	6.455	0.143	46.279	26.192	30.355		
8/2/2010	21.415	22.510	29.605	19.103	7.399	0.140	49.101	20.081	30.810		
12/22/2010	21.250	22.179	23.685	16.038	6.341	0.130	34.872	21.187	27.683		
1/25/2011	32.514	20.480	24.461	11.749		0.199					
2/22/2011	22.759	23.659	23.834	12.478		0.137					
4/14/2011	26.595	31.805	26.951	13.246		0.149	29.130	36.137	31.321	32.66	6.74
5/16/2011	27.793	35.922	30.375	14.648		0.162	27.010	34.221	31.001		
6/10/2011	29.724	37.512	33.773	10.848		0.174	27.000	33.589	33.860	84.56	6.62
9/2/2011							44.413	33.207	33.975		
12/2/2011	27.913	31.025	18.655	10.588		0.174					
1/4/2012	17.715	23.131	20.532	11.015		0.104	21.303	131.293	38.428		
Min	17.72	16.22	18.66	6.25	3.26	0.10	21.30	11.04	27.68	30.99	6.32
Max	45.90	37.51	33.77	19.10	12.90	0.39	63.99	131.29	46.58	84.56	6.88
Mean	26.42	25.09	27.88	11.52	7.00	0.17	41.74	30.78	34.85	53.45	6.58
Median	24.20	23.40	28.84	11.09	6.84	0.15	45.11	24.44	33.92	47.75	6.58
Number of Analyses/detects	18.00	18.00	18.00	18.00	11.00	18.00	16.00	16.00	16.00	10.00	10.00
Standard Deviation	7.04	6.13	4.32	3.15	2.63	0.06	11.46	28.26	5.85	21.42	0.17
Coefficient of Variation	26.63	24.41	15.48	27.31	37.65	35.72	27.45	91.81	16.78	40.08	2.61

Table A.7. MS1 drip water geochemical data.

	Cation concentrations						Anion concentrations				
Detection Limit	0.055	0.175	0.121	0.037	0.053	0.004	0.1	0.1	0.1		
Date	Ca (mg/L)	K (mg/L)	Mg (mg/L)	Na (mg/L)	Si (mg/L)	Sr (mg/L)	Cl (mg/L)	NO3N (mg/L)	SO4 (mg/L)	Alk (HCO_3) (mg/L)	pH
06/26/08	44.903	25.915	14.441	3.629	12.968	0.510	37.455	0.319	18.238		
07/14/08											
07/31/08	71.719	24.211	16.134	4.167	14.240	0.560	45.475	14.286	19.785	76.79	7.80
08/08/08	46.330	17.810	13.820	10.760	13.160	0.470					
09/04/08	58.524	17.933	15.872	5.799	12.953	0.535	35.796	11.101	17.189		
10/10/08			17.811		10.763	13.157	44.000	2.200	17.900	136.01	7.54
11/04/08	47.068	22.231	13.457	11.492	15.528	0.447	32.871	3.294	17.363	138.95	7.74
12/04/08											
01/09/09	49.700	24.670	13.820	13.950	16.170	0.480	52.367	2.934	16.139	118.88	7.95
02/03/09							66.184	1.079	14.829		
03/04/09	54.470	39.880	15.230	20.990	20.180	1.510					
03/19/09											
04/14/09	51.200	13.560	15.780	5.750	12.280	0.440	35.414	5.402	18.783	192.15	7.35
05/14/09	52.615	5.452	16.702	3.479	7.420	0.457	24.033	5.193	20.620	139.48	7.50
06/19/09	54.798	2.699	16.956	3.125	5.662	0.432	23.777	8.161	18.193	164.45	7.40
07/15/09	59.982	6.252	18.526	8.972	7.962	0.479	29.470	1.976	18.213	177.30	7.70
08/14/09	59.470	6.684	18.329	4.055	7.968	0.487	24.495	2.142	17.029	143.77	7.31
09/14/09	58.516	6.870	17.652	3.573	8.024	0.483	20.672	2.658	17.955	146.89	7.85
10/23/09	50.219	6.090	15.787	2.963	8.102	0.425	19.966	3.510	14.730	171.96	7.52
11/23/09	50.195	5.952	15.692	3.000	6.722	0.422	20.795	5.082	19.772	76.94	6.99
12/15/09	52.569	2.717	16.664	3.265	5.602	0.412	23.070	7.775	19.080	130.70	6.84
01/23/10	57.200	3.366	18.596	3.601	5.709	0.470	35.665	12.006	30.111	129.02	7.31
03/01/10	57.612	4.046	17.795	3.937	6.057	0.466	41.180	12.630	31.684	109.72	7.16
03/29/10	54.220	3.812	16.958	3.201	5.891	0.436	39.566	12.212	30.005	133.08	7.37
4/26/2010	52.746	4.857	16.693	5.469	6.527	0.448	26.674	6.364	18.583	148.59	7.05
5/27/2010	60.343	6.420	17.026	3.444	7.615	0.453					
7/1/2010	61.340	6.775	17.206	6.023	6.799	0.460	22.394	2.569	15.576	160.61	7.84
8/2/2010	53.861	6.982	17.178	4.494	6.489	0.452	25.116	1.479	15.553	153.94	6.84
9/2/2010	52.561	0.906	15.454	2.212	4.990	0.358	13.525	6.167	12.309	123.66	7.73
9/30/2010	49.035	1.038	13.975	2.074	4.563	0.333	13.346	5.992	11.079	130.61	7.81
10/28/2010	54.538	1.501	15.808	2.349	5.100	0.377	14.935	6.090	11.962	132.06	7.68
11/22/2010	61.511	2.645	16.247	2.714	5.687	0.375	19.142	6.035	12.250		
12/22/2010	51.460	2.788	15.246	5.539	5.265	0.374	19.735	5.574	13.796		
1/25/2011	42.944	6.240	13.628	5.119	5.705	0.337	18.097	4.069	14.084	107.63	7.81
2/22/2011	40.083	4.126	12.372	5.802	5.952	0.310	14.800	5.191	13.838	98.24	7.65
3/21/2011	64.833	1.710	20.593	3.710	5.4	0.526	24.727	14.266	17.906	146.93	7.18
4/14/2011	58.160	1.652	19.247	3.448	5.393	0.428	24.201	14.641	16.122	147.28	7.13
5/16/2011	61.764	1.367	20.486	3.176	5.53	0.450	21.194	10.547	16.185	149.48	7.53
6/10/2011	62.540	0.960	19.895	2.844	6.089	0.449	20.833	11.259	15.672	143.74	7.30
7/5/2011	60.061	1.122	20.376	3.045	5.432	0.406	18.450	9.399	16.894	152.36	7.47
8/2/2011	62.226	1.025	19.621	2.837	5.206	0.418	18.538	9.342	18.438	182.19	7.57
9/2/2011	62.589	0.997	19.785	2.969	5.242	0.429	18.840	9.945	17.991	148.54	7.21
10/7/2011	61.193	1.083	20.337	2.965	5.403	0.430	18.409	13.633	23.500	166.91	7.62
11/4/2011	56.567	0.909	18.764	2.690	4.94	0.409	18.587	13.631	22.370	150.33	7.37
12/2/2011	47.149	0.744	15.757	2.270	4.495	0.361	16.719	12.031	19.627	102.73	7.41
1/4/2012	70.654	1.601	23.372	3.362	5.547	0.553	22.908	120.845	17.299	164.75	7.66
Min	40.08	0.74	12.37	2.07	4.50	0.31	13.35	0.32	11.08	76.79	6.84
Max	71.72	39.88	23.37	20.99	20.18	13.16	66.18	120.84	31.68	192.15	7.95
Mean	55.60	7.26	17.03	4.84	7.78	0.77	26.59	10.08	17.97	139.90	7.46
Median	54.80	4.05	16.83	3.48	6.00	0.45	22.99	6.13	17.63	143.77	7.50
Number of Analyses/detect	41.00	41.00	42.00	41.00	42.00	42.00	40.00	40.00	40.00	35.00	35.00
Standard Deviation	6.93	8.88	2.36	3.65	3.74	1.97	11.49	18.47	4.52	26.76	0.29
Coefficient of Variation	**12.46**	**122.35**	**13.86**	**75.53**	**48.12**	**256.35**	**43.21**	**183.30**	**25.18**	**19.13**	**3.90**

Table A.8. MS2 drip water geochemical data.

	Cation concentrations						Anion concentrations				
Detection Limit	0.055	0.175	0.121	0.037	0.053	0.004	0.1	0.1	0.1		
Date	Ca (mg/L)	K (mg/L)	Mg (mg/L)	Na (mg/L)	Si (mg/L)	Sr (mg/L)	Cl (mg/L)	NO3N (mg/L)	SO4 (mg/L)	Alk (HCO_3) (mg/L)	pH
06/26/08	68.065	1.614	18.657	3.622	5.138	0.715	16.649	9.944	19.430		
07/14/08											
07/31/08	70.096	1.330	18.360	4.261	5.191	0.717	16.872	9.873	19.755	95.76	7.39
08/08/08	68.540	2.750	18.560	4.770	5.680	0.730					
09/04/08	64.999	1.807	17.795	3.071	5.386	0.703	16.921	9.664	19.874	107.69	7.86
10/10/08	68.543	2.750	18.561	4.771	5.684	0.733	19.600	9.400	22.600	168.49	7.39
11/04/08	66.629	2.067	18.358	5.304	5.890	0.746	19.465	7.519	19.541	173.70	7.06
12/04/08	65.150	1.870	19.020	3.980	5.700	0.790	19.597	10.811	20.962	296.87	7.91
01/09/09	57.410	1.850	18.890	3.490	5.580	0.780	17.371	9.318	18.638	175.63	7.79
02/03/09	63.410	1.070	17.690	3.700	4.920	0.730	17.800	9.422	19.065	144.27	7.65
03/04/09	82.970	1.750	21.510	4.020	7.340	0.850	17.312	9.695	18.065	151.76	7.50
03/19/09	65.650	1.310	16.920	3.160	4.990	0.690	17.347	9.795	18.173	165.74	7.45
04/14/09	65.510	1.150	17.440	3.040	4.930	0.680	18.038	9.766	18.221	161.86	7.51
05/14/09	64.323	1.073	17.096	2.843	5.179	0.645	17.733	10.188	20.959	163.13	7.84
06/19/09	66.263	1.119	17.092	3.116	4.892	0.651	19.788	9.745	18.723	173.34	7.50
07/15/09	75.539	1.391	18.090	6.191	5.629	0.666	20.303	9.853	20.543	136.96	7.32
08/14/09	73.562	1.962	18.912	3.892	5.339	0.689	20.949	9.773	19.139	182.37	7.40
09/14/09	73.370	2.090	19.203	4.292	5.297	0.714	19.799	10.238	21.336	196.75	7.85
10/23/09	64.606	1.552	18.229	3.249	5.472	0.710	18.900	9.379	18.097	188.46	7.51
11/23/09	64.235	1.549	18.346	4.918	5.229	0.712	18.310	9.752	20.836	185.65	6.94
12/15/09	63.432	3.026	18.107	4.990	5.262	0.701	18.835	9.654	20.099	173.30	7.17
01/23/10	64.727	0.701	17.822	4.377	4.806	0.659	28.610	12.599	30.413	190.04	7.60
03/01/10	65.832	1.101	17.438	3.380	5.184	0.680	31.869	13.608	32.339	158.38	7.25
03/29/10	67.670	0.709	17.492	4.847	4.881	0.663	36.966	14.994	28.348	85.22	7.44
4/26/2010	68.042	1.918	17.280	3.942	4.934	0.658	26.616	11.159	19.106	168.87	7.06
5/27/2010	72.443	1.464	17.287	3.354	5.070	0.660					
7/1/2010	77.318	2.697	17.106	3.665	4.856	0.660	23.674	12.521	17.569	164.24	7.52
8/2/2010	69.990	3.573	18.580	3.743	4.892	0.683	26.671	9.719	17.471	127.99	7.49
9/2/2010	65.636	1.680	17.879	3.130	4.922	0.648	23.958	10.248	17.668	139.65	7.72
9/30/2010	62.325	1.655	17.958	3.283	4.885	0.646	24.153	10.347	18.107	117.90	7.83
10/28/2010	57.760	1.875	18.078	3.542	4.968	0.667	22.840	9.367	16.992	147.85	7.90
11/22/2010	63.585	2.135	17.900	3.890	4.893	0.661	23.257	9.761	17.538		
12/22/2010	56.933	1.746	17.039	5.481	4.599	0.664	24.732	10.063	18.336		
1/25/2011	52.044	1.847	16.913	4.954	4.636	0.663	22.251	10.562	19.022	88.37	7.76
	51.133	1.033	16.691	3.647	4.896	0.634	22.018	11.211	19.022	98.87	7.35
3/21/2011	67.837	1.376	18.548	3.766	5.244	0.620	27.342	12.727	17.727	157.43	7.68
4/14/2011	66.186	1.443	18.609	3.761	5.18	0.600	27.704	13.810	17.386	172.78	7.48
5/16/2011	67.254	1.395	19.050	3.884	5.404	0.600	27.459	13.065	16.351	134.86	7.58
6/10/2011	66.249	0.879	18.174	3.658	5.211	0.620	28.073	14.536	16.532	132.39	7.11
7/5/2011	67.650	1.196	19.513	3.473	5.134	0.621	25.782	13.159	16.732	139.42	7.07
8/2/2011	69.981	1.189	18.924	3.302	4.923	0.644	27.462	13.963	18.136	165.41	7.29
9/2/2011	71.035	1.140	18.911	3.491	4.873	0.641	26.554	13.700	28.789	140.05	7.50
10/7/2011	71.393	1.261	19.895	3.262	4.89	0.649	26.042	19.490	23.483	160.56	7.27
11/4/2011	69.413	1.172	19.794	3.483	5.033	0.659	31.951	23.859	24.096	142.46	7.67
12/2/2011	65.250	1.099	19.485	3.342	4.888	0.643	27.136	20.196	25.242	129.90	7.65
1/42012	73.621	1.390	20.203	3.559	5.131	0.645	28.151	134.088	17.104	143.11	7.48
Min	51.13	0.70	16.69	2.84	4.60	0.60	16.65	7.52	16.35	85.22	6.94
Max	82.97	3.57	21.51	6.19	7.34	0.85	36.97	134.09	32.34	296.87	7.91
Mean	66.75	1.62	18.30	3.89	5.18	0.68	23.09	14.48	20.18	153.69	7.49
Median	66.26	1.46	18.23	3.67	5.13	0.66	22.84	10.24	19.02	157.91	7.50
Number of Alyses/detects	45.00	45.00	45.00	45.00	45.00	45.00	43.00	43.00	43.00	40.00	40.00
Standard Deviation	5.89	0.61	0.99	0.74	0.44	0.05	4.91	18.95	3.77	36.45	0.25
Coefficient of Variation	**8.82**	**37.61**	**5.43**	**19.02**	**8.55**	**7.36**	**21.27**	**130.87**	**18.66**	**23.72**	**3.40**

Table A.9. MS3 drip water geochemical data.

	Cation concentrations						Anion concentrations				
Detection Limit	0.055	0.175	0.121	0.037	0.053	0.004	0.1	0.1	0.1		
Date	Ca (mg/L)	K (mg/L)	Mg (mg/L)	Na (mg/L)	Si (mg/L)	Sr (mg/L)	Cl (mg/L)	NO3-N (mg/L)	SO4 (mg/L)	Alk (HCO_3) (mg/L)	pH
06/26/08	86.055	5.640	27.153	5.692	4.821	0.855	55.555	28.421	21.609		
07/14/08											
07/31/08	96.428	5.742	27.746	7.315	5.240	0.877	58.479	34.250	22.456	80.20	7.72
08/08/08	95.070	9.050	24.080	16.570	12.520	0.710					
09/04/08	87.817	7.589	27.277	6.605	5.643	0.832	60.783	28.608	19.068	86.51	7.94
10/10/08	95.073	9.049	24.083	16.569	12.516	0.706	85.400	16.300	21.100		
11/04/08	72.482	39.368	25.179	17.135	10.514	0.749	100.010	0.175	21.936	219.97	7.98
12/04/08											
01/09/09	75.180	56.130	24.020	23.800	11.350	0.730	135.311	2.039	9.229	117.84	8.29
02/03/09							147.390	2.932	10.399		
03/04/09											
03/19/09											
04/14/09	86.350	6.130	26.310	6.160	5.340	0.900	58.938	28.756	21.508	139.37	7.40
05/14/09	85.041	1.974	26.428	4.542	4.717	0.910	52.522	31.467	24.269	140.43	7.63
06/19/09	85.173	2.223	27.380	4.847	4.928	0.877	59.658	28.249	23.333	132.70	7.63
07/15/09	96.584	2.629	29.941	6.256	5.808	0.876	52.142	27.455	24.167	146.57	7.40
08/14/09	101.661	2.457	31.417	6.901	5.488	0.946	52.802	29.046	23.879	163.17	7.45
09/14/09	101.940	3.560	31.769	5.827	6.161	0.919	47.773	13.877	32.341	161.65	7.45
10/23/09	88.944	4.150	30.553	5.620	6.303	0.889	56.490	26.450	20.898	151.88	7.60
11/23/09	82.486	4.459	29.518	6.189	6.044	0.857	53.731	26.106	23.502	153.75	7.30
12/15/09	89.058	3.073	29.096	5.472	5.362	0.901	55.848	25.588	23.245	218.40	7.46
01/23/10	88.178	2.097	27.691	4.974	5.002	0.911	75.883	33.354	37.422	154.70	7.53
03/01/10	89.194	2.229	27.057	5.319	5.304	0.902	87.733	35.800	31.065	131.40	7.48
03/29/10	84.285	1.936	25.931	4.808	4.833	0.846	81.248	34.160	40.985	109.47	7.46
4/26/2010	85.357	1.733	27.875	4.824	5.403	0.723	54.136	23.407	24.343	204.73	7.31
5/27/2010	94.518	1.721	26.327	5.043	4.717	0.810					
7/1/2010	94.402	2.314	26.366	6.223	4.797	0.811	55.546	24.805	21.049	154.03	7.65
8/2/2010	86.729	1.732	27.414	5.962	4.862	0.796	56.323	22.614	20.663	136.68	7.33
9/2/2010	80.995	1.582	27.265	4.916	5.922	0.664	43.317	19.447	17.656	149.22	7.79
9/30/2010											
10/28/2010	71.100	1.488	25.375	4.461	5.402	0.630	45.739	20.788	19.346	135.54	7.84
11/22/2010	77.084	1.289	26.113	4.255	5.132	0.608	46.421	21.482	19.180		
12/22/2010	70.333	1.021	23.783	5.981	4.807	0.628	45.685	20.762	18.656		
1/25/2011	70.307	1.406	23.602	4.867	5.478	0.632	41.937	22.668	19.881	78.03	7.59
2/22/2011	73.673	1.449	23.810	5.093	5.859	0.659	44.475	23.548	20.848	106.03	7.55
3/21/2011	80.026	2.138	28.480	4.678	5.826	0.615	61.802	26.469	26.369	144.47	7.89
4/14/2011	81.150	2.461	25.957	5.015	5.798	0.784	57.399	26.225	25.495	125.84	7.54
5/16/2011	84.961	1.809	28.174	4.808	6.029	0.688	51.871	22.813	21.404	151.63	7.66
6/10/2011	87.244	1.629	25.065	4.855	5.953	0.836	53.387	26.623	21.610	140.21	7.19
7/5/2011	87.609	1.778	29.565	4.962	5.517	0.754	51.534	24.199	22.327	163.09	7.15
8/2/2011	95.208	1.889	30.276	5.003	5.525	0.865	53.475	26.850	22.545	159.78	7.24
9/2/2011	98.952	2.101	31.867	6.143	8.35	0.879	61.461	30.749	23.987	169.49	7.65
10/7/2011	89.915	1.683	31.750	5.022	5.168	0.801	51.575	37.687	28.619	174.97	7.78
11/4/2011	84.385	1.664	31.576	4.965	4.958	0.754	52.091	38.825	29.531	77.76	7.79
12/2/2011	77.394	1.506	30.097	4.650	4.827	0.691	51.956	37.353	30.591	145.40	7.62
1/4/2012	86.368	1.731	32.131	4.596	6.302	0.627	49.595	179.297	20.927	175.47	7.76
Min	70.31	1.02	23.60	4.26	4.72	0.61	41.94	0.18	9.23	77.76	7.15
Max	101.94	56.13	32.13	23.80	12.52	0.95	147.39	179.30	40.99	219.97	8.29
Mean	86.12	5.14	27.64	6.67	6.11	0.79	61.73	28.97	23.27	144.13	7.59
Median	86.36	2.10	27.33	5.07	5.48	0.81	54.14	26.45	22.33	145.98	7.60
Number of Alyses/detects	40.00	40.00	40.00	40.00	40.00	40.00	39.00	39.00	39.00	34.00	34.00
Standard Deviation	8.41	10.29	2.57	4.18	2.02	0.10	22.58	26.23	5.90	34.63	0.24
Coefficient of Variation	**9.77**	**200.10**	**9.28**	**62.60**	**33.06**	**13.12**	**36.58**	**90.56**	**25.36**	**24.03**	**3.22**

Appendix F. Boxplots for Discrete and Composite Geochemical Samples

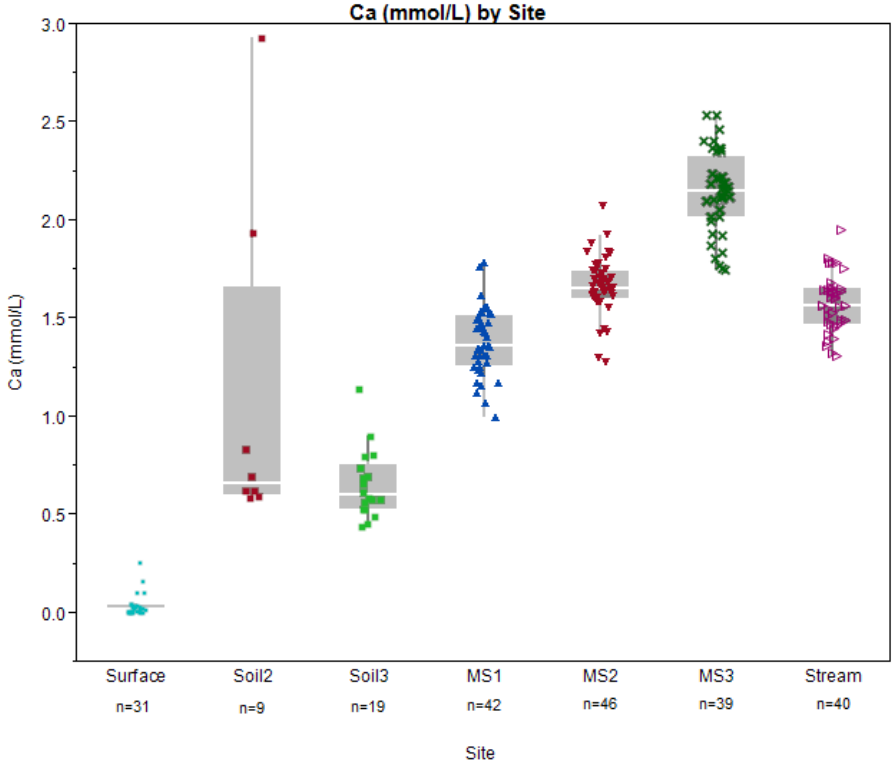

Figure A.4. Calcium concentration boxplot.

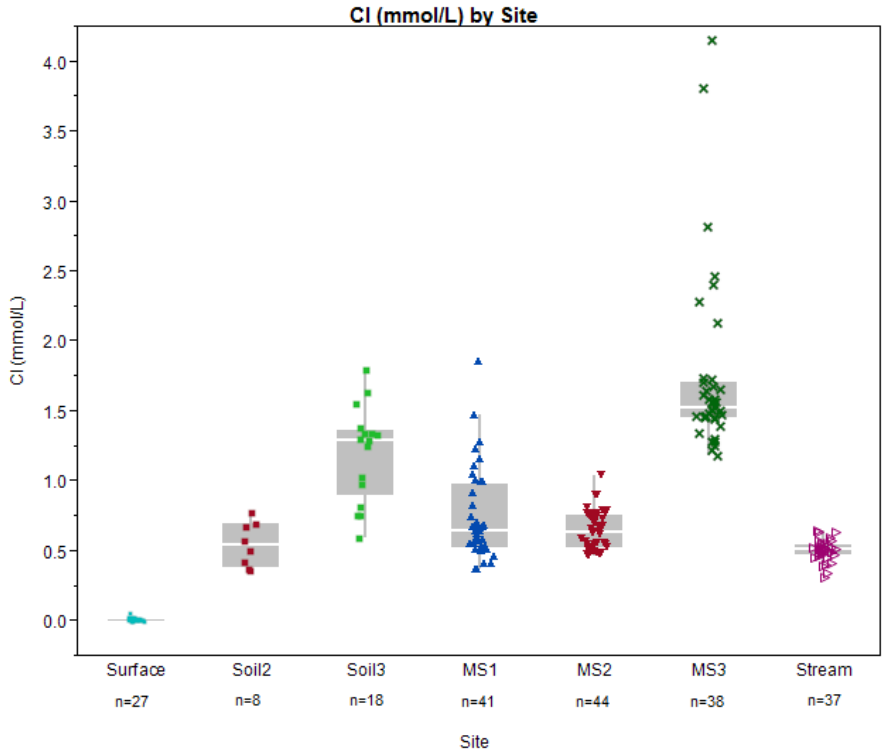

Figure A.5. Chloride concentation boxplot.

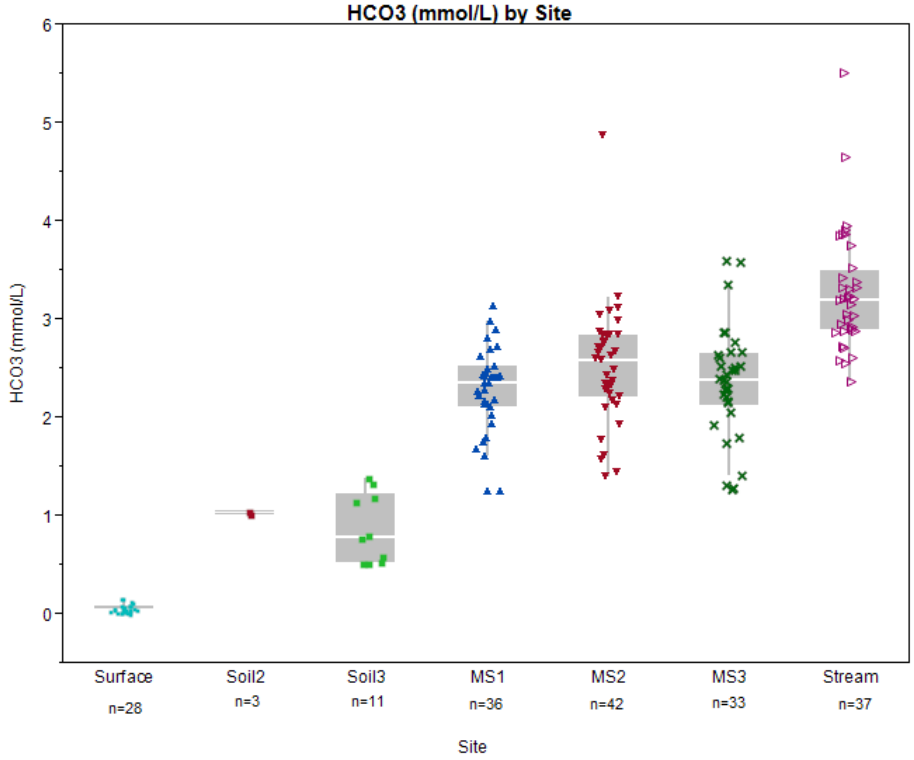

Figure A.6. Bicarbonate concentration boxplot.

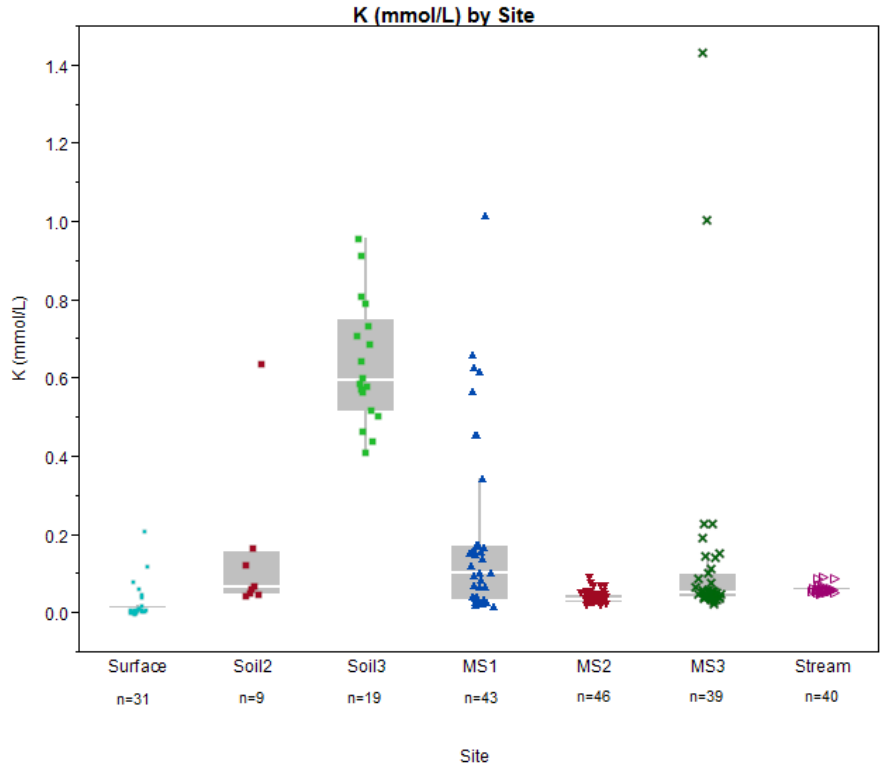

Figure A.7. Potassium concentration boxplot.

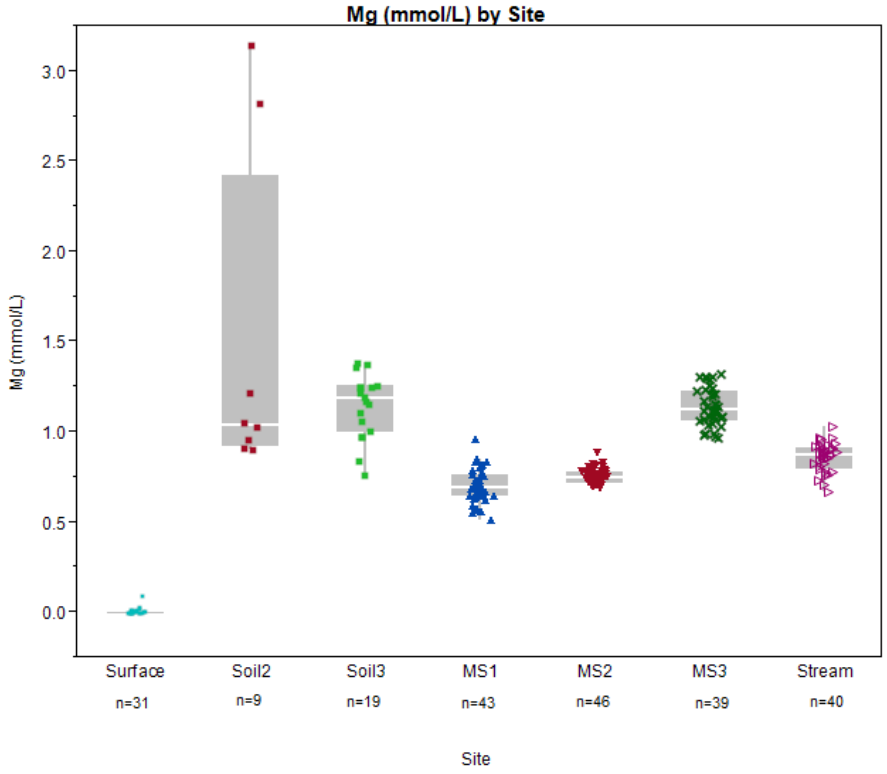

Figure A.8. Magnesium concentration boxplot.

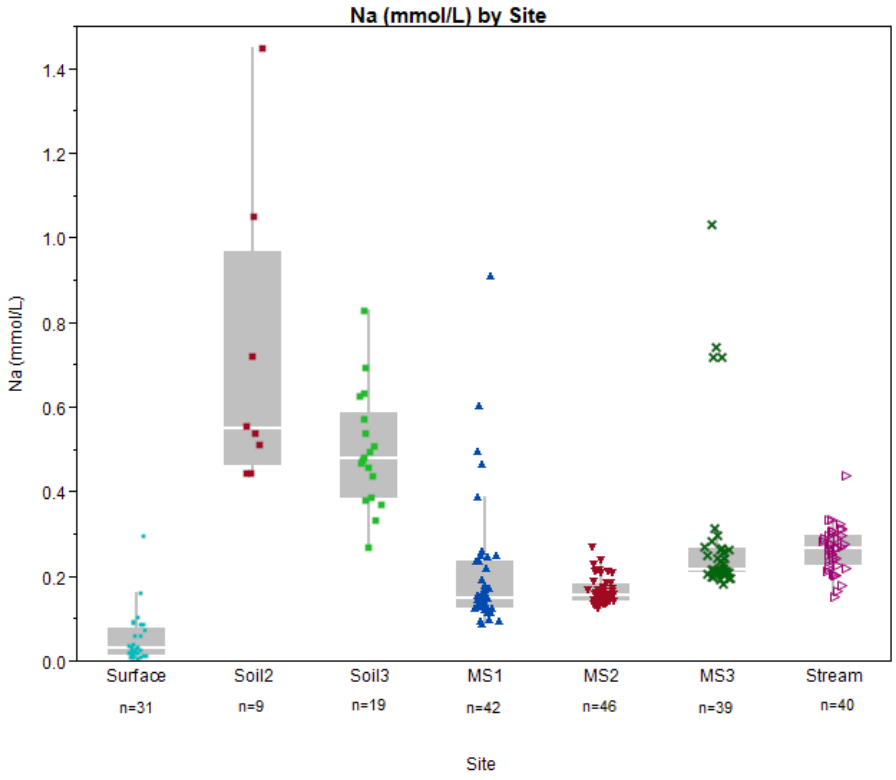

Figure A.9. Sodium concentration boxplot.

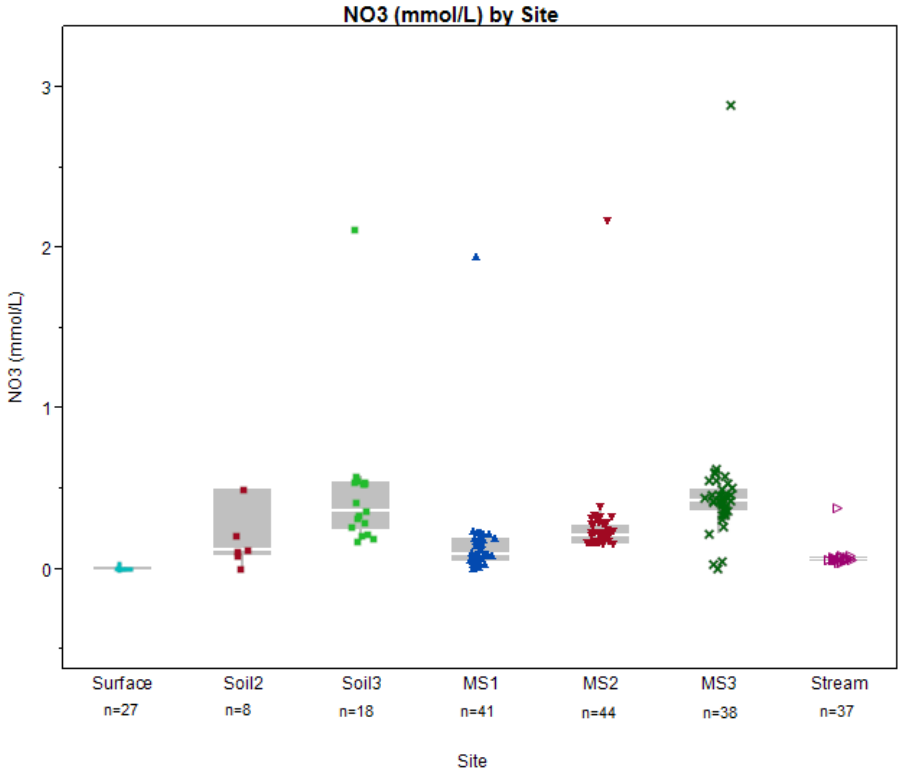

Figure A.10. Nitrate concentration boxplot.

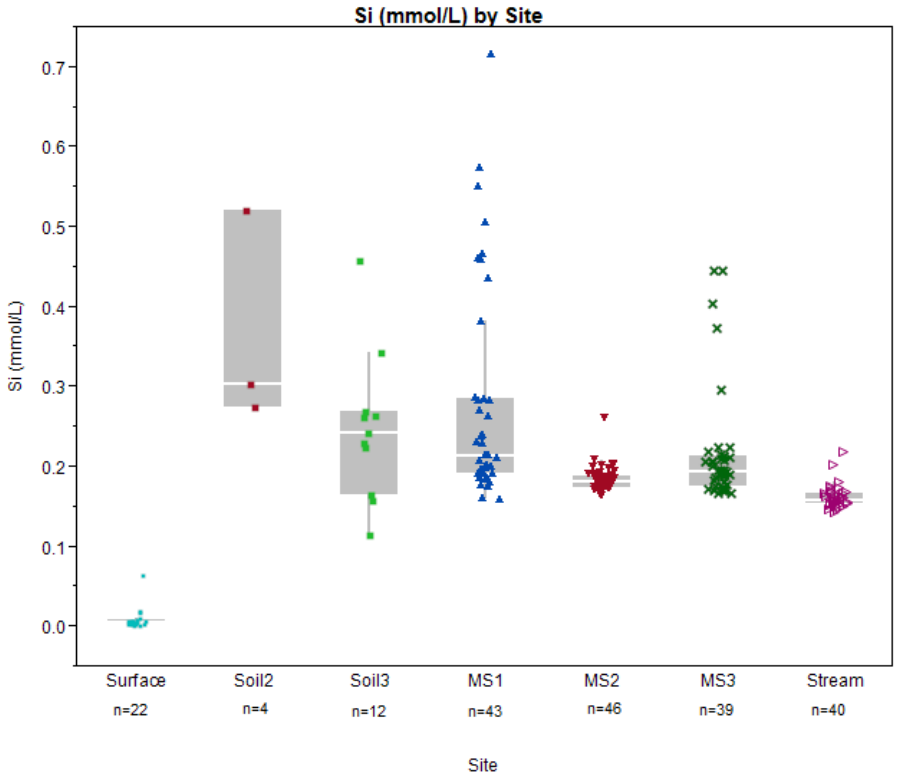

Figure A.11. Silica concentration boxplot.

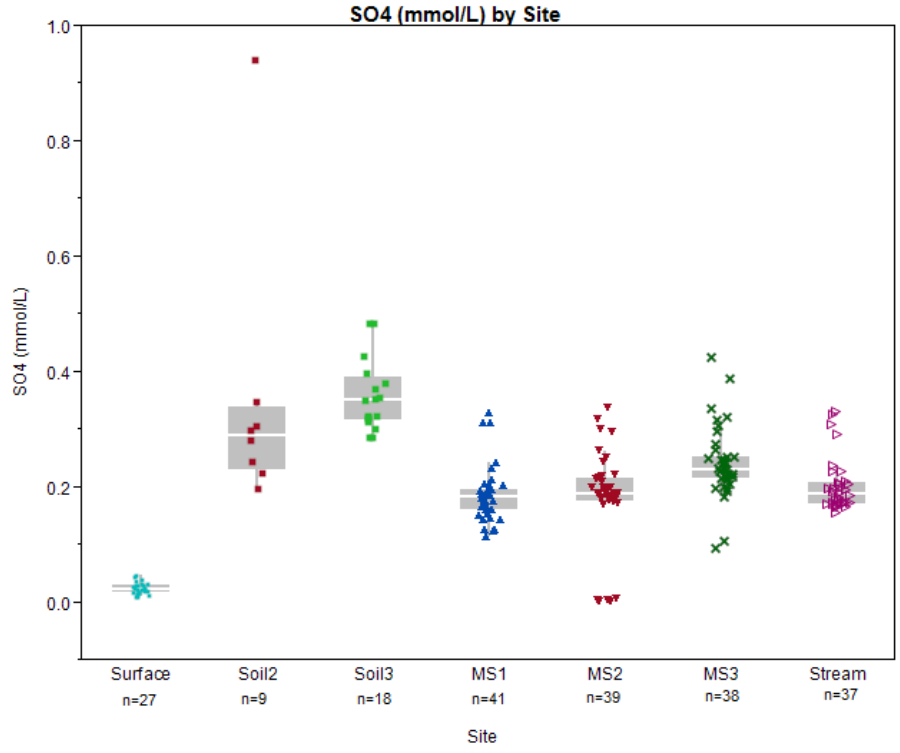

Figure A.12. Sulfate concentration boxplot.

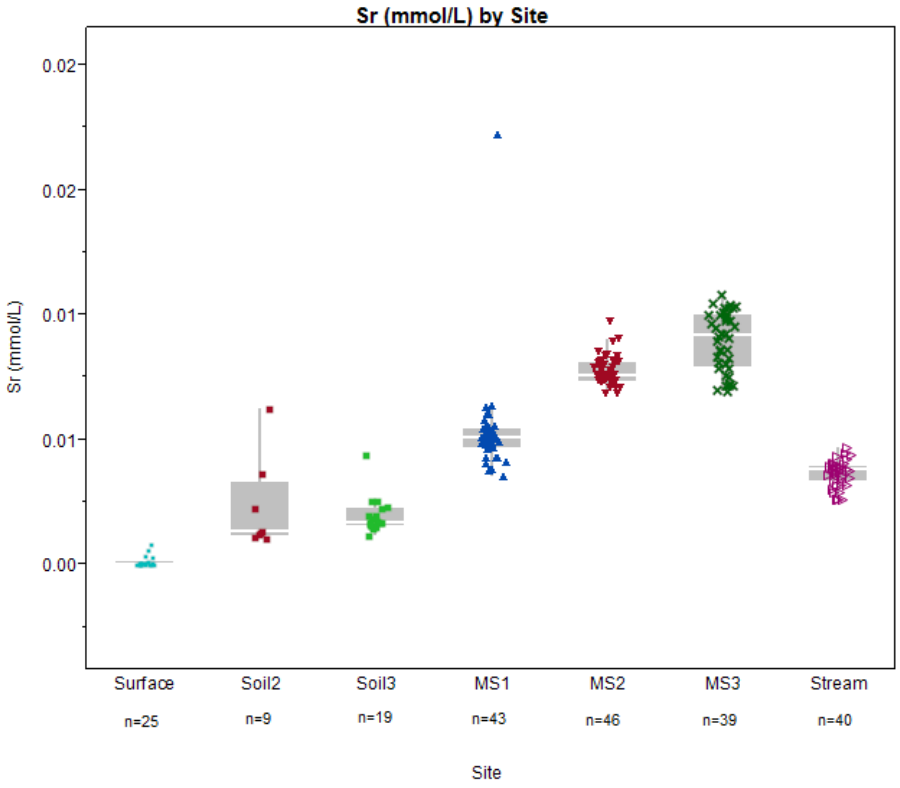

Figure A.13. Strontium concentration boxplot.

Appendix G. Analyte Concentrations by Site and Through Time of Discrete and Composite Geochemical Samples

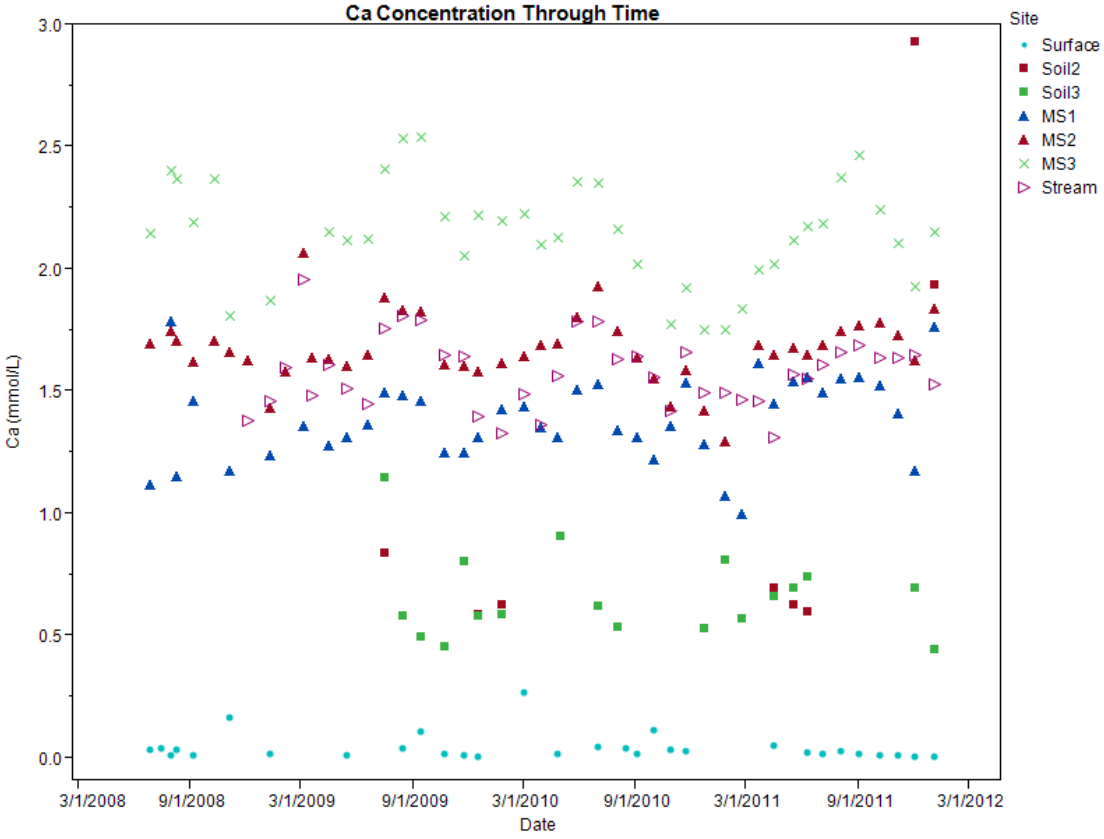

Figure A.14. Calcium concentration through time.

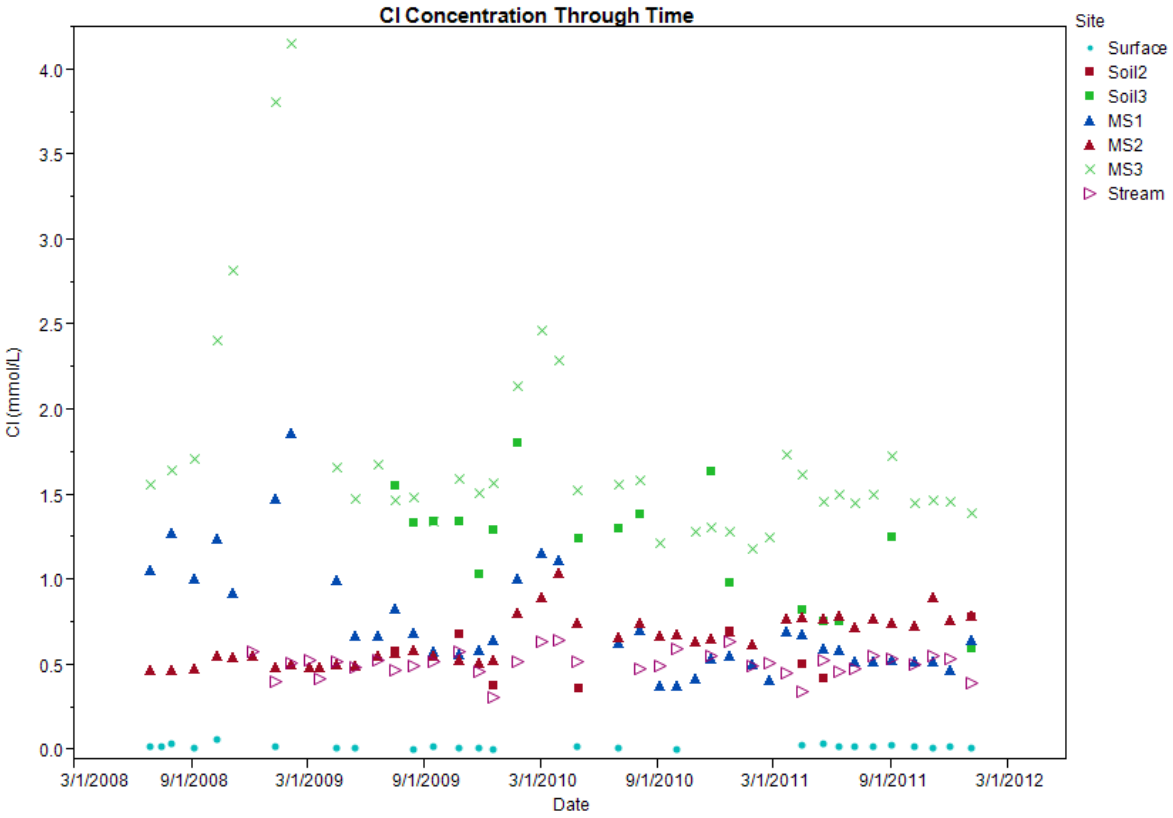

Figure A.15. Chloride concentration through time.

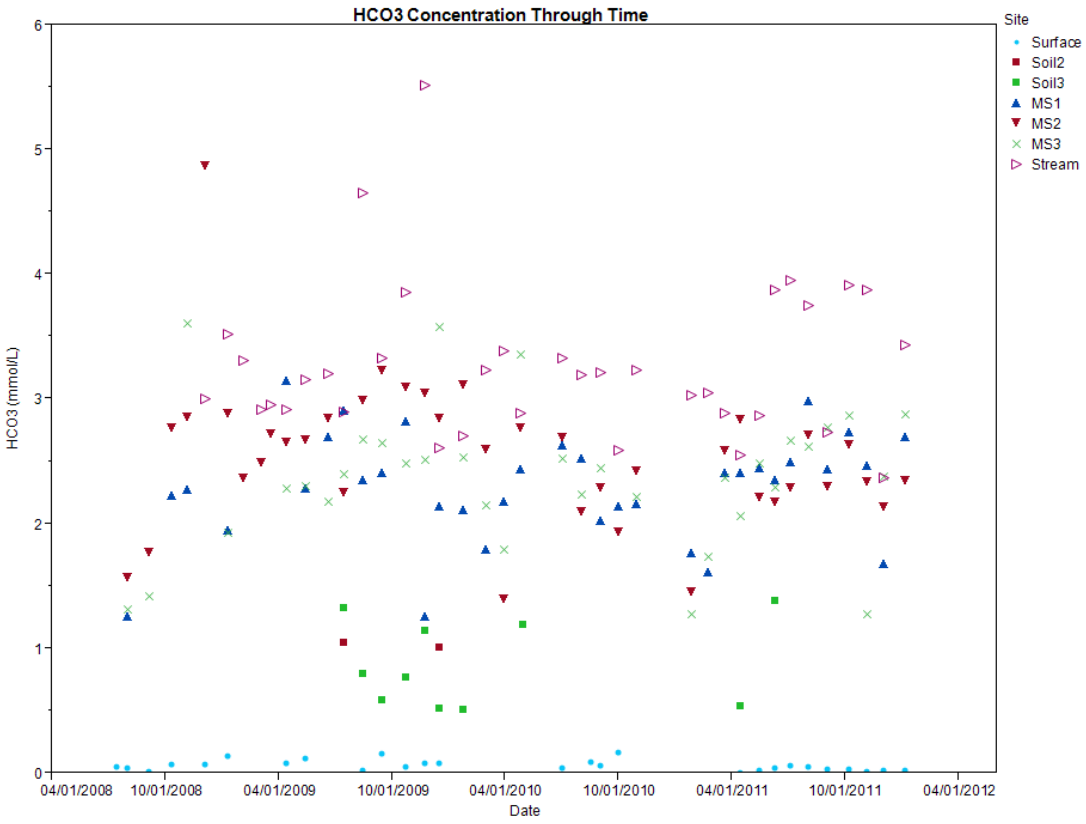

Figure A.16. Bicarbonate concentration through time.

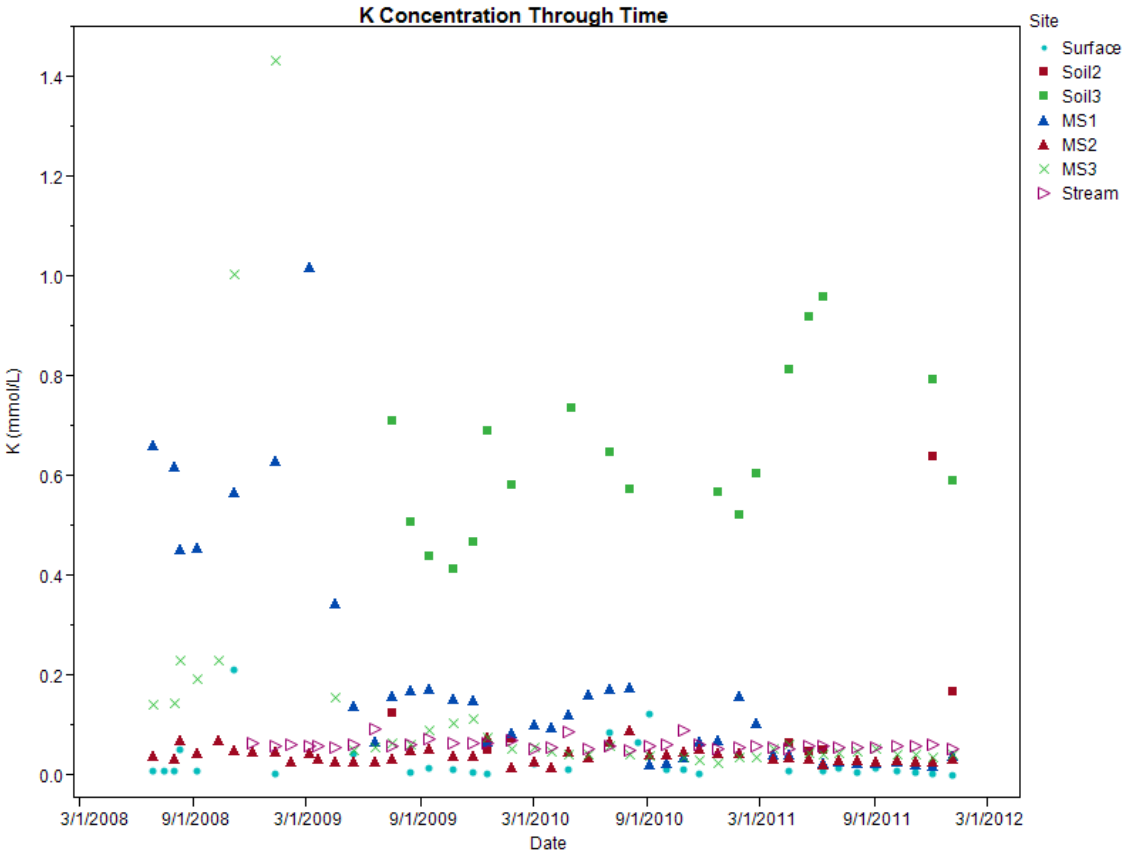

Figure A.17. Potassium concentration through time.

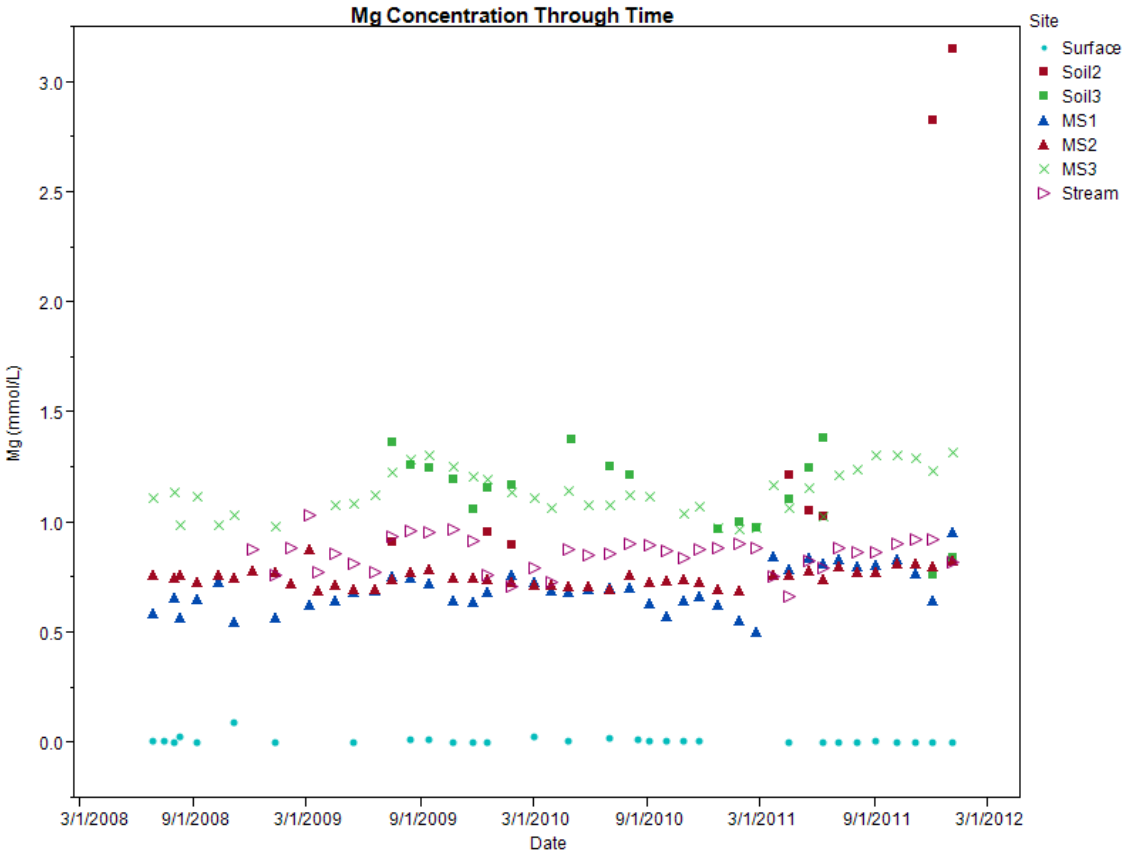

Figure A.18. Magnesium concentration through time.

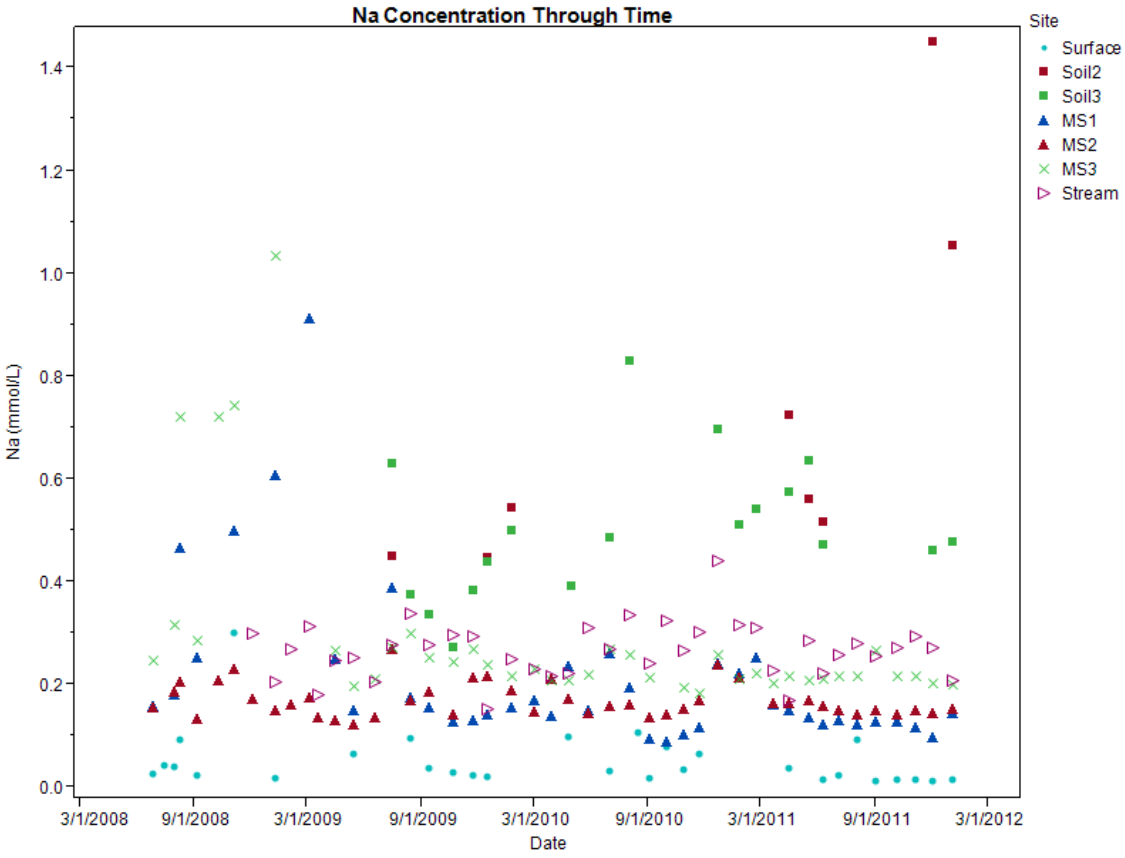

Figure A.19. Sodium concentration through time.

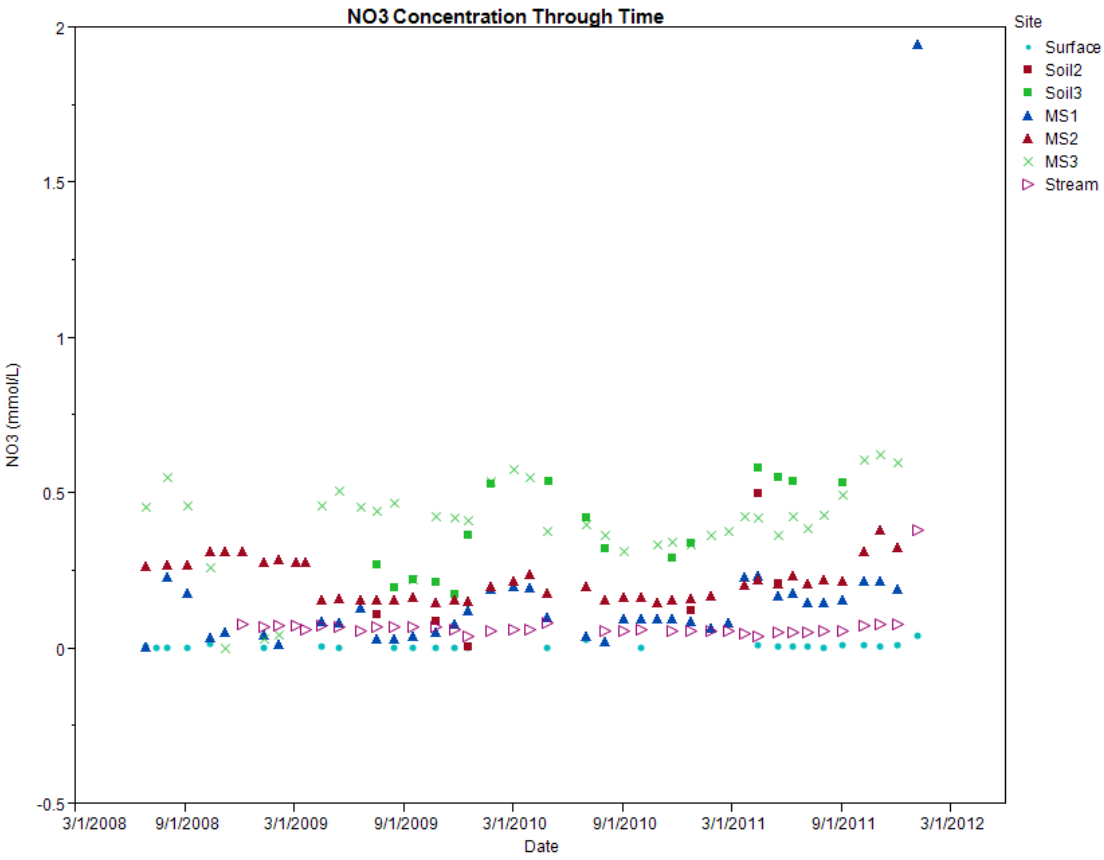

Figure A.20. Nitrate concentration through time.

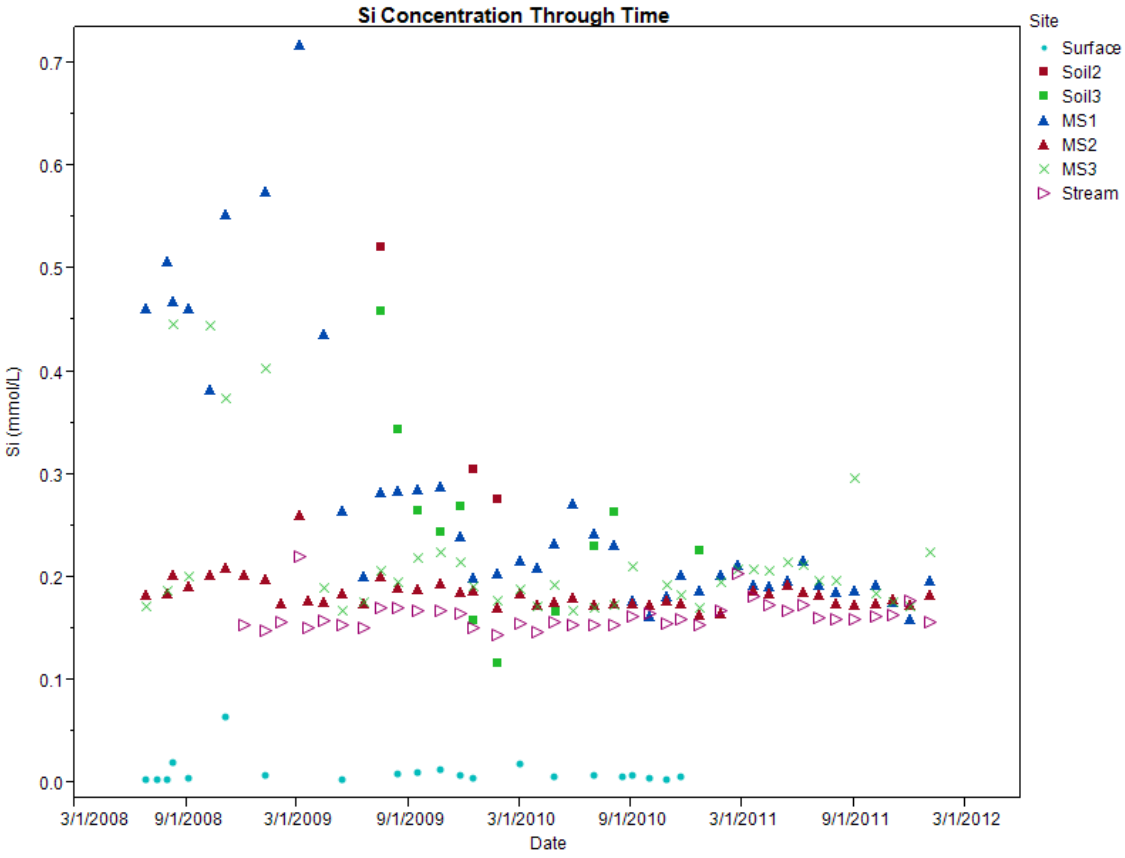

Figure A.21. Silica concentration through time.

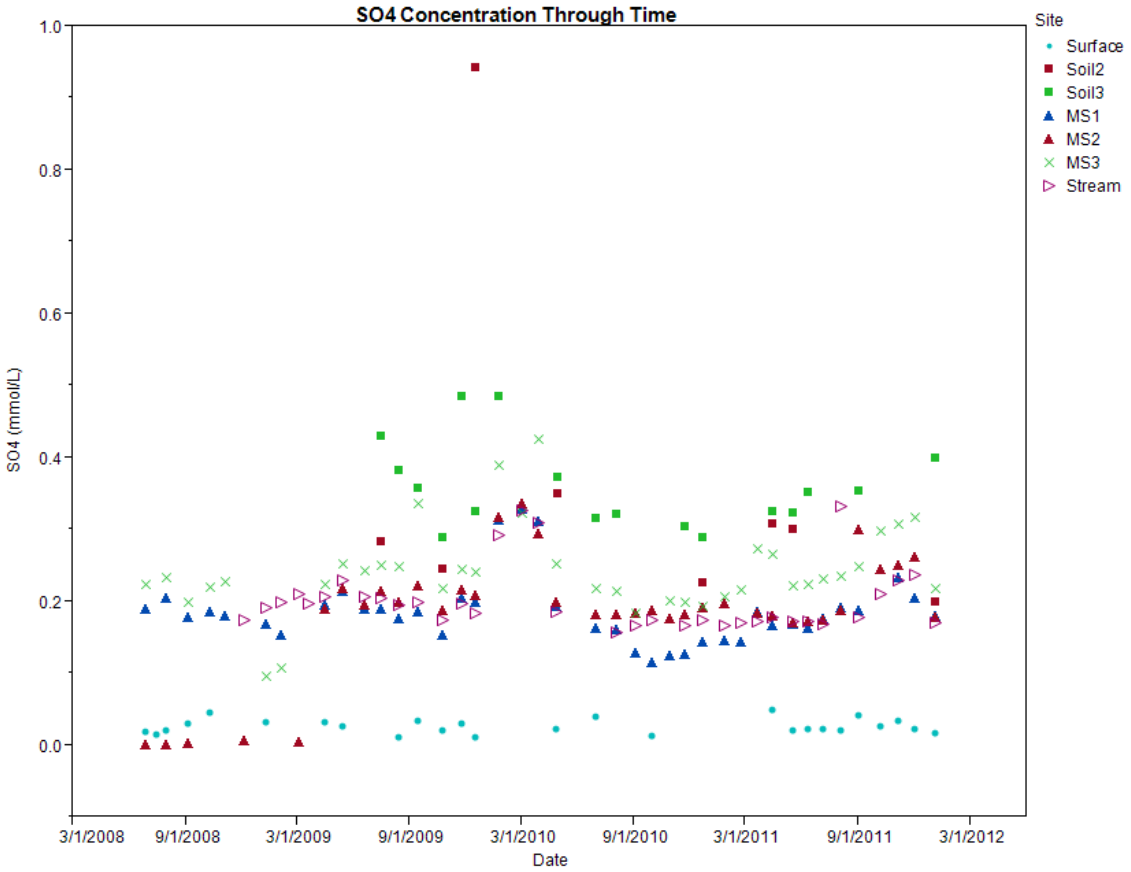

Figure A.22. Sulfate concentration through time.

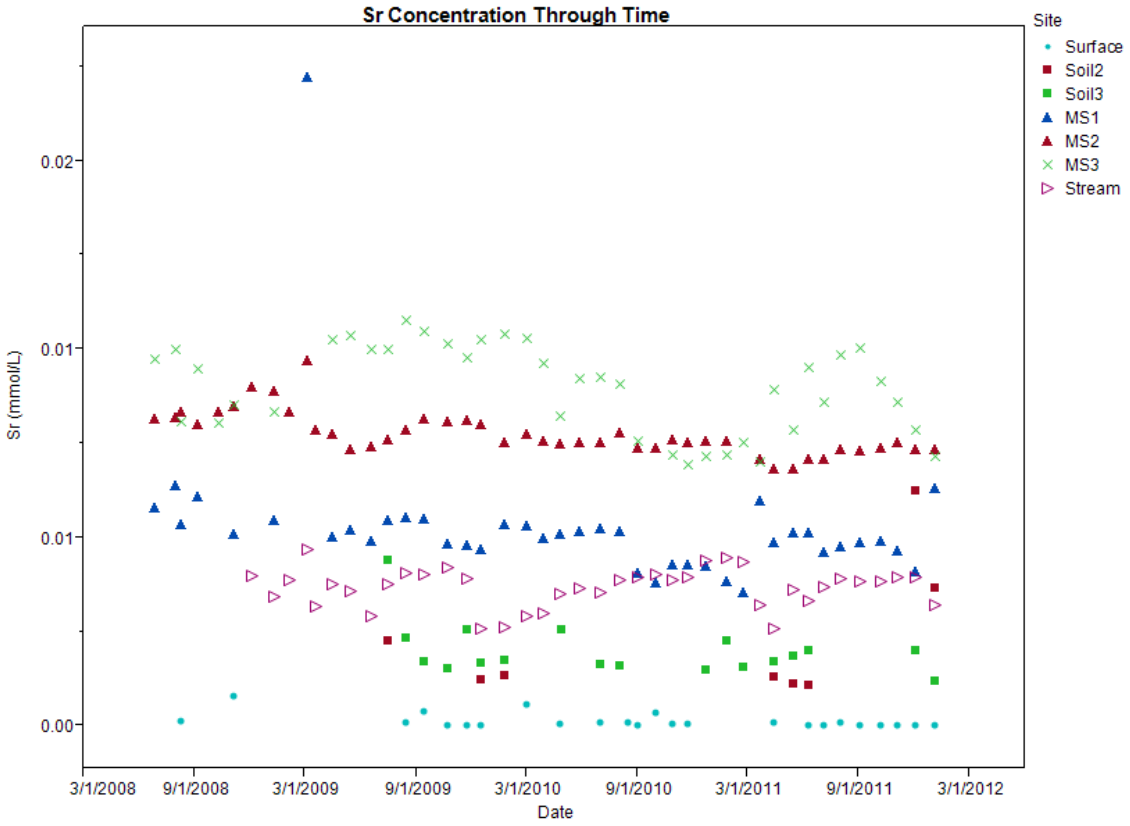

Figure A.23. Strontium concentration through time.

Appendix H. Scatterplot Matrix of Discrete and Composite Geochemical Samples

Figure A.24. Scatterplot matrix of geochemical samples.